Functional Characterization of a Novel Slow Muscle-Specific Methyltransferase – Mettl21c

INAUGURAL-DISSERTATION

zur Erlangung des akademischen Grades

doctor rerum naturalium

- Dr. rer. nat -

vorgelegt dem Fachbereich für Biologie und Chemie (FB 08)

an der Justus-Liebig-Universität

Gießen

eingereicht von

Soraya Hölper

aus Frankfurt am Main

Gießen, 2016

Die vorliegende Arbeit wurde am Max-Planck-Institut für Herz- und Lungenforschung (W.G. Kerckhoff-Institut) in Bad Nauheim angefertigt.

Dekan:	Prof. Dr. Volker Wissemann Fachbereich für Biologie und Chemie (FB 08) Justus-Liebig-Universität Gießen
Erstgutachter:	Prof. Dr. Dr. Thomas Braun Abteilung für Entwicklung und Umbau des Herzens Max-Planck-Institut für Herz- und Lungenforschung, Bad Nauheim
Zweitgutachter:	Prof. Dr. Katja Sträßer Fachbereich für Biologie und Chemie (FB 08) Institut für Biochemie, Justus-Liebig-Universität Gießen
Betreuer:	Prof. Dr. Marcus Krüger Institut für Genetik/CECAD Universität zu Köln, Köln

Datum der Disputation:

Schriftliche Erklärung

„Ich erkläre: Ich habe die vorgelegte Dissertation selbstständig und ohne unerlaubte fremde Hilfe und nur mit den Hilfen angefertigt, die ich in der Dissertation angegeben habe. Alle Textstellen, die wörtlich oder sinngemäß aus veröffentlichten Schriften entnommen sind, und alle Angaben, die auf mündlichen Auskünften beruhen, sind als solche kenntlich gemacht. Ich stimme einer evtl. Überprüfung meiner Dissertation durch eine Antiplagiat-Software zu. Bei den von mir durchgeführten und in der Dissertation erwähnten Untersuchungen habe ich die Grundsätze guter wissenschaftlicher Praxis, wie sie in der „Satzung der Justus-Liebig-Universität Gießen zur Sicherung guter wissenschaftlicher Praxis“ niedergelegt sind, eingehalten.“

Ort, Datum:

Unterschrift: _____

Contents

Summary

In mammals the skeletal muscle is not only essential for movement and force production but comprises also a large reservoir of amino acids and carbohydrates. The maintenance of the muscle homoeostasis is therefore essential for the whole body metabolism. In addition, the skeletal muscle is highly adaptable and responds rapidly to physiological and environmental changes, including nutritional changes, hormonal stimulation, and work loading. This flexibility arises from the dynamic expression of signaling molecules and their reversible post-translational modifications (PTMs). Moreover, the skeletal muscle consists of specific fiber-types with different metabolic profiles designed for endurance and fast contraction. In fact, muscle fibers show cell-type specific regulations and they respond differently to environmental changes [1].

The main focus of this thesis was the characterization of the putative methyltransferase Mettl21c which is highly expressed in slow type I muscle fibers. The inactivation of Mettl21c in mice by homologous recombination showed a clear association of Mettl21c to the skeletal muscle autophagosomal-lysosomal pathway. Notably, it is completely unclear how protein methylation regulates proteolysis in a fiber-type specific manner.

Previous studies indicate that protein methylation can influence the interaction, stability, cellular localization, and activity of proteins. Furthermore, a dysregulation of protein methylation is linked to the pathology of cancer, metabolic, inflammatory and neurodegenerative diseases. Recently, the METTL21 family was discovered as a novel Class I family of lysine methyltransferases that preferentially target and regulate molecular chaperones such as HSP70 and Valosin-containing protein (VCP, also known as p97 and cdc48) [2, 3]. In addition, the METTL21 family might play a role in neurodegenerative diseases like Inclusion Body Myopathy with Paget's disease of bone and Fronto-temporal Dementia (IBMPFD) [4] and some familial forms of Amyotrophic Lateral Sclerosis (ALS) [5].

The presented study revealed that Mettl21c is highly expressed in slow-twitch muscle fibers and localized to Z-disk structures, which is not only a border of the sarcomere but also an important signaling hub to regulate muscle homeostasis [6, 7]. The inactivation of Mettl21c in mice causes a severe reduction in muscle performance, including voluntary and forced running, suggesting a vital function for Mettl21c in maintaining muscle activity. The pathological dysregulation of the autophagic flux interferes with the metabolism of the skeletal muscle during physical exertion [8-10]. To better understand the molecular and cellular function of Mettl21c, comprehensive mass spectrometry based protein-protein interaction studies were performed and revealed a strong

interaction between Mettl21c and several chaperones, including the Valosin-containing protein (VCP). This finding suggests that Mettl21c is associated to the autophagy system since VCP is a key regulator in the maturation of autophagosomes and fusion of lysosomes. Moreover, detailed morphometric analysis using electron microscopy showed a clear accumulation of autophagosomal vacuoles in Mettl21c deficient slow muscle fibers. In vitro methylation assays indicated that VCP is a direct substrate of Mettl21c and this was further confirmed by the mass spectrometric detection of Mettl21c dependent trimethylation sites (K315) of VCP. Consistently, Mettl21c deficient animals show reduced VCP trimethylation in slow soleus fibers, which might enhance the activity of the ATPase/D1 of VCP [2]. Interestingly, the reduced trimethylation of Vcp in Mettl21c deficient slow muscle fibers resulted in a reduced interaction between Vcp and the inhibitory cofactor Nsfl1c (also known as p47). Nsfl1c is an important cofactor for Vcp and a reduced interaction might enhance the ATPase activity of Vcp leading to neurodegenerative diseases and related myopathies [11].

In summary, the expression of a slow fiber-type specific methyltransferase might be a new mechanism to regulate the formation of autophagosomes and the interaction of Mettl21c-Vcp-Nsfl1c represents a new network to modulate protein homeostasis in slow skeletal muscle tissue.

Zusammenfassung

Die Skelettmuskulatur dient nicht nur der Bewegung und Kraftproduktion, sondern sie stellt das größte Aminosäure- und Kohlenhydratreservoir im Körper dar. Die Balance des Aminosäurestoffwechsels im Muskel spielt eine wichtige Rolle für den gesamten Organismus. Die Skelettmuskulatur ist in der Lage schnell auf viele physiologische Impulse, wie Veränderung der Ernährungsgewohnheiten, hormonelle Stimulation, kontraktile Aktivität und körperliche Beanspruchung zu reagieren. Diese Flexibilität des Skelettmuskels wird durch unterschiedliche Proteinklassen und ihre reversiblen post-translationalen Modifikationen (PTMs) reguliert. Ein Charakteristikum des Skelettmuskels sind die unterschiedlichen Fasertypen, die für ausdauernde oder schnelle Kontraktionen ausgelegt sind. In der Tat zeigen Muskelfasern zelltyp-spezifische Regulationen und reagieren unterschiedlich auf Umweltveränderungen [1].

Der Schwerpunkt dieser Dissertation war die Charakterisierung der potentiellen Methyltransferase Mettl21c, welche primär in langsamen Muskelfasern exprimiert wird. Die Inaktivierung von Mettl21c in Mäusen durch homologe Rekombination konnte zeigen, dass Mettl21c den autophagosomalen-lysosomalen Signalweg reguliert. Es ist jedoch völlig unklar, wie Protein-Methylierungen die Proteolyse in unterschiedlichen Fasertypen reguliert.

Vorherige Studien zeigten, dass Methylierungen von Proteinen die Interaktionen, die Proteinstabilität und –aktivität, sowie den Protein-Turnover und die zelluläre Lokalisation beeinflussen können. Folglich wird eine Fehlregulation von Methylierungsmustern mit der Pathologie vieler bekannter humaner Krankheiten wie Krebs, metabolischen, inflammatorischen und neurodegenerativen Erkrankungen assoziiert. Kürzlich wurde die METTL21 Familie als neue Klasse I Methyltransferasen identifiziert, die vorzugsweise Chaperone wie HSP70 und Valosin-containing protein (VCP, auch bekannt als p97 und cdc48) ansteuert und reguliert [2, 3]. Dies bringt die METTL21 Familie in direkten Zusammenhang mit neurodegenerativen Erkrankungen wie Einschlusskörper-Myopathie assoziiert mit einem M. Paget der Knochen und einer frontotemporalen Demenz (IBMPFD - inclusion body myopathy associated with Paget disease of the bone and frontotemporal dementia) [4] sowie familiären Formen der amyotrophischen Lateralsklerose [5].

Im Rahmen dieser Arbeit konnte ich zeigen, dass Mettl21c stark in langsamen Muskelfasern exprimiert wird. Mettl21c ist in der Z-Scheibe lokalisiert, in der sich viele Signalproteine befinden, die vor allem die Muskelhomöostase regulieren [6, 7]. Die Deletion des Mettl21c Gens in Mäusen

verursacht eine massive Abnahme der Skelettmuskelleistung, was klar auf Störungen des Muskelstoffwechsels hindeutet. Eine pathologische Fehlregulation des autophagischen Flusses beeinträchtigt den Stoffwechsel des Skelettmuskels bei körperlicher Anstrengung [8-10]. Um die molekulare und zelluläre Funktion von Mettl21c genauer zu untersuchen, wurden quantitative Protein-Protein-Interaktionsstudien basierend auf massenspektrometrischen Analysen durchgeführt. Diese Experimente zeigten eine starke Interaktion zwischen Mettl21c und mehreren Chaperonen, darunter Valosin-containing protein (Vcp). Vcp wird eine zentrale Rolle bei der Reifung der Autophagosomen und Fusion mit Lysosomen zugesprochen. Somit könnte Mettl21c eine Funktion bei der Regulation des Autophagie-Prozesses spielen. Morphologische Analysen mittels Elektronenmikroskopie zeigten eine Akkumulation von autophagosomalen Vakuolen in Mettl21c defizienten Muskeln. *In-vitro* Methylierungsassays und massenspektrometrische Analysen zeigten, dass Mettl21c Vcp am Lysin-315 trimethyliert. Diese Daten waren in Einklang mit einer verminderten Vcp Trimethylierung in langsamen Soleus Muskelfasern von Mettl21c$^{-/-}$ Mäusen. In einer vorangegangen Studie konnte gezeigt werden, dass eine Methylierung am Lysin-315 die ATPase/D1 Aktivität von VCP herabsetzt [2]. Zudem konnte eine verminderte Interaktion zwischen Vcp und dem inhibitorischen Kofaktor Nsfl1c in Mettl21c$^{-/-}$ Mäusen aufgezeigt werden. Nsfl1c ist als wichtiger Kofaktor für Vcp bekannt und eine reduzierte Interaktion erhöht vermutlich die ATPase Aktivität von Vcp. Ein Verlust der ATPase-Aktivität von Vcp führt zu neurodegenerativen Erkrankungen und hiermit verwandten Myopathien, vermutlich ausgelöst durch die Akkumulation „toxischer“ Proteine [11].

Durch diese Arbeit konnte ein wichtiger Beitrag zum Verständnis für die Regulation der Autophagie im langsamen Skelettmuskel durch das Zusammenspiel von Chaperonen wie Vcp, deren Kofaktoren und skelettmuskelspezifischen Methyltransferasen wie Mettl21c erbracht werden.

1. Introduction

1.1. Skeletal muscle: the main player for whole body homeostasis

Walking, running, sitting, viewing, and even breathing are all possible because of the well-defined and continuous process of contraction and relaxation of skeletal muscle. Besides its role to produce force for maintaining body posture and movement, skeletal muscle has a central function in whole body metabolism and glucose homeostasis. Moreover, by producing an enormous amount of heat as a by-product of its energy metabolism, the muscle tissue helps us to maintain a constant body temperature. The mammalian skeletal muscle accounts for 40-50% of total body mass [12] and therefore plays a fundamental role in whole body homeostasis and represents a major reservoir of amino acids for protein synthesis and energy production. Through evolution, vertebrates developed a variety of skeletal muscles that differ in contractile, biochemical, and morphological features; their function ranges from slow contracting fibers designed for endurance to fast contracting fibers for high-intensity work. In addition, different skeletal muscle and fiber-types vary dramatically in their response to the same stimulus, reflecting their specialized metabolic function [1]. The main focus of this thesis is to expand the understanding of the molecular mechanisms regulating the plasticity and structure of different skeletal fiber-types and the function of a novel class of methyltransferases (Mettl21c) in maintaining protein homeostasis of slow-twitch fibers by modulating the autophagosomal-lysosomal degradation process.

1.1.2. Skeletal muscle architecture

Skeletal muscle is a highly organized tissue and is structured in bundles (fascicles) and coated with connective tissue – the perimysium. Finally, a single muscle fiber is surrounded by a cell membrane or sarcolemma – the endomysium (Figure 1A). The intramuscular region is highly vascularized to supply oxygen and substrates to produce energy and a huge number of nerve branches are connected to each single fiber through the neuromuscular junction [13].

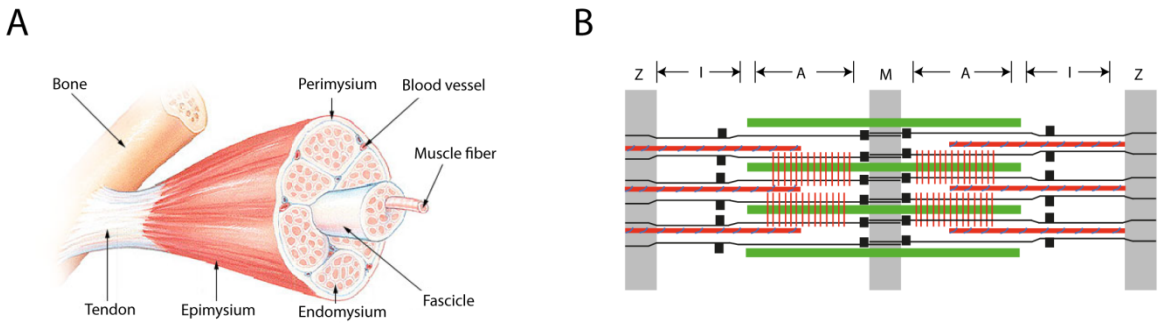

Figure 1. Schematic representation of the skeletal muscle architecture. (A) Skeletal muscle is composed of muscle fibers. Each fiber is composed of myofibrils. (B) The myofilaments are organized in sarcomeres. Each sarcomere is delimited by the Z-disk. The I-band containing the thin actin filaments is adjacent to the Z-disk, followed by the A-band, where the thick myosin filaments are located. The thick myosin filaments are attached end-to-end in the center of the A-band, the so called M-line.

Skeletal muscle does not consist of individual cells but rather forms large, elongated and cylindrical cells termed as myofibers. Each myofiber is a multinucleate syncytium up to several millimeters in length. The nuclei are located in the periphery underneath the plasma membrane – the sarcolemma. Under a light microscope the nuclei from satellite cells, which make up 1% of the nuclei present in the muscle, are not distinguishable from muscle cell nuclei. Satellite cells are muscle progenitor cells, being particular important in regenerating muscle tissue [14].

Besides the contractile apparatus, the most important organelles for skeletal muscle physiology are mitochondria. They regulate a broad range of cellular processes, like energy metabolism, cell signaling, calcium homeostasis, and the regulation of apoptosis. Mitochondrial dysfunction is tightly associated to several diseases affecting mostly skeletal muscle homeostasis, such as Alzheimer, Parkinson and amyotrophic lateral sclerosis.

Muscle fibers possess transverse tubules, also called T-tubules, and they are essential for the conduction of electric impulses to the interior of the fiber. Another tubular structure is the sarcoplasmic reticulum (SR) surrounding each myofibril and the SR is essential for calcium (Ca^{2+}) handling during the process of muscle contraction and relaxation.

The striated appearance of the muscle results from the organization of the myofibril. It is marked by regularly parallel aligned units along its length. The myofibrils are consisting of bundles of myofilaments, which are mainly composed of actin and myosin (70-80% of total protein fiber content) and are organized in thin and thick bands, respectively. A single repeat of the myofibrils is called sarcomere. As seen in Figure 1B the sarcomeres are delimited by the Z-disk, which contains several proteins including alpha-actinin, desmin, nebulin and vimentin. They serve as an attachment point for the actin filament. The broad light band between the Z-disk is called the I-

band. It is mainly composed of the actin filaments that extend beyond a broad band called A-band, which is composed of the thick filaments (myosin). The myosin filaments are attached end-to-end in the center of the A-band, this region is called M-line. Titin filaments are running from the Z-disk to the M-line, thereby supporting the whole assembly of the sarcomere and serving as a molecular spring [15].

1.1.3. Skeletal muscle fiber-type heterogeneity

The flexibility of mammalian skeletal muscles is based on its heterogeneity in the molecular architecture. The function and structure can be correlated to its metabolic and contractile needs. Skeletal muscle fibers were originally identified as oxidative and slow fibers (type I) and as glycolytic and fast (type IIa, IIb, IIx) fibers [16, 17]. Myosin heavy chains (MyHC) are the molecular motors for the contraction and skeletal muscle fibers are usually identified by their content of MyHC isoforms. Type I fibers, also known as slow-twitch fibers, are classified by the expression of Myh7. These fibers have a slow velocity of shortening, are rich in mitochondria and mainly use oxidative metabolism for energy production. Slow-twitch fibers are high resistant to fatigue and have good endurance. Type II fibers, known as fast-twitch fibers, are reflecting fast oxidative properties and can be subdivided into three subtypes. The fastest myosin is the IIb expressed by the gene Myh4, followed by the intermediate IIx isoform (gene Myh1). The “slowest” member of the type II fibers is the IIa expressed by the gene Myh2. In comparison to slow-twitch fibers, type II fibers are required for fast force production and are sensitive to fatigue. In addition, they have a lower number of mitochondria and their metabolic energy production is mainly based on glycolysis. Muscles are classified by the percentage of expression of different fiber-types. Despite fibers containing pure MyHC compositions, there are also skeletal muscle fibers which express more than one MyHC isoform. They are called hybrid muscle fibers. According to their force production they are classified from slow- to fast-twitch 1 ↔ 1/2A ↔ 2A ↔ 2A/2X ↔ 2X ↔ 2X/2B ↔ 2B. Modulation of MyHC molecules allows for a greater flexibility in muscle function and the dynamic fiber-type composition helps to rapidly respond to external stimuli.

In order to understand the molecular mechanisms and signaling pathways underlying the specific muscle phenotypes, intensive morphological and molecular studies have been performed [15, 18]. Recently, it has been shown that not only the MyHC composition reflects the metabolic properties of muscle fibers, but also a complex expression pattern of different classes of proteins and their reversible post-translational modifications determines the skeletal muscle fiber-type and its potential for adaptive changes [19].

Although contractile and metabolic characteristics are predetermined during development, maturated skeletal muscle fiber-types are not static and a given external stimuli as well as defects in muscle homeostasis can induce an extensive fiber-type switching. This property defines the adaptive potential of muscle, also known as muscle plasticity and it was shown that fiber-type switching requires the regulation of specific gene sets [20-22]. Of note, it was shown by experimental models that slow- and fast-twitch fibers vary often drastically in their response to the same physiological or pathological stimulus [23, 24]. Examples for the selective atrophy are shown for instance by Aravamudan and his colleagues when denervating rat diaphragm [23]. This led to atrophy in type IIx and IIb fibers, whereas type I and IIa fibers are unchanged. Similar results are obtained when denervating other fast rat muscles as seen by unpublished data from Schiaffino and Ciciliot [1]. But type I fibers of the slow soleus showed a clear atrophy after denervation.

These examples display that the same fiber-type can undergo opposite changes in different muscles, probably due to different combinations of specific molecular and functional properties of the muscles.

1.1.4. Muscle plays a central role in whole-body protein homeostasis

Proteostasis in skeletal muscle is regulated by a broad range of catabolic and anabolic processes. The constant protein synthesis and protein degradation allows for a rapid adaption in response to different physiological conditions. For example, hormones, physical activity, neuronal stimulation, and stress conditions can activate or inhibit skeletal muscle activity. One characteristic of skeletal muscle is the fast expansion in volume due to increased physical activity. This process is also known as hypertrophy and associated with upregulated protein synthesis or hyperplasia (increased proliferation) [25]. Two main signaling pathways control protein synthesis. The insulin-like growth factor 1-phosphoinositide-3-kinase–Akt/protein kinase B-mammalian target of rapamycin (IGF1-Akt/PKB-mTOR) pathway acts as a positive regulator. On the other hand, myostatin-Smad2/3 pathway is a negative regulator for muscle growth. Furthermore, during the early postnatal developmental stage, the increase of myonuclei through proliferation and fusion of satellite cells regulates muscle growth.

Conversely, skeletal muscle atrophy is delineated by a rapid decrease in the muscle mass, reduced cross sectional area of the fibers, and less protein content. The pathological loss of muscle mass is also called sarcopenia, occurring most often during aging [26]. In addition, human patients with a pathological muscle wasting (cachexia) in combination with systemic diseases including cancer,

diabetes, neurodegenerative and immune disorders [27] usually show a poor survival rate. This reflects the importance of skeletal muscle as an energy reservoir for the whole body. All of these examples have in common that protein degradation overtakes protein synthesis.

During catabolic conditions, several remodeling processes of signaling cascades and cellular organelles including mitochondria and lysosomes are activated. Although the majority of contractile proteins (myosin and actin) are rapidly degraded, a class of proteins named as "atrogenes" are simultaneously activated and/or upregulated to mediate the coordinated protein break down. For example, a number of proteasomal subunits and several E3 ligases like MuRF1 are upregulated during starvation and neuronal denervation (see chapter 1.2.). Conversely, energy-producing systems like mitochondria are down regulated under those conditions. Moreover, physical overload or other environmental factors result in an increased level of reactive oxygen species (ROS), having detrimental effects on mitochondrial proteins and related networks. Thus, skeletal muscle demands an efficient system for removal of unfolded protein aggregates, dysfunctional organelles, and toxic products that otherwise may lead to cell death [28, 29]. In skeletal muscle, there are two main proteolytic systems, the ubiquitin-proteasomal and the autophagosomal-lysosomal pathway, which organize the protein degradation of proteins under regular and perturbed conditions.

1.2. Ubiquitin-proteasomal system

The ubiquitin-proteasomal system (UPS) in muscle is the major degradation system for single proteins or small aggregates and thereby efficiently controls protein concentrations within the cell. It requires the transcription of components of the 26S proteasome, two ubiquitin ligases atrogin-1 and MuRF 1 and the ubiquitination of the substrates [30]. Three specific proteins regulate the process leading to the selection of substrates for degradation by the conjugation of ubiquitin molecules. In brief, first by an ATP-dependent process ubiquitin is connected to the Ubiquitin-activating enzyme (E1) via a high-energy thioester bond. Second ubiquitin is transferred to an Ubiquitin-conjugating enzyme (E2) by linking ubiquitin and a cysteine residue of the E2 enzyme. Finally, although there are a few notable exceptions [31, 32], the Ubiquitin-ligase enzyme (E3) transfers the ubiquitin monomer to the substrate via an isopeptide bond between the ε-amino group of a lysine residue 48 in the substrate and the carboxy-terminal glycine residue 76 in ubiquitin. In order for the substrate to be recognized by the 26S proteasome, the process needs to be repeated a minimum of four times, conjugating ubiquitin monomers to lysine residue 48 of the substrate [33] (Figure 2).

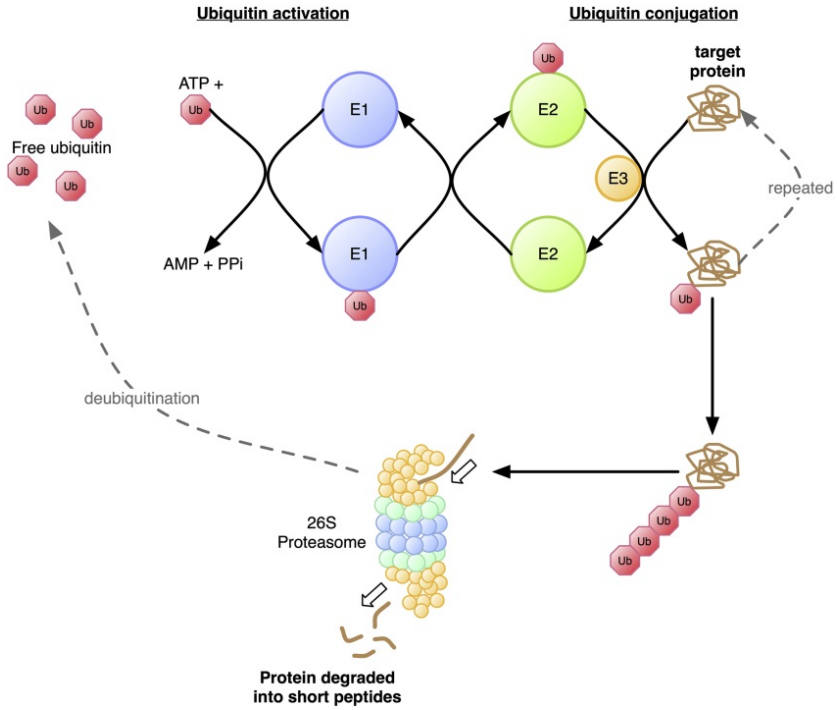

Figure 2. Ubiquitin-proteasomal mediated protein degradation. Three specific proteins regulate the process, which leads to the selection of substrates for degradation by the conjugation of ubiquitin molecules. The Ubiquitin-activating enzyme (E1) binds the ubiquitin monomer first and then transfers it to the Ubiquitin-conjugating enzyme (E2). In order for the substrate to be recognized by the 26S proteasome the Ubiquitin-ligase enzyme (E3) transfers a minimum of four ubiquitin monomers to lysine residue 48 of the substrate (the schematic representation was adapted from Murton et al., 2008 [34]).

Interestingly, it has been shown that the UPS is unable to degrade intact myofibrils [35]. This leads to the assumption that for initial myofibril disruption the activity of other degradation systems is necessary like caspase-3 [36] and calpain [37].

As shown in previous studies, the UPS has a key role in skeletal muscle atrophy [38-40]. However, the inhibition of this UPS by proteasome inhibitors is not sufficient to fully protect from loss of muscle mass during catabolic conditions [41-43], indicating the presence of a further protein degradation system.

1.3. Autophagosomal-lysosomal pathway

Autophagy is a ubiquitous and well-conserved process from yeast to mammals. The word autophagy derives from the Greek word “self-eating”. In contrast to the ubiquitin-proteasomal system, the autophagosomal-lysosomal system has the ability to degrade and recycle entire organelles and large protein aggregates. The balance of this degradation process is the key for muscle health as it is detrimental for muscle homeostasis as the excessive or inhibited activation of

autophagy flux leads to rapid loss of muscle mass [29]. Inhibition of autophagy causes many known myopathies and neurodegenerative diseases like Pompe and Danon disease or Inclusion body myositis. Neurodegenerative diseases are displaying inclusions and abnormal mitochondria.

So far, three independent types of autophagy are described: macroautophagy, microautophagy and chaperone-mediated autophagy (CMA). Macroautophagy (hereafter referred to as autophagy) starts with the formation of a C-shaped double-membrane vacuole called phagophore. It wraps the cytoplasmic components, which should be degraded and finally forms the double membrane autophagsomes. The autophagosome fuses with the lysosome, forming the autophagolysosome. The inner vesicle of the autophagosome together with the cargo substrates are degraded by resistant hydrolases. The resulting macromolecules and amino acids are recovered by lysosomal permeases to fulfill the energy demands of the muscle cells.

However, autophagy is not a non-selective process for bulk degradation as many several types of selective autophagy for mitochondria, peroxisomes, endoplasmic reticulum, cytoplasmic aggregates, and invading pathogens have been described [44].

1.3.1. Autophagy machinery

To date, 38 known autophagy-related genes (Atg) have been identified as regulating the steps of autophagosome formation and breakdown. They are highly conserved and were initially identified in yeast genetic screens [45]. At least four important functional groups of Atg proteins are involved in the process of autophagy: for the regulation of autophagy initiation, the ULK1 protein-kinase and the VPS34–Beclin 1 complex are necessary. The Atg9–Atg2–Atg18 complex regulates expansion of phagophore assembly site (PAS) by carrying lipids and the Atg5–Atg12–Atg16 and Atg8/Map1lc3 (microtubule associated protein 1 light chain 3, LC3) conjugation systems regulate the elongation of autophagosome membranes.

After induction of autophagy the phagophore is formed. The origin of this double membrane is still under debate. It is assumed that highly conserved ubiquitin-like conjugation systems, consisting of the Atg12-Atg5 and the Atg8-phosphatidylethanolamine (PE) system, are assembling at the phagophore assembly site or the pre-autophagosomal structure [46]. Atg7 activates Atg12 in an ATP-dependent manner, functioning like an E1-activating enzyme. Atg12 is then transferred to a cysteine residue in Atg10 by releasing Atg7. Atg10 functions like an E2-conjugating enzyme and links Atg12 to Atg5 and finally to Atg16. This multimeric complex is then required for the elongation

of the expanding pre-autophagosomal membrane that is curved by the asymmetric recruitment of Atg8.

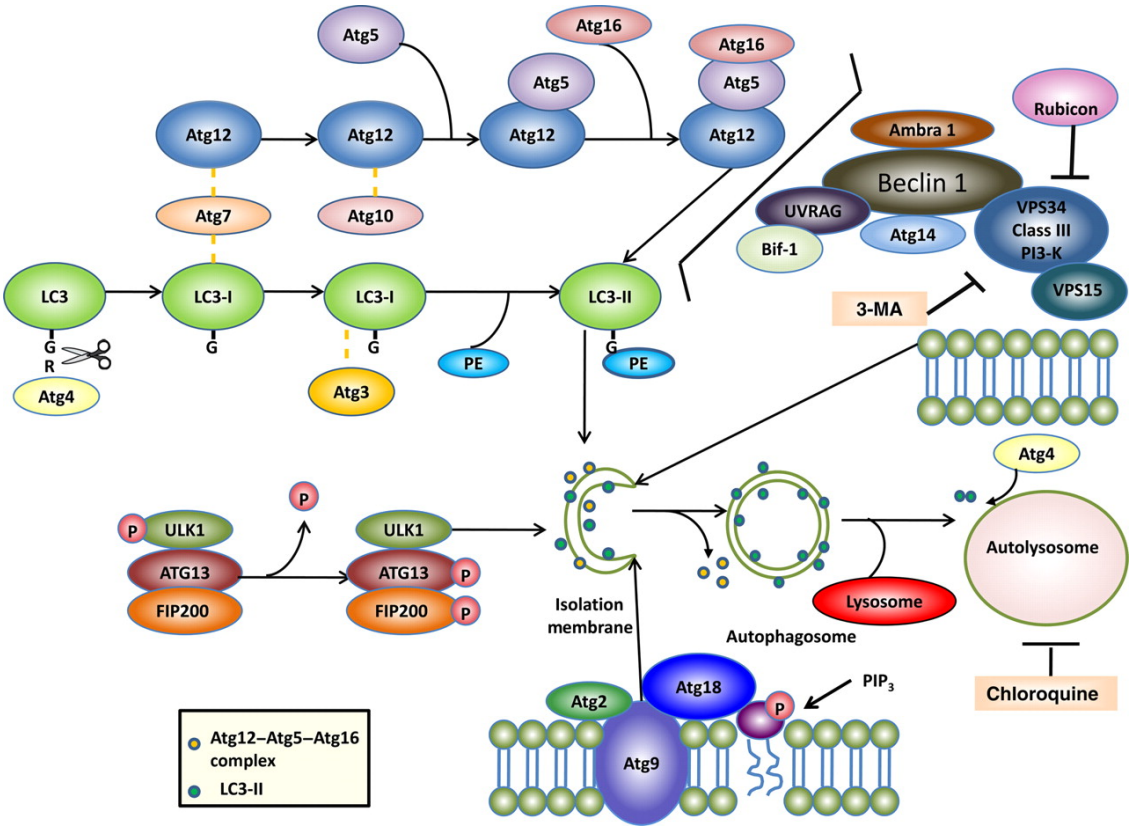

Figure 3. Autophagy machinery. At least four important functional groups of Atg proteins are involved in the process of autophagy: (1) the ULK1 protein-kinase complex and (2) the VPS34–Beclin 1 complex are necessary for regulation of autophagy initiation. (3) The Atg9–Atg2–Atg18 complex regulates expansion of phagophore assembly site (PAS) by carrying lipids and the (4) Atg5–Atg12–Atg16 and Atg8/Map1lc3 (microtubule associated protein 1 light chain 3, LC3) conjugation systems regulate the elongation of autophagosome membranes (the schematic representation was adapted from Ding et al., 2011 [47]).

Early isolation membranes, autophagosomes and autophagic bodies have Atg8 present in their membrane. This ubiquitin-like protein is primarily cleaved by Atg4, which leads to an exposing glycine residue resulting in the activation by binding to Atg7. The transfer to Atg3, an E2-like enzyme, initiates the conjugation of Atg8 with an abundant membrane phospholipid, phosphatidylethanolamine (PE). In order to keep the normal autophagy process running, Atg4 is able to reverse the conjugation of PE. In mammals four Atg8 homologs are identified, among these is LC3, Gate16 (Golgi associated ATPase Enhancer 16 kDa), Gabarap (Gabba receptor associated protein) and Atg8L. LC3 is the most abundant one and is detected in two forms, the soluble LC3-I form and the lipidated LC3-II form. Lipidated and cleaved LC3 is used as a general autophagic marker [48] to monitor autophagic flux [49].

The regulation of autophagy is organized through a set of signaling pathways which are influenced by nutritional status, growth factors, hormones, stress and intracellular energy information. One key regulator and autophagy sensor in mammals is the kinase mTOR. The ULK1 protein-kinase complex (Atg1-Atg13-Atg17) works downstream of mTOR and is required for the early stage autophagosome formation. In order to form this complex, mTOR coordinates the phosphorylation status of Atg13. Cellular stress like starvation leads to the suppression of mTOR, causing activation by dephosphorylation of the serine-threonine protein kinase ULK1. Active ULK1 phosphorylates Atg13 and recruits other downstream Atg proteins. The ULK1 protein-kinase complex recruits Atg9, a transmembrane protein interacting with Atg18, a phosphatidylinositol-triphosphate (PI3-P) binding protein and Atg2, a peripheral membrane protein. This complex is involved in the cargo of additional membranes from trans-Golgi network and the late endosomes necessary for the growth of the autophagosomal membranes.

Atg6 and its mammalian homolog Beclin 1 are also important for the initiation of autophagy. It forms a complex with VPS34, VPS15 and Atg14. The class III PI-3-kinase VPS34 is an essential regulator of autophagy by generating PI3-P. The complex with Atg6/Beclin 1 significantly increases the catalytic activity [50, 51]. Several regulatory proteins that interact with Atg6–VPS34 complex have been identified. The interaction with Bcl-2 and Bcl-xL leads to the dissociation of the Atg6/Beclin 1 and Vps34 complex. Other interaction partners induce autophagy such as ambra-1 [52] and UVRAG (ultraviolet irradiation resistance associated gene) [53]. Rubicon (Run domain protein as Beclin 1 interacting and cysteine-rich containing) [54, 55] and 3-Methyladenine (3MA) [56] are known to negatively regulate autophagy.

Finally, the mature autophagosome fuses with the lysosomal compartment forming the autophagolysosome (Figure 3). This involves the recruitment of the SNARE protein syntaxin and HOPS (homotypic fusion and vacuole protein sorting). This complex promotes the fusion of autophagosomes with lysosomes [57-59]. This process is detrimental for the autophagic flux; any blockage will result in the accumulation of autophagosomes.

Noteworthy, post-translational modulation of the Atg proteins adds additional entry points for crosstalk with other cellular processes and helps define cell-type-specific regulations of autophagy [60].

1.3.1. Autophagy in skeletal muscle

Since muscle is the major reservoir of amino acids, it is one of the most important tissues to control whole body metabolism. Excessive or insufficient protein degradation by autophagy is detrimental for global muscle homeostasis as it leads to atrophy and muscle weakness. The muscle-specific inactivation of two critical autophagy-related genes in mice, Atg5 and Atg7, helped to understand the basal mechanisms of autophagy in skeletal muscle. The inactivation of Atg5/7 leads to severe muscle wasting combined with ultrastructural alterations of cytosolic organelles and myofiber degeneration. Furthermore, the Atg5/7 inactivation results in an increase of polyubiquitinated proteins and the accumulation of concentric membranous structures without any obvious changes of the proteasome activity, indicating an important role of lysosomal protein degradation via autophagy in muscle cells [61-63]. Consistently, collagen VI deletion mutants, a model for Bethlem myopathy and Ullrich congenital muscular dystrophy, are not able to activate autophagy in skeletal muscles causing the accumulation of dysfunctional organelles, increased ROS levels and myofiber damage [8].

Notably, another report revealed an important link between physical exercise and induction of autophagy [10]. Since exercise usually improves glucose and energy metabolism in the liver and pancreas in high-fat diet mouse models of obesity, the beneficial effect of exercise was perturbed in stimulus (exercise- or starvation-) induced autophagy-impaired mice. These mice carry a mutation in Bcl-2 that prevents its release from an inhibitory interaction with the autophagy protein Beclin 1, resulting in a blockage of the beneficial metabolic effects. This reveals that autophagy is a key contributor for metabolic benefits of physical exercise.

Reduction in autophagy causes muscle wasting due to toxic accumulation of protein aggregates, resulting in a pathological phenotype after several months or years. Conversely, an increase of autophagic flux causes a rapid loss of muscle mass within days and weeks [29]. Although the balance in the autophagic flux is one key point in muscle health, there are still many open questions about the role of autophagy in skeletal muscle. Elucidation of autophagy regulators is of great importance as an imbalance is associated in several myopathies and dystrophies.

As mentioned before, there is increasing evidence that ubiquitin is used as a signal for autophagic degradation of protein aggregates and other cellular substrates. It is still not clear which degradation pathway is activated upon accumulation of polyubiquitinated protein. Nevertheless, the two main cargo proteins responsible for the selective recognition and delivery to the autophagosomes are p62/SQSTM1 and NBR1. They contain a C-terminal ubiquitin-binding domain containing (UBA) and a short LC3-interacting region (LIR) sequence responsible for LC3 interaction

[64, 65]. This enables the cargo proteins to bind polyubiquitin chains of proteins and LC3 [28]. Furthermore, there is evidence that aggregates containing p62 and ubiquitinylated proteins serve as nucleating scaffold for autophagosome biogenesis by binding multiple Atg proteins [66-68].

Arndt et al. depicted that chaperone-assisted selective autophagy is essential for muscle maintenance. Before p62 binds its cargo, the substrate needs to be recognized by molecular chaperones or other cellular systems. The co-chaperone BAG3 forming a complex with Hsc70, HspB8 and the ubiquitin ligase CHIP binds filamin, a muscle sensitive protein prone to irreversible damage. The ubiquitination of filamin and BAG3 by CHIP results in the binding of p62 and finally autophagic clearance [69]. Another chaperone called Valosin-containing protein (VCP/p97) seems to play a pivotal role in the fusion of autophagosomes to lysosomes [70] by regulating the integrity of a dynamic tubular lysosomal network [71].

1.3.2. Valosin-containing protein (VCP/p97) is required for autophagy

Valosin-containing protein is a ubiquitously expressed hexameric AAA-ATPase (ATPase associated with various activities). It is implicated in several cellular processes, like cell cycle regulation, nuclear envelope formation, Golgi biogenesis and the ubiquitin proteasome system [72]. VCP has two ATPase domains, D1 and D2, which are organized as two stacked rings with a central channel. The regulatory N-domain is at the periphery of the D1 ring. Several cofactors have been shown to be responsible for modulating VCP-mediated processes [4]. Mutations of VCP gene cause inclusion body myopathy (IBM), Paget's disease of the bone (PDB) and frontotemporal dementia (FD) [73], spastic paraplegia [74], scapuloperoneal muscular dystrophy [75] and Charcot-Marie-Tooth disease [76] which are rare multisystem degenerative disorders. Muscle weakness is the first symptom in over 50% of VCP associated diseases [70]. Typical symptoms are the accumulation of non-digested autophagosomes that form morphological structures called rimmed vacuoles and poly-ubiquitin aggregates [70]. A recent study of Johnson et al. depicted a role for VCP in the dynamic of lysosome tubules. VCP deficiency causes defects in lysosome tubular lattice leading to a disruption in autophagic clearance. However, the exact mechanism by which VCP regulates autophagic and lysosomal protein degradation needs to be elucidated. Furthermore, it was long believed that autophagy and the ubiquitin-proteasomal system act as complementary systems with no point of intersection. But several studies revealed that ubiquitinated proteins can be degraded by both catalytic pathways [77-79] and ubiquitin-binding proteins such as VCP appear to play a major role in this crosstalk [80].

Several Atg proteins were identified and they are regulated by transcriptional, translational, and post-translational mechanisms. But the impact of these PTMs on the degradation systems still needs to be elucidated.

1.4. Methyltransferases: an enzymatic group with diverse functions

Complex molecular networks are necessary to maintain the intracellular homeostasis under normal and stimulated conditions. Methyltransferases are important regulators that keep the balance in these critical cellular events by enzymatically methylating a great variety of substrates. They transfer methyl groups to nucleotides, lipids, small molecules, and proteins. The donor of the methyl group is a small cofactor called S-adenosylmethionine (SAM also known as AdoMet). In 1887, the German physician Wilhelm His reported the results of experiments in which he administered pyridine to dogs and found that they excreted *N*-methylpyridine in their urine. About 60 years later, it was found that the reaction is catalyzed by S-adenosylmethionine-dependent methyltransferases [81]. Several years later it was shown that methylation occurs on lysine residues of proteins [82], in particular histones [83], and nucleic acids [84]. So far more than 200 potential methyltransferases in humans have been identified and they are involved in epigenetic control, tissue differentiation, and lipid biosynthesis (Figure 4) [85].

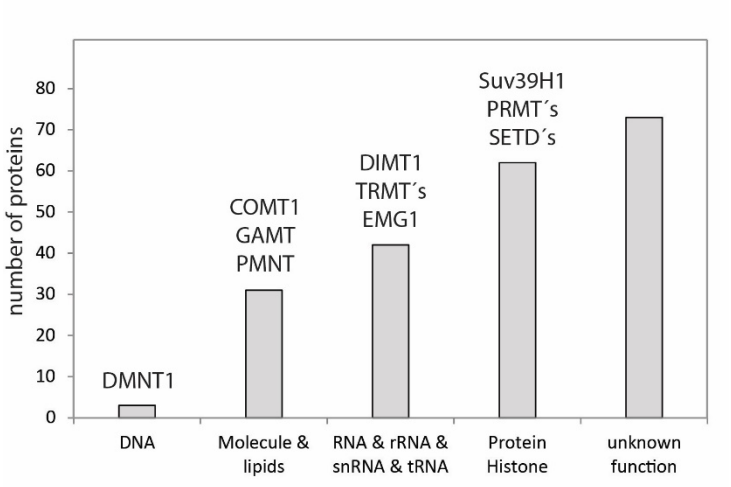

Figure 4. Composition of the methyltransferome. Methyltransferase domain containing proteins were grouped into biological functions. The annotation of biological functions is adopted from the Swiss-Prot database and in most cases the assignments are based on similarities.

Mammalian DNA methyltransferases transfers a methyl group to DNA either at the C-5 carbon atom of cytosine or the C-6 nitrogen atom of the adenine purine ring. DNA methylations, also

known as epigenetic marks, are involved in numerous processes including genomic imprinting, carcinogenesis, and gene expression control. Increased DNA methylation on regulatory DNA sequences is generally associated with decreased gene activity and is the basis for epigenetic regulation of gene expression. The most abundant DNA (cytosine-5)-methyltransferase is DNMT1. It methylates CpG dinucleotides and the inactivation of this gene results in a clear reduction of DNA methylation and to a lethal phenotype during embryonic mouse development [86].

Another class of mammalian methyltransferases transfers the methyl group to mainly lysine and arginine residues of proteins. In several cancer types a dysregulation of these methyltransferases was found. SMYD2, a protein lysine methyltransferase, is upregulated in esophageal squamous cell carcinoma [87] and bladder cancer cells [88]. Similarly, an increased expression for SMYD3 was revealed in breast carcinoma [89] and for G9a, a histone methyltransferase, in hepatocellular carcinoma [90].

The lack of guanidinoacetate N-methyltransferase causes a deficiency of creatine in tissues with high-energy demand like muscle and brain due to an accumulation of the creatine precursor guanidinoacetic acid (GAA) [91].

In addition to its function in cancer SMYD2 plays also an important role for proper muscle function. The deletion of Smyd2 in zebrafish resulted in loss of Hsp90 methylation, causing a decreased complex formation of titin and Hsp90. As a consequence, Smyd2 deletion mutants showed reduced titin stability and altered muscle function [92].

It was initially thought that methyltransferases are highly substrate-specific. But several examples suggest a remarkable substrate promiscuity that is characterized by methyltransferases acting on diverse substrates [93-95]. This classification and identification of substrates of methyltransferases might be one of the biggest challenges in the characterization of these proteins.

1.4.1. The “protein” methylation reaction

The transfer of a methyl group by S-adenosylmethionine-dependent methyltransferases works via a SN2 displacement mechanism to nucleophilic atoms like carbon, oxygen, nitrogen, sulfur or halides. These residues are present on a wide range of amino acids such as lysine, arginine, glutamate, asparagine, histidine, and cysteine as well as several amino acids at the amino or carboxyl terminus of proteins [96]. S-adenosylmethionine is produced and regenerated via the SAM cycle [97]. The by-product of the methylation reaction S-adenosyl-homocysteine (SAH) is a strong inhibitor of these methyltransferases. Thus, SAH is normally converted to homocysteine and

adenosine by the action of SAH hydrolase [98]. Defects in methyltransferases are associated with elevated intracellular levels of homocysteine, which results in the premature onset of cardiovascular and neurological diseases [37, 99]. Furthermore, methyl groups can be also transferred to electrophilic carbon atoms by an indirect "ping-pong" mechanism with an intermediate methylation step on a conserved cysteine residue. For example, the methyltransferases RlmN (YfgB) and Cfr belong to the radical SAM-dependent enzymes and methylate C-2 and C-8 of adenosine 2503 (A2503), respectively. In neither case is a methyl group transferred directly from SAM to the RNA. Instead this class of methyltransferases is able to cleave SAM to a 5'-deoxyadenosyl 5'-radical (5'-dA•), which is further, used to abstract key hydrogen atoms from the substrate. One prerequisite is at least one [4Fe-4S] cluster that is typically coordinated by the cysteine residues of a CxxxCxxC motif. This [4Fe-4S] cluster supplies the electron for the reductive cleavage of SAM [100].

1.4.2. Methylation on proteins

One of the first reports about protein methylation was already described more than 50 years ago [82] and identified the methylation on core histone proteins. The methylation of histone proteins is part of the "histone code" which is important for transcriptional activation and the recruitment of DNA binding partners.

Several studies also showed that non-histone proteins are methylated at lysine, arginine and the N-terminus [2, 92, 101-104]. The first methyltransferase was identified twenty years ago and it is responsible for the trimethylation of lysine-14 of the large subunit RUBISCO, the plant enzyme required for fixing much of the carbon dioxide in the biosphere [105, 106]. This methyltransferase was later designated as a SET-domain protein, though the function still needs to be elucidated. The SET-domain stands for three Drosophila genes associated with development: Su(var)3–9, enhancer of zeste, and trithorax. The knowledge that the SET-domain is important for plant methyltransferases led to the understanding that it is the catalytic core of protein methyltransferases and that each of these Drosophila proteins catalyze histone lysine methylation [107].

In contrast to protein acetylation, methylation does not alter the overall charge of the protein and the nucleosome. However, the function of both modifications is to recruit proteins responsible for regulatory processes like transcription, mRNA splicing and DNA repair and thereby determine cell fate and identity [108]. Initially, protein methylation was considered irreversible due to its high thermodynamic stability of the N–CH_3 bond. The first enzyme identified that could erase methyl

marks from histones was the amine oxidase LSD1 [109] (KDM1 according to the newly suggested nomenclature [110]). This changed the understanding, and during the last years many families of demethylases have been identified underscoring the dynamic nature of methylation [111].

A unique feature of histone methylation is that it leads to a repression or activation of gene activity depending on the modification site and the modification state. For example, the trimethylation on H3K4 is associated with active genes [112], in contrast to H3K9, which is found at silent loci [113]. Furthermore, trimethylation of H3K4, H3K9, H3K27 and H4K20 proved to be stable through mitosis and over several cell generations [114, 115]. These features make histone methylation suited for propagation and inheritance of epigenetic states.

One prominent example for non-histone protein methylation is the tumor suppressor p53. It is the most studied non-histone protein being methylated at the several lysine residues. Clearly, the activity of p53 is mainly regulated on post-translational level. In addition to phosphorylation, ubiquitination and acetylation, methylation can enhance or suppress the activity of p53. It was shown that p53 is methylated at lysine K320 and K327, which regulate its activity [116-118]. In the methylation field it was a significant finding that Smyd2, a Set and MYND domain containing methyltransferase, is one of the methyltransferase regulating the methylation process of p53 and its downstream targets [118]. Other examples for protein methylation are the activation of the transcription factor TAF10 by the methyltransferase SET9 [119] and the VEGFR1 methylation by Smyd3 [120]. There is a great influence of the Smyd methyltransferase family (Smyd1-3) in the development and assembly of skeletal muscle tissue. Smyd1 is expressed in heart and fast skeletal muscle tissue, and it is localized at sarcomeric M-line structures. In zebrafish flatline mutants where Smyd1 is mutated the assembly of thick myosin filaments is dysregulated and results in a severe malformation of heart and fast skeletal muscle tissue [121]. As mentioned before, the family member Smyd2 is essential for the methylation of the Hsp90 protein that subsequently stabilizes Z-disk structures in zebrafish [92]. However, the inactivation of the Smyd2 gene in mouse does not show any obvious phenotype in the heart [122].

Another important protein regulating a wide range of physiological processes throughout eukaryotic organisms is Calmodulin, a key mediator of calcium-dependent signaling, which has an important role in skeletal muscle excitation. Several studies revealed that Calmodulin is subject to many regulatory post-translational modifications, including trimethylation of lysine 115 [102, 123, 124]. A recent study revealed that an enzyme named Calmodulin-lysine N-methyltransferase is responsible for the trimethylation of lysine residues on Calmodulin [102].

Taken together, these examples prove that protein methylation is an important regulator for protein stability [125, 126], activity [116-120, 127], turnover [128], localization [117, 129-131], protein-protein [92, 132-134] and protein-nucleic acids interaction [135].

1.4.3. Methyltransferases share homologue structures

S-adenosylmethionine-dependent methyltransferases represent 0.6-1.6% of all genes in the genomes of bacteria, yeast and humans. It is predicted that there are over 200 methyltransferases in humans [85, 136] and for most of them the function/substrate is completely unclear.

These methyltransferases are classified into five distinct families, namely Class I-V, based on their different structural features. The majority of identified methyltransferases contains a seven-strand twisted beta-sheet and is summarized as Class I enzymes. The smallest families with very distinct structures are Class II (TIM beta/alpha-barrel alpha/beta) and III (tetrapyrrole methylase alpha/beta). Class IV (SPOUT alpha/beta) act as homodimers and methylate RNA substrates like tRNA and rRNA. One of their characteristics is the knot-like structure formed by the C-terminus compromising of several catalytic residues [137]. The SET domain containing enzymes represent Class V also displaying a knot-like structure, but they catalyze the methyl transfer to proteins like histones and ribosomal proteins [93]. Based on the yeast methyltransferome, Wlodarski and his colleagues claim for the existence of at least four more methyltransferase classes [138]. The majority of methyltransferases, however, have a structure similar to the Class I fold, and this group is characterized by a seven-stranded beta-sheet adjoined by alpha helices. Although the sequence similarity is rather low, their tertiary structure shares the well-known S-adenosylmethionine-dependent methyltransferase fold, which is structurally similar to the NAD(P)-binding Rossmann fold [85, 93]. This class displays four distinct motifs, namely Motif 1, Motif Post 1, Motif 2 and 3 [139, 140]. Important for the binding of cofactors are two conserved positions; the first one is a GxGxG motif localized in Motif 1. It is characteristic for a nucleotide-binding site and is used to bind the adenosyl part of S-adenosylmethionine. The second position is an acidic residue located C-terminal to Motif 2 that forms one hydrogen bond to each hydroxyl of the S-adenosylmethionine ribose part [141].

1.4.4. The Methyltransferase-like 21 (METTL21) family

Recently, the METTL21 family was discovered as a novel Class I family of lysine methyltransferases that preferentially target and regulate molecular chaperones [2, 3]. It was shown that METTL21D catalyzes the trimethylation of VCP, while METTL21A methylates the heat shock protein HSP70. Moreover, it seems that cofactors play an important role. VCP trimethylation of lysine-315 by

METTL21D was stimulated by the direct interaction of the UBX cofactor ASPSCR1 [2]. Interestingly, the stimulatory effect of the of the UBX cofactor ASPSCR1 is diminished when using the VCP mutants (R155H, R159G and R191Q) which are known to be responsible for Inclusion Body Myopathy with Paget's disease of bone and Fronto-temporal Dementia (IBMPFD) and/or some familial forms of Amyotrophic Lateral Sclerosis (ALS) [2]. These amino acids are localized to the N-terminal domain that is crucial for the interaction with several cofactors [142]. The lysine-315 on VCP is in close proximity of the Walker B domain of the first ATPase/D1 domain, and it is suggested that it negatively affects the ATPase activity [3].

It has been shown that methylation of Hsp70 has a beneficial impact on the formation of stress granules induced by arsenite treatment. In times of cellular stress cells produce stress granules. Several proteins (for example Ataxin-2 [143] and the survival motor neurons [144]) which are involved in neurodegeneration are known to interact with stress granules [145]. These cytoplasmic inclusions result in the repression of RNA processing. Several studies implicate that the dysfunctional stress response facilitates the onset of the pathogenesis of neurodegenerative diseases [146, 147]. This brings protein methylation in context with degenerative disorders like IBMPFD and ALS [2].

Furthermore, Huang and co-workers suggested an important role for Mettl21c in musculoskeletal biology and sarcopenia. They showed that siRNA mediated knockdown of Mettl21c mRNA expression in mouse myogenic C2C12 precursor cells causes a slight reduction in myofiber formation, which was claimed to be caused by effects of the NFκB pathway [148].

In *Saccharomyces cerevisiae,* an uncharacterized methyltransferase encoded by the *YNL024C* gene shows high sequence similarity to METTL21A and METTL21D, as well as to their uncharacterized paralogues METTL21B and METTL21C. The study of Jakobsson et al. provided evidence that it methylates the eukaryotic translation elongation factor eEF1A at lysine-390 [149]. For the eukaryotic translation elongation factor eEF1A in yeast four methylation sites have been reported (Lys30, Lys79, Lys318 and Lys390). With the identification of YNL024C, all four methyltransferases regulating these methyl modifications have now been identified [149-152].

Taken together, protein methylation by members of the METTL21 family is an important regulator for protein-protein interactions and associates most likely chaperone activity and protein turnover to modulate skeletal muscle plasticity.

1.5. Mass spectrometry based proteomics

Multicellular organisms have a complete genome in every single cell of their body and the diversity between different cell types and organs derives from epigenetics, transcriptional, post-transcriptional as well as post-translational processes. In order to better understand the complex molecular system and the crosstalk between signaling pathways in a cell, one needs to survey all proteins (termed proteome) at different physiological conditions at once. Therefore, mass spectrometry has emerged as a powerful tool and the method of choice for the identification and quantification of proteins and post-translational modifications in a biological sample [153-155]. Mass spectrometry became popular in the 1980s, when the two main techniques, matrix-assisted laser desorption/ionization (MALDI) [156] and electrospray ionization (ESI) [157, 158], were introduced. Initially, proteomics was performed with 2-dimensional gel electrophoresis techniques, which suffer from several limitations, including sensitivity and reproducibility [159]. 2-dimensional gel electrophoresis was later replaced by protein and peptide separation techniques based on liquid reversed phase chromatography coupled online to mass spectrometers (LC-MS).

Currently, the bottom-up approach is the most popularly used approach in mass-spectrometry based proteomics for the identification and quantification of proteins, post-translational modifications, and protein-protein interactions in complex biological samples. This approach is also known as shotgun proteomics. Here, proteins are first enzymatically digested into peptides using proteases and purified peptides are then subjected to LC-MS/MS analysis (Figure 5). The generic workflow contains four stages and starts usually with the lysis of the cells and solubilisation of proteins. Within the second step the proteins are proteolytically digested by endopeptidases like trypsin or LysC. Protein digestion is performed either in solution (in-solution digestion) or after separation of proteins by 1-dimensional SDS-PAGE (in-gel digestion). In addition, combination of in-solution digestion and filter-based peptide separation, named as filter-aided sample preparation (FASP) technique, were recently invented. This third method for sample preparation was invented by Wisniewski et al., proving to be the method of choice for single-run analysis with in-depth coverage of proteome [160].

The major challenge in shotgun proteomics is the dynamic range of proteins in a given sample. For example, the concentration of blood proteins comprises up to 12 orders of magnitude and the detection limit in protein concentration differences are only 5 orders magnitudes for modern mass spectrometers [161]. This fact makes it impossible to detect very low abundant proteins in complex biological samples, such as blood and skeletal muscle.

To bypass this problem, several different approaches were developed to reduce the complexity of biological samples. A useful strategy is the improvement of peptide separation in front of the mass spectrometers. Longer columns filled with smaller bead size increase the resolution of the reversed phase chromatography significantly. Other approaches to reduce the sample complexity are based on size exclusion chromatography (SEC), strong cation exchange chromatography (SCX), strong anion exchange chromatography (SAX) or (high pH) reversed-phase liquid chromatography (RPLC). After digestion, peptides are cleaned and desalted by C18 STAGE-tip technique (Stop and Go extraction tips) [162].

During the third step, peptides are separated online by ultra-high pressure reversed phase chromatography (UHPLC). Peptides are separated by reversed phase chromatography and ionized by electrospray (ESI) at the tip of the column and transferred into the mass spectrometer. Next, tandem mass spectrometry allows isolating and fragmenting individual peptides (MS) and detecting the fragment mass spectra (MS/MS) [153]. Peptide masses (MS) and the fragment spectra (MS/MS) are used to accurately identify proteins and peptides. The quantification is based on peptide intensities. The spectra are obtained as raw files and they are analyzed using a search engine for comparison to databases, which were digested with the same enzyme in silico.

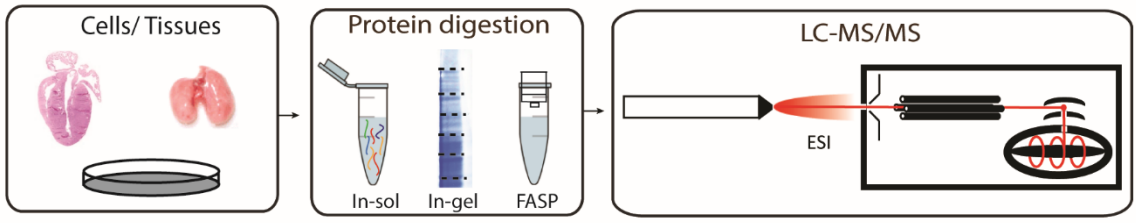

Figure 5. Generic workflow of LC-MS-based proteomics. It is based on four different steps: 1. Extraction of proteins from cells or tissue. 2. Proteolytic digestion of proteins, usually in-solution, in-gel or in a filter-aided sample preparation protocol. 3. + 4. Peptide mixtures are separated by UHPLC, ionized by electrospray (electrospray ionization, ESI), and measured in a mass spectrometer detecting the masses and fragment masses.

Due to the quality of the MS/MS spectrum in large-scale analysis, the main issue is to assign correct peptide sequences to a spectrum. This score-based result will inevitably have some mismatches (false positives). There are several strategies for a multiple testing correction to discriminate the false positive hits. The most frequently used is the target-decoy database search. The principle of this is the usage of a combinatory database consisting of a normal (target) fasta sequence and a reversed/random (decoy) fasta sequence. A peptide would be considered to be a false positive if it

would be aligned to the decoy database. The false discovery rate (FDR) is finally calculated by dividing the number of target and the decoy peptide spectrum match (PSM) [163, 164].

In comparison, the top-down approach detects intact proteins, including their PTM pattern, and measures them directly with the mass spectrometer.

1.5.1. Quantitative methods in mass spectrometry

Mass spectrometry is able to qualitatively analyze thousands of proteins in complex biological mixtures, but is not inherently quantitative. Variabilities in sample preparation and instrument performance very often hamper a direct comparison of large-scale samples. However, a number of techniques have recently emerged. In principle there are three major quantification techniques I.) the label-free protein quantification approach, II.) the chemical modification and derivatization with labeled isotopes [165], and III.) the metabolic incorporation of "SILAC" amino acids into the proteome (stable isotope labeling by amino acids in cell culture) (Figure 6).
In this thesis, I either used stable isotope labeling with amino acids in cell culture (SILAC) [166], the SILAC mouse [167] or label-free quantification techniques [168-170].

Relative quantification strategies compare the abundances of individual peptides between two samples of interest. Clearly, the SILAC technology has become the most often used approach for in vivo isotopic labeling. Cells are usually labeled with lysine and arginine, containing stable isotopes of carbon and/or nitrogen. Cells were usually incubated with the SILAC amino acids for approximately five cell doublings, resulting in a complete exchange from the non-labeled (light) to the labeled (heavy) form. For relative protein quantification, both non-labeled and labeled protein extracts are mixed 1:1 according to their protein concentration. After mass spectrometric analysis each peptide is then measured as a peptide pair. The relative intensity of the light and heavy peak indicates the abundance of the peptide/protein within the sample. The advantage of SILAC is that the samples are mixed at the beginning of the workflow and each error will affect both conditions equally. This makes the quantification independent of variations due to sample preparation or the mass spectrometric measurement. Depending on the SILAC amino acid combination, a multiplexing of three different biological conditions can be performed [166].

Recently, the SILAC technology was expanded to also label living animal models, including yeast, worms, flies, and rodents. For the labeling of intact animals, the essential amino acid lysine is preferred since this amino acid does not get converted into other amino acids, contrary to arginine. Thus, to obtain peptides containing at least one lysine, the protease LysC, which cleaves proteins only after lysine, is used for proteolytic digestion [167].

Besides these labeling approaches, label-free quantification has emerged as a powerful tool by comparing the signal intensity from the extracted-ion chromatogram (XIC) of individually measured peptides derived from any biological sample. Nowadays, the combination of single shot analysis and sophisticated software tools has shifted the label-free approach to the same level of accuracy compared to SILAC quantification [169]. In addition, the absolute concentration or the amount of a given protein in copy number per cell can be determined with absolute quantification techniques. This is mainly done with spiking in isotopic labeled peptides of known concentrations.

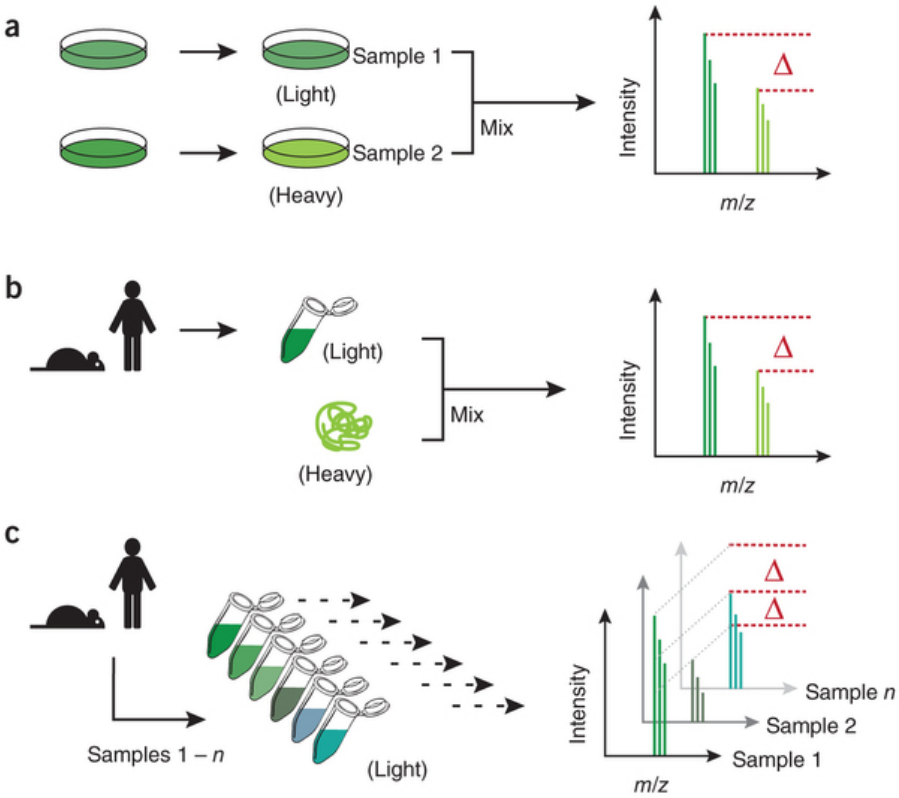

Figure 6. Relative and absolute quantification strategies. (A) The SILAC approach metabolically labels the entire proteome with isotopically stable amino acids. Before the analysis, the samples with different conditions are mixed. (B) Absolute proteomic quantification uses isotopic peptides of known concentrations to analyze the exact concentration or the amount of a given protein in copy number per cell of a target protein. (C) Label-free quantification has emerged as a powerful tool by comparing the signal intensity of individually measured peptides derived from any biological sample (the schematic representation was adapted from Meissner et al., 2014 [171]).

1.5.2. Mass spectrometry instrumentation

Mass spectrometry is a powerful analytical technology for complex mixtures. Providing precise measurements of mass, composition, and structural properties of analytes, it makes it a versatile tool in many fields, for example medicine, life and pharmaceutical sciences, physics, and organic

chemistry. The first experiments in mass spectrometry were made by J.J. Thomson who was interested in the behavior of electrical discharges in gases. This led to the discovery of the electron in 1897. He could show that the movement of charged particles in vacuum under the influence of an electric or a magnetic field depending on the mass to charge ratio (m/z). This led to the construction of the first mass spectrometer. For his great discovery, he received the Nobel Prize in 1906 in physics. From that time point on the application of mass spectrometry rapidly expanded.

In general, a mass spectrometric measurement starts with the ionization of an analyte in an ion source. The m/z ratio of the ions is measured in a mass analyzer, while a detector registers the number of ions at each m/z value and outputs them as intensities. The intensity values are plotted as a function of m/z values to obtain the mass spectrum, which is finally processed with several computational strategies in order to correlate the m/z with the analytes.

The first step in any mass spectrometry experiment involves the formation of gas phase ions derived from the solid, liquid, or gas of interest and during the decades, several different methods were developed. From the ion source, the ionized analyte molecules are sprayed into the mass analyzer, facilitated by pressure and electric potential differences. An enormous number of different ionization methods have been developed. Currently, mainly soft ionization methods are used that do not fragment the analyte upon ionization. The most popular approaches to ionize molecules are the chemical ionization or matrix-assisted laser desorption (MALDI) [156] and the electrospray ionization (ESI) technique [157, 158]. The principle of ESI is based on two main theories, the Ion Evaporation Model (IEM) developed by Iribarne and Thomson, and the charge residue model (CRM). Both the IEM and CRM assume that evaporation causes the droplets to shrink, resulting in large field strength at their surface. In contrast to the CRM, the IEM postulates that the field strength is large enough to cause the field desorption of solvated ions [172, 173]. The CRM suggests that when the field strength increases at the location with the highest surface curvature, a Taylor Cone is formed. From the tip of the Taylor Cone other highly charged smaller droplets are emitted until the droplets contain only one analyte molecule [157, 174].

A great advantage for the detection of peptides from biological samples was the combination of ESI and liquid-chromatography (LC). This method is the most commonly used technology to analyze proteomes, and it is nowadays possible to measure complete proteomes from mammalian cells [163].

There are different types of mass analyzers that can be used for the separation of ions like quadrupole, magnetic sector, time-of-flight (TOF), ion trap, and Fourier transform ion cyclotron resonance analyzer (FT-ICR). In principle, the charged analytes are analyzed by their motion based

on their characteristic mass to charge ratio under the influence of magnet and/or electric field. The quadrupole and the linear ion trap use the stability of the ion trajectory in oscillating electric fields. In comparison, the TOF and the FT-ICR use velocity and frequency of oscillation. After passing through the mass analyzer ion beams strike on a detector. The selection of detector is based on the required detection sensitivity, the speed, and application-specific requirements [153]. Resulting from the complexity of peptides in biological samples with high dynamic ranges, mass spectrometers are constantly developing towards higher sensitivity, sequencing speed and resolution [175, 176].

The Orbitrap analyzer is one of the latest developments in the field of mass spectrometry [177, 178]. The basic principle is like the Kingdon trap as described by K.H. Kingdon in 1920 [179]. The Orbitrap analyzer consists of an outer barrel-shaped electrode and an inner spindle-shaped electrode. The ions are injected in packages from the C-trap, an ion storage device. The electric field of the inner electrode is ramped and the ions are forced to enter a circular motion (electrodynamic squeezing) resulting from the interaction of centripetal and centrifugal forces generated from the tangential movement and the electric field between the electrodes. The oscillating frequency by the axial motion of the ions is a direct value for the mass of the ions. The generated current is Fourier Transformed (FT) and displayed in high-resolution mass spectra.

The Orbitrap analyzer was first integrated into a hybrid mass spectrometer in 2005. It was released as a LTQ Orbitrap [177, 178, 180] in a combination of a low resolution but fast linear ion trap and a high resolution Orbitrap analyzer. The Orbitrap detects the MS scans, while the ion trap fragments the peptides by collision induced dissociation (CID) and scans the resulting peptide fragments [177, 178, 181]. In 2009, a new version of the hybrid Orbitrap, the LTQ Orbitrap Velos, was developed containing a new inlet system, the S-lens. This new system contains apertures to which RF voltage is applied and results in a 10-fold improvement in the transmission of ions compared to the skimmer lens.

In addition, a dual linear ion trap and a higher energy collisional dissociation (HCD) were implemented. This allows for peptide fragmentation and peptide detection in the Orbitrap detector [182]. In the collision-induced dissociation (CID) mode of the LTQ Orbitrap Velos, the LTQ and Orbitrap operate as separate mass spectrometers, while in the HCD mode the precursor ion is selected for fragmentation in the HCD cell. Although the fragmentation and detection of peptides is much slower via the HCD and Orbitrap detector, the mass accuracy is much higher resulting in peptides with significant better scores. The use of two separated mass analyzers is referred to as ‘tandem in space’ as it is commonly employed in a combination of an ion trap and Orbitrap mass

analyzer or FT-ICR. In contrast, the sequential use of the same analyzer can be viewed as 'tandem in time', like it is commonly used in Q Exactive instruments (as described in section 2.15.1.).

1.6. Aim of this thesis

Skeletal muscle fibers are highly differentiated cells and the development of a highly efficient contractile apparatus ensures a lifelong contraction. In mammals the skeletal muscle is the most abundant tissue and supports the whole body with energy. Thus, the metabolic function of skeletal muscle tissue plays a vital role for whole body homeostasis. The presence of specific fiber-types enables the skeletal muscle to perform simultaneously long lasting workload as well as fast movements. Moreover, individual fiber-types are able to rapidly respond to external stimuli, including loading conditions, nutrition status, and hormonal signals [18, 19]. Earlier studies showed that not only the abundance of proteins in the cell is important but also the presence of post-translational modifications (PTM), such as phosphorylation, ubiquitination and acetylation. Another PTM, the methylation of lysine and arginine residues is mainly known as an essential regulator of hetero- and euchromatin, which is achieved by the formation of methyl marks on histone tails. However, it has been shown that protein methylation is not only restricted to epigenetic regulation but also modulates the activity, stability, and interactions of many non-histone proteins. According to these functions, a dysregulation of methyltransferases is closely associated to many human diseases, such as cancer, inflammation, metabolic syndromes and neurodegeneration [183].

The aim of the presented thesis is the functional characterization of a slow-muscle specific putative methyltransferase annotated as Mettl21c (Methyltransferase-like 21c). To elucidate the function of this enzyme in muscle tissue, a transgenic mouse model with an inactivated Mettl21c gene should be generated. Besides the analysis of morphometric and physiological parameters, a comprehensive analysis of the transcriptome and proteome is aimed in order to understand the molecular consequences of the inactivation of Mettl21c. Moreover, protein-protein interaction studies based on high-resolution mass spectrometry should help to decipher the molecular network and identify potential substrates for this enzyme. It will be central to investigate, whether muscle tissue of Mettl21c deficient mice is able to properly respond to external stimuli such as atrophy induction to understand the alterations of the dynamics.

Together, the goal of this study is to understand how non-histone methyltransferases regulate the homeostasis of muscle fibers under basal and disease related conditions.

2. Materials and Methods

2.1. Materials and chemicals for biochemistry methods

cOmplete protease inhibitor cocktail	Roche
Needles and syringes	B.Braun
BSA protein standard	Sigma Aldrich
Dithiothreitol (DTT)	Sigma Aldrich
Iodacetamide	Sigma Aldrich
Ammonium bicarbonate (ABC)	Sigma Aldrich
Methanol	AppliChem
NuPAGE 4-12% Bis-Tris Gel	Life Technologies
NuPAGE LDS sample buffer 4x	Life Technologies
NuPAGE SDS MOPS running buffer	Life Technologies
InstantBlue	Expedeon
Ethanol	Carl Roth
Acetonitrile	Sigma Aldrich
Acetone	Carl Roth
Trifluoroacetic acid	Applied Biosystems
Sodium dodecyl sulphate (SDS)	Carl Roth
Urea	Sigma Aldrich
Thiourea	Sigma Aldrich
HEPES	Sigma Aldrich
Tris	Carl Roth
Hydrochloric acid	AppliChem
S-adenosylmethionine	NEB
Potassium phosphate	AppliChem
Potassium chloride	Carl Roth
Potassium hydrogen phosphate	Sigma Aldrich
Sodium chloride	AppliChem
3M Empore C8 extraction disk	Sigma Aldrich
3M Empore C18 extraction disk	Sigma Aldrich
Sepharose G beads	Life Technologies

Bicine	Sigma Aldrich
Bis-Tris	AppliChem
Tween-20	Carl Roth
Whatman (Rotilabo blotting) paper	Carl Roth
Nitrocellulose blotting membrane	GE Healthcare Life Sciences
RedAlert western blot stain 10x	EMD Millipore
Albumin bovine fraction	Serva
NP-40	Fluka
Sodium desoxycholate	Sigma Aldrich
Skim milk powder	Serva
Glass teflon homogenizer	Kontes Glass Co.
Ethylenediamenetetraacetic acid (EDTA)	Carl Roth
Phenylmethanesulphonyl fluoride (PMSF)	Sigma Aldrich
Sodium carbonate	Carl Roth
Trichloroacetic acid	J.T. Baker Chemicals
Triton-X 100	Carl Roth
Paraformaldehyde	Sigma Aldrich
Mowiol 4-88 reagent	Sigma Aldrich
Collagenase P	Sigma
Mayers heamalaun	Chromo 2E038
Eosin	Chromo 2C140
Xylol	Roth
Trichrom Stain (Masson) Kit	Sigma Aldrich
FITC Lectin	Sigma Aldrich

2.2. Materials and chemicals for mass spectrometry methods

Fused-silica PicoTip Emitter	DNU-MS GbR
C18-AQ Reprosil Pur beads	Dr. Maisch GmbH
Nano electrospray ion source	Proxeon
LTQ Velos ESI positive ion calibration solution	Pierce
Methanol	AppliChem
Formic acid	Thermo Scientific

Acetonitrile	Sigma Aldrich

2.3. Materials and chemicals for molecular biology methods

LB Carl Roth and agar	Sigma Aldrich
Glycerol	Sigma Aldrich
DMSO	Sigma Aldrich
dNTP mix	Life Technologies
***PfuUltra* High-Fidelity DNA polymerase AD**	Agilent Technologies
DpnI restriction enzyme	New England Biolabs
T4 DNA ligation buffer 10x	Promega
T4 DNA ligase	Promega
2-propanol	Carl Roth
Agarose	Biozym
Ethidium bromide	AppliChem
TRIzol reagent	Life Technologies
Chloroform	Merck
Diethylpyrocarbonate (DEPC)	Sigma Aldrich
RQ1 Dnase buffer	Promega
RQ1 Dnase	Promega
RQ1 Dnase stop solution	Promega
First strand buffer 5x	Promega
Rnase IN	Promega
Rnase H	Promega
Superscript II reverse transcriptase	Promega
Calcium chloride	AppliChem
Magnesium chloride	Carl Roth
Bacto-tryptone	BD Biosciences
Bacto-yeast extracts	BD Biosciences
Bacto-agar	BD Biosciences
Ampicillin	Sigma Aldrich
Kanamycin monosulphate	Sigma Aldrich
Tris-acetate	Sigma Aldrich

Glucose	Sigma Aldrich
Sodium hydroxide	Carl Roth
Potassium acetate	Carl Roth
Acetic acid	Carl Roth
1 kB DNA molecular mass standard	Invitrogen

2.4. Materials and chemicals for cell culture methods

DMEM medium	Sigma Aldrich
Fetal bovine serum (FBS)	Life Technologies
Penicillin-Streptomycin-Glutamine 100x	Sigma Aldrich
PBS tablets	Gibco (Life Technologies)
Trypsin EDTA	Sigma Aldrich
SILAC DMEM medium	Silantes
Dialyzed fetal bovine serum (dFBS)	Silantes
L-lysine	Sigma Aldrich
L-arginine	Sigma Aldrich
$^{13}C_6$ L-Lysine HCl (Lys4)	Silantes
4,4,5,5-D_4-L-Lysine (Lys4)	Cambridge Isotope Lab (CIL)
$^{13}C_6$ $^{15}N_2$-L-Lysine HCl (Lys8)	Silantes
$^{13}C_6$ $^{15}N_4$-L-Arginine HCl (Arg10)	Silantes
Dimethyl Sulphoxide (DMSO)	Sigma Aldrich
Sodium hydrogen phosphate	Carl Roth
Calcium chloride	AppliChem
TurboFect transfection reagent	Thermo Scientific
Opti-MEM medium	Gibco (Life Technologies)
Bafilomycin A1	Sigma
Rapamycin	Sigma

2.5. Materials and chemicals for mouse methods

10% Ketamine	CEVA Sante Animale, Düsseldorf
2% Xylazin	CEVA Sante Animale, Düsseldorf
5-0 Vicryl	Ethicon
Tissue-Tek® O.C.T. Polyfreeze™ Freezing media	Miles Inc., Diagnostic Division, Elkhart, USA
Running Wheel	TSE Instruments
Treadmill	Columbus Instruments

2.6. Enzymes

Lysyl endopeptidase (LysC)	Wako
Sequencing grade Trypsin	Promega
Proteinase K	Sigma Aldrich
RNase A	Sigma Aldrich

2.7. Kits

DC protein assay kit	Bio-Rad
Phusion High-Fidelity DNA polymerase kit	New England Biolabs
QIAquick Gel Extraction kit	Qiagen
NucleoBond Xtra Maxi Kit	Macherey Nagel
SuperSignal West femto max. sensitivity substrate kit	Thermo Scientific
PCR clean up and Gel extraction Kit	Macherey-Nagel
RNA-Seq Kit v2	Thermo Fisher
miRNeasy micro Kit	Qiagen
Rnase free Dnase Set	Qiagen
Ribo Minus Kit	Thermo Fisher

2.8. Antibodies

2.8.1. Primary antibodies

Antibody	Company	Catalog number	Application
Flag	Sigma Aldrich	#F1804	IF
Anti-Flag M2 affinity gel	Sigma Aldrich	#A2220	IP
Flag M2 peroxidase HRP	Sigma Aldrich	#A8592	WB
GFP	Evrogen	#AB121	IP
Pan-actin	Cell Signaling Technology	#4968	WB
Sequestosome (p62)	abcam	#ab91526	IP, WB
Valosine-containing-protein (p97)	abcam	#ab11433	IP, WB
Microtubule-associated proteins 1A and 1B (Map1lc3)	Cell Signaling Technology	#2775	WB
a-Actinin 2	Sigma	#A7811	
Myomesin clone B-4	Kind gift from Dr. H.M. Eppenberger, Switzerland		

2.8.2. Secondary antibodies

Antibody	Company	Catalog number	Application
Anti-mouse IgG-peroxidase	Sigma Aldrich	#A5278	WB
Anti-rabbit IgG-peroxidase	Sigma Aldrich	#A9169	WB
Cy2™	Dianova GmbH	#715-225-151 (mouse) #711-225-152 (rabbit)	IF
Cy3™	Dianova GmbH	#715-165-151 (mouse)	IF

#711-165-152 (rabbit)

2.9. Buffers and solutions

SDS lysis buffer	4% SDS
	0.1M Tris/HCl pH 7.6
RIPA lysis buffer	100mM Tris/HCl pH 7.5
	300mM NaCl
	2% NP-40
	2mM EDTA
	0.2% Sodium deoxycholate
Urea (UA) buffer	6M Urea
	2M Thiourea
	0.1M HEPES pH 7.4
Buffer A	0.1% formic acid
Buffer B	80% acetonitrile
	0.1% formic acid
Buffer C	5% Acetonitrile
	1% Trifluoroacetic acid
KCM buffer 5x	500 mM KCl
	150 mM CaCl2
	250 mM $MgCl_2$
LB (Luria-Bertani) medium per litre	10g Bacto-tryptone
	5g Bacto-yeast extracts
	5g NaCl
	950 ml deionized water added and dissolved,
	pH adjusted to 7.0 with 5N NaOH,
	filled up to 1l with deionized water,
	sterilized by autoclaving
LB-Agar plate per litre	10g Bacto-tryptone
	5g Bacto-yeast extracts
	5g NaCl
	7g Bacto-agar
	Sterilized by autoclaving,
	cooled to 50-60°C and antibiotic added

Antibiotics (1000x stocks)	Ampicillin 50mg/ml in H2O
	Kanamycin monosulphate 10mg/ml in H2O
Tris-EDTA (TE) buffer 10x	100 mM Tris/HCl pH 7.6
	10mM EDTA pH 8.0
TAE buffer	40mM Tris-acetate
	1mM EDTA
Mini prep solution A	25mM Tris pH 8.0
	10mM EDTA
	50mM Glucose
	10µg/ml RNase A
Mini prep solution B	0.2N NaOH
	1% SDS
Mini prep solution C	3M Potassium acetate
	8.9% Acetic acid
HBS (HEPES Buffered Saline) 2x	50 mM HEPES
	280 mM NaCl
	1.5 mM Na2HPO4
	pH 7.0 adjusted using HCl and
	filter sterilized
Western blot transfer buffer 20x	500 mM Bicine
	500 mM Bis-Tris
	20 mM EDTA
TBS-T	50 mM Tris/HCl pH 7.6
	150 mM NaCl
	0.1% Tween-20
Methyltransferase-Buffer	100 mM Tris pH 8.5
	10 mM MgCl
	8 mM DTT
Sodiumposphate buffer	77,4 ml 1 M NaHPO
	22,6 ml 1 M NaHPO
	in 1 l MilliQ-H_2O, pH 7,4
X-Gal fixation solution	Sodiumphosphate buffer pH 7.4
	0.2% GDA
	2 mM $MgCl_2$
	5 mM EGTA pH 7.5

X-Gal washing solution	2 mM $MgCl_2$
	0.01% Na-Desoxycholat
	0.02% NP-40
	Sodiumphosphate buffer pH 7.4
5% X-Gal	50 mg/ml X-Gal in Dimethylformamide
X-Gal staining solution	5 mM K_3FeCN_6
	5 mM K_4FeCN_6
	0.1% X-Gal
	in X-Gal washing solution
Blocking solution	2% BSA
	0.5% NP40
	3% Horse Serum
	in PBS
Mowiol 4-88	2.4 g Mowiol 4-88
	6 g Glycerin
	6 ml MilliQ-H_2O
	12 ml Tris-HCl pH 8.5
2x HBS	50 mM HEPES
	280 mM NaCl
	1.5 mM na2HPO4 x $2H_2O$, pH 7.05
4% PFA/PBS	40 mg/ml Paraformaldehyd (PFA)
	in PBS, pH 7.4
1x TE	10 mM Tris-HCl
	1 mM EDTA
	pH 8
TENS Lysis buffer	50 mM Tris-HCl, pH 8
	100 mM EDTA
	100 mM NaCl
	1% SDS
	200 µg/ml Proteinase K (freshly added)
PBT	0.1% Tween20 in PBS
0.2% collagenase solution	0.2% Collagenase P in DMEM
10x TBS	2 M Tris-HCl pH 6.7
	1.4 M NaCl
	in MilliQ-H_2O

1x MOPS-SDS Running Buffer	dilution of 20x MOPS-SDS Concentrate (Invitrogen) in ddH2O
1x TAE	1:50 50x TAE, in ddH2O

2.10. Devices used

FLUOstar galaxy spectrophotometer	BMG Labtech
SpeedVac concentrator plus	Eppendorf
MilliQ water purification system	Merck Millipore
Thermomixer	Eppendorf
ÄKTA purifier	GE Healthcare Life Sciences
Easy nLC 1000 UHPLC	Thermo Scientific
QExactive mass spectrometer	Thermo Scientific
PCR labcycler	Sensquest
NanoDrop 2000c spectrophotometer	Peqlab
ChemiDoc MP imaging system	Bio-Rad
Ion Torrent Proton sequencing platform	Thermo Fisher
LSM700 confocal microscope	Carl Zeiss
Transmission electron microscope	Philips CM 10
Zeiss Axioimager Z1	Carl Zeiss
Leica with DFC 420C camera	Leica
Cryostat Leica CM3050	Leica
Running Wheel	TSE Instruments
Treadmill	Columbus Instruments
Bead mill	Retsch, MM301
Bioanalyzer 2100	Agilent
Ion OneTouch2 instrument	Thermo Fisher

2.11. Cell lines

Cell line	**Company**	**description**
C2C12	ATCC CRL-1772™	Murine myoblast cell line
HEK293T	ATCC CRL-11268™	Human embryonal

		kidney cell line
U-2 OS	ATCC® HTB-96™	Homo sapiens bone cells

2.12. Primer

2.12.1. Primers for genotyping

Wild type and Mettl21c$^{-/-}$ fw: CTGTGAAACTAGCTCCTTGG

Wild type: GATTGACCGTAATGGGATAG

Mettl21c$^{-/-}$ rev: TTCTTATGGCTGAGAAATGC

2.12.2. Primers for Phusion PCR amplification

NdeI- Mettl21c fw 5'-GGG AAA GGG CAT ATG GAT CAG CAT CTC CAC ATA GCC CAG CAG CCC CT-3'

BamHI- Mettl21c fw 5'-GGG AAA GGG GGA TCC ATG GAT CAG CAT CTC CAC ATA GCC CAG CAG CCC CT-3'

Mettl21c -nostop-SlaI rev 5'-CCC TTT CCC CTC GAG CTC CCA CTT TAA TAT CCC TTT AAA CAG CTT GAC AG-3'

NdeI- Mettl21e fw 5'-GGG AAA GGG CAT ATG GAC CTC ACA GTA ACT CAC ATT ACT CAC AAA GA-3'

BamHI- Mettl21e fw 5'-GGG AAA GGG GGA TCC ATG GAC CTC ACA GTA ACT CAC ATT ACT CAC AAA GA-3'

Mettl21e -nostop-SlaI rev 5'-CCC TTT CCC CTC GAG GGC ACT CCT CCG ATT TTT CTT CAT AGC TTT GTA CA-3'

2.12.3. Primers for methyltransferase domain mutation

Mettl21c-GGG/AAA fw 5'-GCT AAA ATA CTT GAA ATT GCT GCT GCA GCA GCC CTT GTT TCC-3'

Mettl21c -GGG/AAA rev 5'- GGA AAC AAG GGC TGC TGC AGC AGC AAT TTC AAG TAT TTT AGC-3'

Mettl21e -GGG/AAA fw 5'-AAT GTG ATT GAA ATT GCA GCT GCG ACA GCG CTT GTC TCC-3'

Mettl21e-GGG-AAA rev 5'- GGA GAC AAG CGC TGT CGC AGC TGC AAT TTC AAT CAC ATT-3'

2.12.4. Empty plasmids used in this study

pGemTeasy (Promega)

pcDNA5/TO (life technologies)

pcDNA5/TO EGFP (provided by MPI collection, Marten Szibor)

pcDNA5/TO Flag-stop (provided by MPI collection, Natalie Al-Furoukh)

pcDNA5/TO HA-stop (provided by MPI collection, Natalie Al-Furoukh)

pcDNA5/TO Myc-stop (provided by MPI collection, Natalie Al-Furoukh)

2.12.5. Plasmids generated during this thesis

Mettl21c:

pGemTeasy-Nde1-Mettl21c-Sla1

pcDNA5/TO-Mettl21c-Flag

pcDNA5/TO-Mettl21c-HA

pcDNA5/TO-Mettl21c-Myc

pcDNA5/TO-Mettl21c-EGFP

pGemTeasy Nde1-Mettl21c(GGG/AAA)-Sla1

pcDNA5/TO-Mettl21c(GGG/AAA)-Flag

pcDNA5/TO-Mettl21c(GGG/AAA)-HA

pcDNA5/TO-Mettl21c(GGG/AAA)-Myc

pcDNA5/TO-Mettl21c(GGG/AAA)-EGFP

pET26b-Mettl21c

pET26b-Mettl21c(GGG/AAA)

Mettl21e:

pGemTeasy-Nde1-Mettl21e-Sla1

pcDNA5/TO-Mettl21e-Flag

pcDNA5/TO-Mettl21e-HA

pcDNA5/TO-Mettl21e-Myc

pcDNA5/TO-Mettl21e-EGFP

pGemTeasy Nde1-Mettl21e(GGG/AAA)-Sla1

pcDNA5/TO-Mettl21e(GGG/AAA)-Flag

pcDNA5/TO-Mettl21e(GGG/AAA)-HA

pcDNA5/TO-Mettl21e(GGG/AAA)-Myc

pcDNA5/TO-Mettl21e(GGG/AAA)-EGFP

pET26b-Mettl21e

pET26b-Mettl21e(GGG/AAA)

2.13. Working with the model organism Mus musculus

2.13.1. Transgenic mouse line Mettl21c

The construct for the targeting vector replacing Mettl21c gene with a LacZ cassette was commercially obtained from VELOCIGENE (http://www.velocigene.com/komp/detail/15237). For inactivation of Mettl21c, the ZEN-UB1 velocigene cassette was used that contains the beta-galactosidase coding sequence from E.coli (LacZ Gene) and a polyadenylation signal. In addition, the promoter of human ubiquitin C genes together with the neomycin phosphotransferase and a polyadenylation signal flanked by loxP sites were used for positive selection. The generation of the knockout mouse was performed the in-house service of the MPI mouse facility. The targeting vector was linearized and used to electroporate pluripotent embryonal mouse ES cells (F1 hybrid Bl6/129). Transformed ES cells were cultured for 8-10 days with G418 antibiotics. G418 resistant clones were isolated and expanded. ES cells with homologous recombination into the correct locus were injected into C57Bl6 mouse blastocytes. These blastocysts were transplanted into pseudopregnant C57Bl6 mice. Resulting chimera mice were mated with cre-deleter mice, which express the Cre-Recombinase in the germ line, to cut out the neomycin-resistance cassette at the loxP sites. The Cre-Recombinase expression is driven by a beta-actin enhancer element and a human cytomegalovirus promotor (CMV) followed by a rabbit beta-globin polyadenylation signal [185]. For seven generation back crossing C57BL6/J was used. The official authorization for the genetic manipulation was given by the Regierungspräsidium in Gießen (B2-250).

2.13.2. Maintaining of transgene mouse colony

The transgene mouse line Mettl21c$^{-/-}$ was housed in the animal facility of the Max-Planck-Institute for Heart and Lung Research in Bad Nauheim under regular conditions with ambient temperature of 20-22°C and in a 12 hour light-dark cycle. They were provided with food and water ad libitum.

2.13.3. Genotyping - isolation of genomic DNA from murine tail biopsy

Murine tail biopsies (0.5 cm) were digested with Proteinase K (200 µg/ml) in 500 µl lysis buffer overnight at 56°C shaking. After precipitation with 500 µl Isopropanol and washing with 70%

Ethanol the genomic DNA was diluted in 300 µl MilliQ H_2O. For the following genotyping 2 µl were used.

2.13.4. Isolation of mouse muscles tissue

All animal procedures were performed in accordance with institutional guidelines. For the isolation of mouse muscle tissue the animals were sacrificed by cervical dislocation. For muscle isolation the skin at the leg was opened and the fascia was carefully removed. Several muscles, including the tibialis anterior, extensor digitorum longus, soleus muscle, gastrocnemius muscle, gluteus maximus, and the diaphragm were isolated for biochemical and histological analysis.

2.13.5. Sciatic nerve transection

The sciatic nerve transection is a validated and reproducible model for denervation-induced skeletal muscle atrophy in rodents. It was performed on Mettl21c$^{-/-}$ and littermate control males ages 8-12 weeks. Animals were anesthetized with an intraperitoneal injection of 100 mg/kg ketamine and 10 mg/kg xylazine. Mice were denervated by surgical removal of approx. 5 mm of sciatic nerve from the left hindlimb. The right hindlimb served as the control leg. Wounds were closed by suturing with 5-0 Vicryl. The operative limb was check daily for infections. After 7 days the animals were euthanized and skeletal muscles were dissected, flash-frozen in liquid nitrogen or imbedded in optimal cutting temperature (OCT) compound (Tissue-Tek) for cryostat sectioning. The official authorization for the sciatic nerve transection was given by the Regierungspräsidium in Darmstadt (B2-1082).

2.13.6. Running Wheel

To study the physiological ability and the spontaneous motion behavior of mice deficient for Mettl21c, voluntary running experiments were performed. Each mouse was given access to a cage that was equipped with a running wheel (drum diameter 115 mm, drum width 40 mm, rod distance 8.9 mm) and with ad libitum access to food and water in a 12-hour light/dark cycle. After an initial one day acclimation period the running performance was recorded by the PhenoMaster Software for three days. The official authorization for the running wheel experiment was given by the Regierungspräsidium in Darmstadt (B2-1083).

2.13.7. Treadmill

To study the physiological ability and the time to exhaustion of mice with a deletion of Mettl21c forced running experiments were performed. The official authorization for the treadmill experiment was given by the Regierungspräsidium in Darmstadt (B2-1083). The treadmill model from Columbus Instruments allows low-intensity electric shock to the mouse's paws when the mouse stops. Mice are trained in acclimation runs on two consecutive days, during which animals become familiar with the apparatus. The duration of the acclimation run is 12 minutes and the speed increases from 0 to 12 m/min. This is done by starting the treadmill at 5 m/min and slowly (once per minute) adding 1 meter per minute, until the speed reading is 12 m/min (7 minutes time), and the speed of 12 meters per minute is continued for an additional 3 minutes. The mouse is then removed from the treadmill, placed back in its home cage and returned to the mouse room by free access to water and food. On the third day mice were fasted for 4 hours (from ~9 am -1 pm). The exercise protocol consists of a 60 minutes run beginning with a 5 min warm-up period from which the mice progress from 0 to 12 m/min (0.2 m/sec). To do this, the treadmill is started at 5 m/min and increased by 1 m/min every 20 seconds. Following the warm-up stage, mice were then exercised at 12 m/min for the remainder of the 60 min protocol.

The exercise session is terminated at any point at which a mouse meets either of these exhaustion criteria:

1. Spending greater than 5 consecutive seconds on the shock grid without attempting to reengage the treadmill.
2. Spending greater than 50% of its time on the shock grid (in other words, it continues to go back to the shock grid repeatedly).
3. The third time a mouse is willing to sustain 2 seconds or more of shock without attempting to reengage the treadmill.

Following the 60 minutes run, mice were returned to their home cage, given access to food and water.

2.14. Sample preparation methods for mass spectrometry

2.14.1. Protein extraction – tissue homogenization and cell lysis

Frozen tissue was cryogenically grinded with mortar and pestle and then suspended in lysis buffer (4% SDS in 0.1 M Tris/HCl pH 7.6) completed with protease inhibitor cocktail (Roche cOmplete

tablets 1 tablet per 100 mL buffer) using a 1:10 (w/v) sample to buffer ratio. For complete cell lysis samples were heated for 10 minutes at 95°C. The homogenate was spun centrifuged at 16000 g for 10 minutes at room temperature. For immunoprecipitation experiments or complex muscle samples, the tissue was lysed using modified RIPA buffer completed with protease inhibitor cocktail (Roche cOmplete tablets 1 tablet per 100 mL buffer) using a 1:15 (w/v) sample to buffer ratio. The lysates were homogenized on a rotating wheel at 4°C for 30 minutes. Crude extracts were clarified by centrifugation at 15000 rpm at 4°C for 10 minutes. The lysis procedure was similar for SDS-PAGE or western blot.

2.14.2. Myofiber isolation

For the purpose of this experiment 8-12 weeks old Mettl21c$^{-/-}$ and littermate controls were used. Different muscles were isolated very carefully and placed in 0.2% collagenase solution (Collagenase P in DMEM) and incubated at 37°C. The incubation time was adjusted depending on the collagenase activity and on the size, age and muscle condition. To avoid over-digestion the muscle was checked regularly. To stop the digest, the muscles were carefully transferred to a Petri dish with prewarmed DMEM. To release the myofibers, the muscle was carefully pipetted using a large glass pipette. The fibers were washed with PBS and after a while of settling the supernatant was removed. After three repetitions the single fibers can be collected under a stereo microscope (Leica).

2.14.3. Determination of protein concentration

The determination of protein concentration was determined with the DC Protein assay according to the manufacturer's instructions using a FLUOstar galaxy spectrophotometer. It is based on the Lowry method [186] and is based on the principle of complex formation of proteins with copper ions at an alkaline pH. After this the aromatic amino acids in the sample reduce the phosphomolybdate phosphotungstic acid present in Folin Reagent. The amount of proteins can then be estimated via reading the absorbance at 750 nm from the end product of the Folin reaction against a standard curve of a Bovine Serum Albumin (BSA) solution.

2.14.4. In-solution digestion

Proteins in lysis buffer (SDS or RIPA lysis buffer) were precipitated for 1 hour using 4 volumes of ice-cold acetone at -20°C. Centrifugation at 15,000 rpm at 4°C for 10 minutes precipitated the

proteins. The protein pellet was washed with 90% ice-cold acetone and again centrifuged. The resulting protein pellet was dissolved in 6 M urea, 2 M thiourea, 10 mM HEPES, pH 8 and subjected to digestion in solution. Next, protein disulfide bonds were reduced with 10 mM dithiothreitol (DTT) for 30 minutes. This is followed by alkylation of free sulfhydryl groups of the cysteins with 55 mM iodoacetamide for 20 minutes in the dark. For the first digestion step LysC (Wako) (protein to LysC ratio = 100:1) was added for 3 hours, which cuts after lysine, which is used for samples containing Lys6 labeled proteins (from SILAC mouse). For any other samples, proteins were first digested with LysC under denaturing conditions. Then, the samples were diluted to 2 M urea with 50 mM ammonium bicarbonate (ABC), and sequencing-grade trypsin (Promega, Madison, WI) was added to the samples (protein to trypsin ratio = 100:1) overnight. For both digestion conditions proteolysis were carried out at room temperature. Digestions were quenched by acidification (Buffer C) and desalted with stop and go extraction tips (Stage Tips). Stage Tips were made in-house by stacking two layers of C18 material in pipette tips. Before loading the samples on the Stage Tips, they were activated with 20 µl 100% methanol, washed with Buffer B to elute any dirt from the C18 material and twice with Buffer A to remove any remaining acetonitrile from Buffer B. The digested peptides were then loaded onto the equilibrated C18 material. Centrifugation is at 2600 rpm for 2 (equilibration) and 4 (sample loading) minutes, respectively. Due to hydrophobic interaction, peptides bind to the C18 material. Finally, the Stage Tips were washed with 20 µl Buffer A and dried using a syringe. Stage Tips were stored at 4°C until elution for measurement at the mass spectrometer.

2.14.5. In-gel digestion

Protein mixtures were separated according their molecular weight by subjecting them to SDS-PAGE (4-12% NuPage BisTris Gel, Invitrogen) followed by Instant Blue Staining for 15 minutes on a shaker. After this the gel was washed twice with distilled water. Gel lanes were cut into equal pieces and digested in gel as described by Shevchenko et al. [187]. At first, the gel pieces were destained by incubating them twice with 100 µl 50 mM ABC solution for 20 minutes. Dehydration took place by incubating twice with 100 µl ethanol for 10 minutes, followed by drying using the SpeedVac for 5 minutes at 30°C. Proteins were reduced with 10 mM dithiothreitol (DTT) at 56°C for 45 minutes with shaking at 600 rpm in a Thermomixer. The free sulfhydryl groups were alkylated with 55 mM iodoacetamide (IAA) in the dark for 30 minutes. Following this, the gel pieces were washed with 100 µl 50 mM ABC for 15 min, dehydrated with 100 µl ethanol for 15 min, again washed with 100 µl 50 mM ABC for 15 min and dehydrated twice with 100 µl ethanol for 15 min. The dehydrated gel pieces were dried using SpeedVac for 5 min at 30°C. Then 50 µl 12ng/µl LysC or trypsin was added

to the gel pieces, which were incubated on ice for 15 min for swelling. Then 80 µl 50 mM ABC was added and the gel pieces were incubated at 37°C overnight. On the next day, generated peptides were extracted using an increasing acetonitrile (ACN) concentration. At first, to stop the enzymatic digestion the gel pieces were incubated with 100 µl 30% ACN / 3% trifluoroacetic acid (TFA) for 20 minutes. This is followed by twice with 100 µl 70% ACN for 20 min and then twice with 100 µl 100% ACN for 20 min. Collected peptide mixtures were concentrated by using a SpeedVac to ~80 µl and mixed with 80 µl Buffer C. Finally they were desalted using the stop and go extraction (STAGE) technique as described earlier.

2.15. Liquid Chromatography – Tandem Mass Spectrometry (LC-MS/MS)

2.15.1. The Q Exactive series mass spectrometers

The combination of a quadrupole mass filter with an Orbitrap analyzer called Q Exactive was introduced in 2011 [188]. Its ability to perform multiplexed operation at MS and MS/MS modes makes the Q Exactive to a highly efficient and fast mass spectrometer for complex proteomic analyses. Due to its fast switching times the Q Exactive is able to select the ions almost instantaneously, resulting from the fact that ions within a specified m/z (mass/charge) range have stable trajectories. The ions are fragmented in the HCD cell on a similar time scale.

The Q Exactive instrument is coupled to a nano electrospray ion source, where ions are formed under atmospheric pressure and transferred through a capillary into the S-lens. The ions pass the S-lens through an injection flatapole into a bent flatapole. The 2 mm gaps between the rods of the bent flatapole allow for clusters and droplets to fly unimpeded out of the flatapole. After the transmission through a lens they are brought into a hyperbolic quadrupole mass filter, which separates the ions of interest. On their way to the C-trap the ions pass through the quadrupole's exit lens and a split lens, which target the ion beam through an octapole directly into the C-trap, the ion storage device. The gas-filled HCD cell fragments multiple precursor ions by adjusting the offsets of the RF rods and the axial field resulting in collision energy. The ion population is transferred back into the C-trap and finally injected into the Orbitrap mass analyzer where they are detected. The ions are filled into the HCD cell and in parallel the ions from the previous detection cycle are being analyzed in the Orbitrap mass analyzer resulting in enhanced speed and quality of the spectra (Figure 7). Thereby, the cycle time in the Q Exactive instrument is achieved at the rate of 1 s for a top 10 HCD method. A doubling of the resolution of the spectra was obtained from the enhanced Fourier Transformation (eFT) algorithm [189]. All these advances in instrumentation

resulted in a compact, high performance quadrupole Orbitrap instrument with great analytical properties.

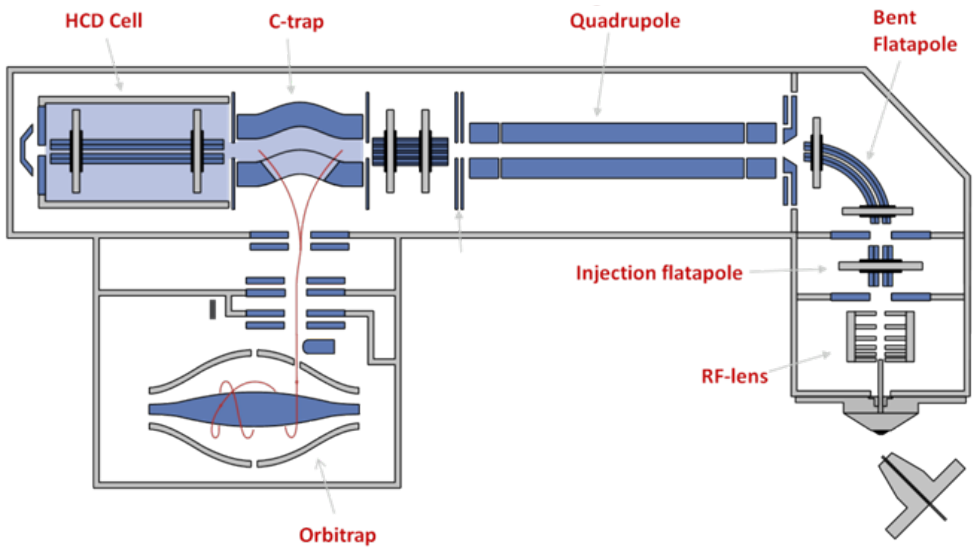

Figure 7. Construction of the Q Exactive. The ions are directed towards the S-lens, the bent flatapole, the mass selective quadrupole, the C-trap for ion storage, the HCD cell for fragmentation to the Orbitrap mass analyzer (the schematic representation was adapted from www.planetorbitrap.com).

Recently, the Q Exactive and the Q Exactive High Field (HF) mass spectrometers have emerged. The Q Exactive features an ultra-high-field Orbitrap analyser, resulting in a doubling of the spectra. It is built on the proven performance of the Q Exactive Plus series which features a low resolution mass filter incorporated within the injection flatapole so that unwanted ions do not enter deep into the instrument. Furthermore, they contain a segmented quadrupole resulting in enhanced isolation efficiency with a 2-fold improvement at narrow isolation windows and it uses a cycle time of 1 s for a top 15 to top 20 HCD method. These features make the Q Exactive Plus and Q Exactive HF instruments very stable systems with exceptional analytical performance for single-shot analysis of complex biological samples and post-translationally modified peptides [190].

Data dependent analysis on the quadrupole-Orbitrap and linear iontrap-Orbitrap mass spectrometers have proven to be leading in the field of MS-based proteomics, still most of the eluting peptides are not selected for fragmentation. Therefore, increasing sequencing speed would improve identification and quantification. The ultra-high-field Orbitrap analyzer doubles the sequencing speed at the same resolution like the Q Exactive Plus, resulting from a size reduction of the Orbitrap mass analyzer and thus leading to increased field strength [190].

2.15.2. Reversed phase liquid chromatography (LC)

For elution of the peptides from the Stage Tips 30 µl Buffer B was pipetted on the C18 material and incubated for 20 minutes. Following, the elution by pushing it through with a syringe into a 96-well plate and evaporating the acetonitrile by using a SpeedVac. The concentrated peptides (~2 µl) were resuspended in 10 µl Buffer A. A binary buffer system consisting of buffer A (0.1% formic acid) and buffer B (80% Acetonitrile, 0.1% formic acid) was used for peptide separation on an Easy nano-flow UHPLC system (Thermo Fisher Scientific). This system was coupled via a nano electrospray ionization source to the Q Exactive or Q Exactive Plus mass spectrometer. Peptide elution from the in-house packed 20/50 cm (1.8 µm Reprosil Pur Beads, 75 µm ID, Dr. Maisch Germany) column was achieved by increasing the relative amount of B from 7% to 38% in a linear gradient within 150 min or 240 min at a column temperature of 40°C. Followed by 5 min at 95% B and gradients were completed by re-equilibration time of 5 min to 5% B.

2.15.3. Tandem Mass Spectrometry (MS/MS)

Tandem Mass Spectrometry contains multiple stages of mass analysis, with some form of fragmentation occurring between the stages. Peptides are eluted via an increasing acetonitrile gradient from the C18 column and are then ionized by electrospray under atmospheric pressure (electrospray ionization, ESI). The nano-electrospray ion source sprays the peptides onto the transfer capillary of the Q Exactive mass spectrometer. The Q Exactive was operated in a data-dependent mode, where full MS scans (300-1750 m/z) were acquired by the Orbitrap. MS Spectra were recorded at 70,000 resolution (200 m/z, 3E6 ions as AGC target) within a maximum injection time of 20 ms. Acquisition of MS/MS spectra in a data-dependent mode after high collision induced dissociation (HCD) fragmentation (Top10) was carried out at 17,500 (200 m/z) in the highly accurate Orbitrap mass analyser using 1E6 as the AGC target and 60 ms for maximal injection time. Separation width was set to 1.7 m/z. A spray voltage of 1.8 kV and capillary temperature of 280°C were among the general settings applied. For mass accuracy the Q Exactive instrument was calibrated once in three days using LTQ Velos ESI positive ion calibration solution.

2.15.4. Data processing with MaxQuant

All acquired raw file were processed using the MaxQuant software versions 1.3.7.4 to 1.5.2.8 as well as the implemented Andromeda search engine. For protein identification HCD MS/MS Spectra were correlated and compared to the latest Uniprot mouse (Mus musculus) data set involving 74,265 protein sequence entries. An additional list of common contaminants was used, addressing

the filtering of those proteins. Searches were performed with tryptic or LysC specificity allowing two miscleavages and a mass range window of 4.5 ppm for MS spectra. For first MS/MS searches I allowed a mass range of 7 ppm and for main searches 4 ppm. Carbamidomethyl at cysteine residues was set as a fixed modification. Oxidation at methionine, acetylation at the N- terminus and lysine residues were considered as variable modifications. PSM (peptide spectrum match) and protein FDR (False Discovery Rate) were set to 0.01 and the minimal peptide length to 7 amino acids. For SILAC quantification the minimal ratio count was set to 2.

Perseus (version 1.4.1.3) and R package was used for following data analysis and visualization as well as the statistical environment R. Distance matrix for hierarchical clustering was computed by Pearson correlation and for clustering the average linkage method was used.

2.16. Molecular Biology

2.16.1. Concentration measurement of DNA and RNA

Determination of the concentration of nucleic acids was performed with the NanoDrop2000 photometer (Peqlab). Parameters: OD_{260}=1=50 µg/ml dsDNA, OD_{260}=1=40 µg/ml ssRNA. Sample solvent was used to calibrate the photometer.

2.16.2. Polymerase chain reaction, PCR

Polymerase chain reaction (PCR) was used for the amplification of double stranded DNA fragments with specific primers. The reaction always contains the following steps: denaturing of double stranded DNA, primer annealing, extension and final extension. For genotyping the following protocol was used. A 25 µl reaction with 2.5 µl PCR buffer, 1 µL 2 mM $MgCl_2$, 1µL 10 mM dNTP mix, 0.2 µl forward primers and 0.2 µl reverse primers, 0.2 µl 0.2 U Taq DNA polymerase, 2 µl DNA and MilliQ H_2O was performed in a thermocycler. The initial denaturating step (3 min, 95°C) was followed by 34 cycles with 30 s at 95°C (denaturing), 30 s 55°C (oligonucleotide annealing) and 1 min/kb, 72°C (extension). After the last cycle there was a final extension period for 5 min at 72°C. The reaction was then loaded on to an agarose gel where the separation of the DNA is based on size. A 1 kB DNA molecular mass standard (Invitrogen) was used as a reference.

2.16.3. Agarose gel electrophoresis

Agarose gel electrophoresis is used to separate DNA molecules by size when a current is applied. Based on the fact that the phosphate backbone of the DNA is negatively charged, the DNA fragments will migrate to the positively charged anode. According to the size of the DNA molecules, 1-2% agarose gels were prepared by melting the agarose powder in 1xTAE buffer in the microwave. By adding 5-10 µl ethidium bromide to the agarose solution DNA can be visualized under UV light. After the gel was polymerized in the gel chamber, the PCR reaction mixed with loading buffer was loaded on the gel and run for 30-40 minutes at 160 V. Finally the separated and ethidium bromide incorporated DNA fragments were visualized using an UV trans-illuminator. These fragments are either documented or excised with a scalpel and purified using the QIAquick Gel Extraction Kit (QIAGEN) following the manufacturer's instructions. The DNA was eluted with sterile water and the concentration was measured.

2.16.4. Amplification of the coding sequences of Mettl21c and Mettl21e from mouse cDNA using Phusion polymerase

RNA was isolated from mouse myoblasts (C2C12 cells) with the Trizol reagent and generated cDNA using the Superscript II Reverse Transcriptase according to the manufacturer's recommendations. The resulting cDNA was used as a template for Phusion amplification of the Mettl21 genes.

To facilitate subcloning of the Mettl21 genes from the pGemTeasy plasmid into the different expression plasmids, specific enzymatic restriction sites were introduced at the 5' and 3' end of the amplification product by primer design. For subcloning into the pcDNA5/TO and related plasmids BamH1 was used as a 5' restriction site, while Nde1 was chosen for targeting the pET26b(+) plasmid. For all constructs a Sla1 site was introduced at the 3' end. The coding sequences were amplified without stop codon. Phusion PCR (Finnzymes) amplification was performed in a 20 µl volume according to the manufacturer's recommendations using 3% DMSO and the following PCR protocol: 1-98°C-30sec, 2-98°C-10sec, 3-68°C-20sec, 4-72°C-30sec, 5-72°C-5min, repeat from 2-4 for 25 cycles.

2.16.5. Gel elution and A-tailing

The Phusion PCR product was mixed with 6x DNA loading dye and run on a 1% TAE agarose gel with ethidiumbromide (10 µg/ml) at 150 V. Then the size of the amplified band was checked using a UV table and then the band was excised with a scalpel and the DNA was eluted from the gel using the PCR clean up and Gel extraction Kit (Macherey-Nagel) according to the standard protocol. The PCR

product was eluted with 20-50 µl MilliQ H_2O and the concentration was determined using the Nanodrop photometer (Thermo Scientific).

For subcloning into the pGemTeasy plasmid a 3:1 ratio (plasmid:insert) was used. Since Phusion polymerase results in the amplification of blunt end fragments the corresponding amount of eluted PCR product was subjected to A-tailing prior to ligation. For A-tailing the gel purified PCR product was mixed with 3 µl of 10x Taq Polymerase buffer with $MgCl_2$, 1 µl 1 mM dATP, 1 µl Taq DNA Polymerase (5PRIME) and MilliQ H_2O was added to a final volume of 30 µl. The A-tailing mix was incubated for 30 minutes at 70°C and then cooled on ice.

2.16.6. Ligation in pGemTeasy and transformation in XL1Blue E.coli

For ligation of the Mettl21 genes into the pGemTeasy plasmid the 30 µl A-tailing mixture containing the gel eluted PCR products was mixed with 1 µl pGemTeasy plasmid (50 ng/µl), 5 µl 10x T4 DNA Ligation buffer, 2 µl T4 DNA Ligase and water to a final volume of 50 µl. The ligation was performed overnight in a temperature controlled heating block at 16°C.

The next day 5 µl of the ligation mixture was added to 35 µl MilliQ H_2O and 10 µl 5x KCM and cooled on ice. 50 µl competent XL1Blue E.coli were added and then incubated for 10 minutes on ice, for 20 minutes at room temperature and then 1 ml of LB-0 medium was added and the transformations were incubated for 1 hour at 37°C under shaking (650 rpm). Then the medium was removed (1000 g, 1 min, room temperature) and the transformed bacteria were plated on LB-agar plates containing the corresponding antibiotics (Ampicillin for pGemTeasy and pcDNA5/TO, Kanamycin for pET26b). The plate was incubated overnight at 37°C and transformants were analyzed by mini-DNA preparation and sequencing using the T7 sequencing primer for the pGemTeasy plasmids.

2.16.7. Subcloning the Mettl21 genes from pGemTeasy in the final expression plasmids

To generate tagged versions of the Mettl21 genes for the expression in mammalian cells, the following plasmids were used: pcDNA5/TO-Flag, pcDNA5/TO-HA, pcDNA5/TO-Myc plasmids. These plasmids contain a Flag-tag (amino acid sequence: DYKDDDDK), HA-tag (amino acid sequenceYPYDVPDYA) or Myc-tag (amino acid sequence: EQKLISEEDL) followed by a stop codon (5'-TGA). The tag-stop sequences were cloned into the pcDNA5/TO plasmid using the Xho1 (5') and Xba1 (3') restriction sites downstream of the multiple cloning site. This insertion results in a C-terminal tagging of the protein of choice. For bacterial expression of Mettl21 the pET expression system and the pET-26b(+) plasmid (Novagen) was used.

The subloning was done by enzymatic digestion of the pGemTeasy plasmids containing the Mettl21 genes with either BamH1/Sla1 or Nde1/Sla1 flanking restriction sites and the corresponding target plasmids. In general 1 µg of plasmid was digested with 1 µl enzyme 1, 1 µl enzyme 2 and 5 µl of the corresponding 10x buffer in a total volume of 50 µl for 4 hours at 37°C.

2.16.8. Mutation of the methyltransferase domains of Mettl21c and Mettl21e

Coding sequences of the Mettl21 genes:

Mettl21c coding sequence (NM_001013799): 747 bp length

ATGGATCAGCATCTCCACATAGCCCAGCAGCCCCTACTCTCGGGGACTCCACAGGAAGATGGTTTTGCAGGA
CCCTCAGTAGAGTTCGACAGGATAGAATCATCTCTTCGTAGCATCCAGAAATTTGTTCCTACAGACTATGCCA
GCTACACACAAGAGCATTATCAGTTCGCAGGCAAGAAGATCATCATTCAAGAATCCATTGAGAACTATGGCA
CAGTGGTGTGGCCAGGGGCTACAGCTCTGTGTCAATATTTAGAAGACCATACAGAGGAATTAAATCTCCAAG
ATGCTAAA**ATA**CTT**GAAATTGGTGCTGGAGCAGGC**CTTGTTTCCATTGTATCCAGTCTTTTAGGAGCTCAAG
TCACAGCAACAGACCTGCCTGATGTTCTAGGAAATCTTCAATACAATATTTTAAAAAACACACTAGAATGCAC
AGCTCATCTACCTGAAGTGAGAGAACTGGTATGGGGGGAAGACCTGGAGCAGAGCTTCCCTAAGTCAACCT
GTTGTTATGACTACGTGCTGGCCTCTGATGTTGTCTACCACCACTACTTCCTGGACAAGCTGCTCGCTACCAT
GGTGTACCTTTCCCAGCCAGGCACTGTGGTGCTGTGGGCAAACAAATTCAGATTTAGTGCTGACTATGAATT
TTTAGGTAAGTTTAAGCAAGCCTTTGATACCACTCTCTTGGCTGAATATTCAGAATCATCTGTCAAGCTGTTTA
AAGGGATATTAAAGTGGGAGTGA

Mettl21e coding sequence (NM_207281): 735 bp length

ATGGACCTCACAGTAACTCACATTACTCACAAAGAGACCTACAAAGAGCCCAGAGACGATGATGATGACAA
GCAGGTGGTCGCAGAGATCATGGCAAGAAGTTTTATCCCAACTCTGATAACGACTATTCCTTGGGAAGGCTT
TCACTTTGCTGGTCATGAGATTCAGATTACTGAAGGCAAAGATTGCTATGGTGCATTTGTCTGGCCATCGGCC
CTTGTTCTATGCTATTTTCTGGAAACACATGCCAAGCAATATAACATGGTTGATAAAAATGTGATT**GAAATTG
GAGCTGGGACAGGG**CTTGTCTCCATTGTGGCAAGCTTACTTGGTGCTCGTGTGATTGCTACAGACTTACCTG
AATTACTTGGAAACCTGCAATATAATATTTCCAGAAACACCAAAATGAAATGCAAGCATCTGCCTCAGGTCA
AAGAACTATCCTGGGGAGTAGCATTAGACAGGAATTTCCCCAGGTCTTCCAATAACTTTGACTACATCCTGGC
AGCAGATGTTGTCTATGCCCATCCGTTCCTGGAGGAGCTTCTCATGACCTTTGACCATCTCTGCAAAGAAACT
ACCATTATACTCTGGGCTATGAGATTCAGGCTGGAGAAAGAAAATAAATTTGTAGATAAATTTAAGGAACTG
TTTGACCTGGAAGAAATTTCTAGTTTCCCTAGCCTGAATATTAAGTTGTACAAAGCTATGAAGAAAAATCGGA
GGAGTGCCTAG

Enzymes that are not cutting in this sequence and therefore can be used for the cloning process were determined with the "NEBcutter"-software: BamH1, XhoI/SlaI, and Nde1.

2.16.9. Methyltransferase domain mutation with site-directed mutagenesis

A methyltransferase domain (conserved in Motif 1) has the following consensus motif 1: (oEoGoGoG). Since the mutation of glycins in this domain is known to impair/abolish SAM binding, I mutated the three glycins into alanins using site-directed mutatgenesis PCR. First, Clustal W alignment showed that the glycin residues of the putative methyltransferase domains of both, Mettl21c and Mettl21e, are highly conserved.

Q8BLU2 Mettl21c 248 amino acids

MDQHLHIAQQPLLSGTPQEDGFAGPSVEFDRIESSLRSIQKFVPTDYASYTQEHYQFAGKKIIIQESIENYGTVVWP
GATALCQYLEDHTEELNLQDAK**ILEIGAGAG**LVSIVSSLLGAQVTATDLPDVLGNLQYNILKNTLECTAHLPEVREL
VWGEDLEQSFPKSTCCYDYVLASDVVYHHYFLDKLLATMVYLSQPGTVVLWANKFRFSADYEFLGKFKQAFDTTL
LAEYSESSVKLFKGILKWE

Q8CDZ2 Mettl21e 244 amino acids

MDLTVTHITHKETYKEPRDDDDDKQVVAEIMARSFIPTLITTIPWEGFHFAGHEIQITEGKDCYGAFVWPSALVLC
YFLETHAKQYNMVDKNV**IEIGAGTG**LVSIVASLLGARVIATDLPELLGNLQYNISRNTKMKCKHLPQVKELSWGV
ALDRNFPRSSNNFDYILAADVVYAHPFLEELLMTFDHLCKETTIILWAMRFRLEKENKFVDKFKELFDLEEISSFPSL
NIKLYKAMKKNRRSA

For site-directed mutagenesis of the methyltransferase domains in Mettl21c and Mettl21e I used the oligonucleotides, which have alanine codons instead of the three central glycine codons.
For the mutagenesis reaction the Agilent Pfu Polymerase AD was used with the following reaction mixture: Primer fw (10 pmol/µl) 0.64 µl, Primer rev (10 pmol/µl) 0.64 µl, 10x Buffer 2.5 µl, dNTPs (10 mM) 0.5 µl, Pfu AD Polymerase 0.5 µl, plasmid template (10 ng/µl of the pGemTeasy Mettl21c or Mettl21e plasmids, respectively) 1 µl. The PCR was run with the following PCR program: 1-95°C-1min, 2-95°C-30sec, 3-annealing Tm-5°C-30sec, 4-72°C-1min per kilobase, 5-72°C-10min, repeat from 2-4 for 20 cycles.
5 µl of the mutagenesis PCR mixture was analyzed on a 1% TAE agarose gel. The residual 20 µl were precipitated with 80 µl MilliQ H_2O, 100 µl 4M NH_4Acetate and 400 µl Isopropanol (15 min incubation at room temperature and 15 min precipitation at max speed in the centrifuge). The

pellet was washed with 70% ethanol and precipitated again for 5 min at maximum speed. The pellet was dissolved in 13 µl water and 1.5 µl Jena Buffer B2 was added with 0.5 µl Dpn1 enzyme. The template DNA plasmid was digested for 4 hours at 37°C. Then 5 µl of this mixture was subjected to transformation (+ 35µl MilliQ H_2O, 10 µl 5x KCM) in E.coli XL1 blue and analyzed by miniprep and sequencing.

2.16.10. Chemical competent bacteria

After growing 10 µl of an *E.coli Xl1Blue* cryostock in 1 ml LB medium for 1 hour at 37°C with 700 rpm shaking, the cells were plated on a LB agar plate without antibiotics (LB-0) and incubated over night at 37°C. On the next day 5 ml LB-0 medium was inoculated with a single bacteria clone and incubated over night at 37°C shaking with 200 rpm. Next morning, 5 ml of the culture is transferred to 100 ml LB-0 and incubated for 1 hour at 37°C until the OD_{600} reached a value of 0.5-0.6, which resembles the logarithmic phase. Subsequently, the bacteria are harvested by centrifugation at 2500 g at 4°C for 15 minutes and then resuspended in 7.5 ml TSB buffer. This suspension was incubated on ice for 1 hour. Afterwards aliquots of 110 µl bacterial suspension were snap frozen in liquid nitrogen and stored at -80°C. Test transformations were performed to test the chemical competence.

2.16.11. Plasmid DNA isolation

For analytical plasmid isolation (Mini-prep) a small-scale mini preparation (from 5 ml bacterial culture) and for preparative plasmids isolation (Maxi-prep) a large-scale preparation (200 ml bacterial culture) was used. LB-medium containing 100 µg/µl selective antibiotics was inoculated with a bacteria clone from an agar plate and incubated overnight (14-16 hours) at 37°C with shaking at 200 rpm.

For the Mini-prep the bacteria overnight culture was pelleted by centrifugation for 5 minutes at 14000 g. Optional a glycerol stock was kept by mixing 225 µl glycerol/1xTE and 500 µl of the overnight culture which can then be stored at -80°C. To break the cells the pellet was resuspended with 150 µl Miniprep Solution A containing RNase and incubated for 10 minutes at room temperature.

Induction of alkaline lyses of the genomic DNA resulted from the addition of 200 µl Solution B for 10 minutes. Then 175 µl Solution C was added for neutralization and incubated on ice for 10 minutes. After centrifugation at 14000 g for 10 minutes at 4°C the supernatant was transferred into a new tube containing 500 µl isopropanol. This is followed by precipitation of the DNA by centrifugation for 20 minutes at 20000 g at 4°C. By using 500 µl 70% ethanol the DNA pellet was

washed, subsequently air dried and resuspended in sterile water. The plasmid concentration as well as the quality was determined using Nanodrop2000 Spectrophotometer.

For the Maxi-prep of plasmid DNA NucleoBond Xtra Maxi Kit was used following the manufacturer's instructions.

2.16.12. Sequencing of DNA

Sequencing of plasmids is based on the chain termination method by Sanger and was performed by the company Seqlab in Göttingen. A mixture of 7 µl of DNA solution with a concentration of ~200 µg/ml with 1 µl sequencing primer (10 pmol/µl) was submitted for sequencing.

2.17. Morphological and immunostaining methods

2.17.1. Immunofluorescence

C2C12 cells were cultured on coverslips and transfected with Flag-tagged Mettl21c and control plasmid (empty vector with Flag-tag) for 24 hours, fixed with 4% paraformaldehyde for 10 minutes, permeabilized with 0.1% Triton X-100 in Phosphate-buffered saline (PBS) for 10 minutes and stained with anti-Flag antibody for 1-2 hours at RT. Alexa dye conjugated secondary antibodies were purchased from Life Technologies. Nuclear counterstaining was done with DAPI (4',6-diamidino-2-phenylindole), which emits blue fluorescence upon binding to AT regions of DNA. The coverslips were mounted in Mowiol 4-88 Reagent. Imaging was performed with a Zeiss Axioimager Z1.

2.17.2. Immunohistochemical stainings

All muscle immunolabeling experiments started with embedding the muscle tissue in Optimal Cutting Temperature compound (OCT, Tissue-Tek® O.C.T.Polyfreeze™) media prior to frozen sectioning. The muscle was positioned in liquid OCT avoiding any air bubbles and then immersed in isopentane (2-methyl-butan), which was cooled down by liquid nitrogen. Frozen tissue was stored in the -80°C freezer.

The muscles were then cut into 10-20 µm thick sections on a cryostat (-25°C) and mounted on lysine coated slides (Superfrost). The slides were air dried for 1 hour before freezing (-20°C) or staining the slides.

On the day of immunostaining the slides were allowed to reach room temperature for 30 minutes before 4% paraformaldehyde/Desoxycholate/NP40 fixation for 5 minutes. This is followed by proteolytic digestion with 0.02% pepsin in 0.2 N HCl for about 1.5 minutes. After several washing

steps in PBS, pH 7.4 the slides were incubated with blocking solution (2% BSA, 0.5% NP40, 3% Horse Serum) for 45 minutes. Followed by primary antibody incubation overnight at 4°C in a wet chamber.

When performing serial sectioning one slide per sample was incubated with anti-MyHC slow antibody (1:450 dilution) and the other one was incubated with anti-MyHC fast antibody (1:900 dilution). A third serial section slide was stained for X-Gal to detect the LacZ activity.

The following day, sections were rinsed three times with PBS and incubated with biotinylated second antibody in blocking solution for 1 hour at room temperature. Slides were again rinsed three times with PBS. After this it was incubated with the VECTASTAIN® Elite ABC Staining solution for 1 hour, which functions with an advanced avidin/biotin technology and allows sensitive binding to biotinylated targets. The avidin-peroxidase complex is formed by mixing 2 droplets of Reagent A (Avidin DH) and Reagent B (biotinylated peroxidase H) in PBS with 0.1% Tween20 (PBT). For detection of the antibody-stained sections DAB (3, 3'-diaminobenzidine) as a HRP substrate was used and incubated for about 2-5 minutes at room temperature under constant supervision under the microscope. One tablet DAB (10 mg) was diluted in 17 ml PBT und activated with 1 µl 30% H_2O_2 in 1 ml PBT. DAB produces a dark brown reaction product. Finally, the stainings are rinsed three times with PBT and then mounted in Mowiol 4-88 reagent.

2.17.3. X-Gal staining of mouse tissues

Mettl21c deletion mutants (8 weeks) were euthanized by cervical dislocation. Skeletal muscles were isolated, washed with PBS and then placed in X-Gal fixation solution (Sodiumphosphate buffer pH 7.4, 25% GDA, 1M MgCl, EGTA pH 7.5) for 5 minutes. After rinsing several times with X-Gal washing solution (Sodiumphosphate buffer pH 7.4, 2% NP40, 1M MgCl, 1% Na-desoxycholat) for 10 minutes, the pups were incubated in the X-Gal staining solution (X-Gal washing solution, 0.5 M K3FeCN6, 0.5 M K4FeCN6, 0.1% X-Gal) overnight protected from light with gentle shaking. The next day, the skeletal muscles were washed three times and stored at 4°C until the clearing.

2.17.4. Clearing of stained muscle tissues

The X-Gal stained skeletal muscles were cleared in Cedar Wood Oil. First they were dehydrated through graded ethanol steps up to 100% and then placed in Xylene-Ethanol (1:1) mixture for 1 hour up to 1 day. Finally, the skeletal muscles were transferred to high quality cedar wood oil and gently rocked until the desired clearance was achieved. The cedar wood oil was replaced once. The imaging of the whole mount mouse skeletal muscles was carried out using a 6 cm dish with a 0.5%

agarose layer and a stereomicroscope. The skeletal muscles were placed onto the dish and covered with 1xPBS and imaged using the AxioVision3.1 software.

2.17.5. X-Gal staining on cryosections

The beta-galactosidase activity on cryosections of postnatal and adult tissues was detected using X-Gal staining. The cryosections of OCT embedded tissues were placed in a glass cuvette with X-Gal fixation solution for 5 minutes and then immediately treated with washing solution three times for 5 minutes. Staining was then carried out for 1 up to 12 hours in the X-Gal staining solution. Thereafter, the sections were washed again 3 times for 5 minutes, then mounted in Mowiol 4-88 Reagent and stored at 4°C until imaging at a Zeiss Axioimager Z1.

2.17.6. Haematoxylin/Eosin (H&E) staining

H&E staining is a widely used histological method that allows visualizing different tissue structures. It contains the two dyes haematoxylin and eosin. Eosin is an acidic dye, which stains basic or acidophilic structures like cytoplasmic structures and connective tissue red or pink. Haematoxylin is considered a basic dye, which stains acidic or basophilic structures such as DNA and RNA in a purplish blue.

The cryosections were treated with hematoxylin (Mayers heamalaun) for 10 minute and after that with tap water. Subsequently, samples were treated with eosin for 6 minute and after that with tap water. Then they were dehydrated in 95% and 100% ethanol series for 2 minutes, each. Finally, they were washed in xylol for 2 times 5 minutes and mounted in Mowiol 4-88 reagent.

2.17.7. Masson's Trichrome Staining

Masson’s Trichrome staining consists of Weigert’s iron hematoxylin, which stains the nuclei in black, Biebrich scarlet-acid fuchsin, which stains cytoplasm and muscle fibers in red and after treatment with phosphotungstic and phosphomolybdic acid, collagen is stained in blue with aniline blue. Briefly, slides are fixated with 4% PFA at room temperature for 15 minutes. Slides are placed in Weigert’s iron hematoxylin for 10 minutes, rinsed in running water for 10 minutes, placed in Beibrich scarlet-acid fuchsin solution for 15 minutes, and rinsed until clear. Then the slides are placed in phosphomolybdic-phosphotungstic acid solution for 15 minutes, followed by aniline blue solution for 20 minutes, rinsed, and then placed in 1% acetic water for 5 minutes. Finally, the slides are dehydrated and protected with cover slips, mounted using Mowiol 4-88 reagent.

2.17.8. Lectin staining

After fixation with 4% PFA at room temperature for 15 minutes and washing with PBS 3 times for 5 minutes, the slide were incubated for 1 hour in moist chambers in the dark with the FITC-conjugated lectins diluted to 0.05 mg/ml in PBS. The slides were then washed in PBS and mounted in Mowiol 4-88 reagent and photographed in a fluorescence microscope.

2.18. Biochemistry methods

2.18.1. SDS Polyacrylamide Gel Electrophoresis (SDS-PAGE)

For electrophoretic separation by means of their molecular size protein samples were diluted with lysis buffer and 1xLDS protein sample loading buffer. The samples were heated at 70°C for 10 minutes to denature the proteins for SDS binding. The samples were loaded on 4-12% Bis-Tris Gels and run with MOPS buffer at 180 V for 50 minutes.

2.18.2. Immunoprecipitation

Cells or tissues were lysed in RIPA buffer supplemented with protease inhibitors (1:100 v/v) and incubated on a rotating wheel for 30 min at 4°C. The crude lysates were cleared by centrifugation at maximum speed for 10 min at 4°C. Protein concentration was measured using the Bio-Rad DC protein assay and typically 500 µg lysate was used for immunoprecipitation. A pre-clearing step with 30 µl Sepharose G beads was performed for 30 min. Beads with unspecific protein binding were removed by centrifugation at 2000g for 2 min at 4°C and the supernatant was incubated with 5-10 µg antibody (for analysis with mass spectrometry) or 2 µg (for analysis with western blot) on a rotating wheel for 30 min at 4°C. Subsequently, fresh 30 µl Sepharose G beads were added and incubated overnight on a rotating wheel. While using antibody coupled to beads, this was added directly after the pre-clearing step. On the next day, beads with bound proteins were washed 3-4 times with RIPA buffer by centrifuging at 2000 g for 2 min at 4°C each time. Proteins were then eluted from the beads by heating with 1.5x Laemmli buffer and 40 mM DTT for 10 min at 70°C.

2.18.3. Western blotting

Proteins eluted from immunoprecipitated beads or otherwise 20-40 µg proteins (heated with 1.5x Laemmli buffer and 40 mM DTT for 10 min at 70°C) were loaded on a 4-12% Bis-Tris gel and separated using SDS-PAGE, which was run using MOPS buffer at 180 V for 50 minutes. Subsequently, proteins were transferred from the gel to a nitrocellulose membrane sandwiched between two Whatmann papers at 35 V for 2 hours. Transfer buffer was used in the inner chamber

and water with ice in the outer chamber to maintain the system at low temperature. Following the transfer, the membrane was stained using Red Alert for 5 min on a shaker and the excess stain was then washed with MilliQ water to visualize the protein bands. The membrane was washed with TBS-T buffer on a shaker for complete removal of the stain and then blocked with 5% BSA or 5% non-fat dry milk in TBS-T for 1 h at room temperature on a shaker. Following blocking, the membrane was incubated with primary antibody diluted in blocking buffer at 4°C overnight with gentle shaking. On the next day, the membrane was washed 5 times for 5 min with TBS-T with rigorous shaking to remove any unbound primary antibody. The washed membrane was incubated with horseradish peroxidase-coupled secondary antibody diluted in blocking buffer for 1 h at room temperature with gentle shaking. The membrane was washed 5 times with rigorous shaking to remove any unspecific binding of secondary antibody. Antibody-bound proteins were detected on a VersaDoc using enhanced chemiluminiscence method with an equal proportion of peroxide solution and luminol enhancer.

2.18.4. In vitro methylation assay

In vitro methylation assays are used to determine the specificity of PKMT and to discover new PKMT substrates. The analysis of protein methylation was performed in vitro using an immunoprecipitated Mettl21c in the presence of selected substrates.

The methyltransferase Mettl21c, its family member Mettl21e and the substrates Valosine-containing protein (VCP, p97), Sequestosome (Sqstm1, p62) are immunoprecipitated from overexpressed HEK 293T cells or C2C12 cells. In a 1.5 ml Eppendorf tube the beads with the immunoprecipitated substrate, 2 mM S-adenosylmethionine (stock solution 32 mM), 25 µl Methyltransferase buffer and H_2O up to 50 µl are mixed. The methylation reaction is initiated with beads that carry the immunoprecipitated Mettl21c-Flag. The reaction is mixed gently by tapping and then incubated at 37°C for 30 minutes. To stop the reaction 1xLDS protein sample loading buffer was added and heated at 70°C for 10 minutes. The sample was run on a 4-12% SDS-PAGE gel at 180 V for 50 minutes using MOPS running buffer. The separated samples are then subjected to in-gel digest and the peptides are measured on the Q Exactive mass spectrometer.

2.19. Cell culture methods

2.19.1. Maintenance of cell lines

Human embryonic kidney (HEK) 293T cells and C2C12 cells were cultured in high glucose Dulbecco's Modified Eagle's Medium (DMEM) containing 4.5 g/L glucose. The medium was

supplemented with 10% Fetal Bovine Serum (FBS) and 1% Penicillin-Streptavidin-L-Glutamine (PSG). The incubator was maintained at 37°C and with 10% CO_2. Confluent cells in 10 cm dishes were washed once with 5 ml PBS and treated with 1 ml trypsin-EDTA for about 2 min to allow detachment of cells. Standard cell culture medium containing FBS was added to stop the activity of trypsin. Cells were split 1:3 or 1:6 for HEK or C2C12 respectively, for experiments on the next day.

2.19.2. SILAC labeling

Cells were labeled by culturing in SILAC DMEM medium containing high glucose of 4.5 g/L and supplemented with 10% dialyzed FBS and 1% PSG. Additionally, L-lysine (Lys0) and L-arginine (Arg0) were supplied to the 'light' medium, 4,4,5,5-D_4-L-Lysine (Lys4) and $^{13}C_6$-labeled L-arginine (Arg6) were supplied to the 'middle' medium, and $^{13}C_6$ $^{15}N_2$-labeled L-lysine (Lys8) and $^{13}C_6$ $^{15}N_4$-labeled L-arginine (Arg10) were supplied to the 'heavy' medium. The concentrations of lysine and arginine used were 84 g/L and 147 g/L respectively. Cells were cultured for 5 passages to ensure complete labeling.

2.19.3. Cell storage

Cells were washed with PBS, trypsinized and pelleted by centrifugation at 1500 rpm for 5 min. The cell pellet was frozen in 90% FBS and 10% DMSO. Cells obtained from a confluent 10 cm dish were frozen as two aliquots and stored at -80°C over the first night. On the next day, frozen cell stocks were transferred to a liquid nitrogen tank maintained at -180°C for longer storage. Frozen cells were recovered by thawing, resuspending in the culture medium and centrifuging to remove DMSO.

2.19.4. Calcium phosphate transfection

Calcium phosphate transfection method was used for HEK 293T cells. For transfection of a 10 cm dish, 10 µg plasmid was precipitated in 61 µl 2M $CaCl_2$ and filled up to 500 µl with sterile water. This mixture was added to 500 µl 2x HEPES buffered saline (HBS) and mixed. The 1 ml transfection reagent was added as drops onto the cells carefully. Cells were maintained in the transfection medium for 24 hours.

2.19.5. Transfection with TurboFect

TurboFect transfection reagent was used for transfection of C2C12 myoblasts. To transfect a 10 cm dish, 10 µg plasmid was diluted in 1 ml reduced serum Opti-MEM medium after which 20 µl

TurboFect transfection reagent was added and vortexed thoroughly. This mixture was incubated at room temperature for 20 min and carefully added to the cells as drops. Cells were maintained in the transfection medium for 24-36 hours.

2.19.6. Induction of autophagy in cell culture

C2C12 and HEK 293T cells were cultured on 6 well plates and transfected for 24 hours with Mettl21c-Flag plasmid or control plasmid (empty plasmid with Flag-tag), respectively. For the induction of autophagy Rapamycin (through inhibition of TORC1) was used. Cells were incubated for 5 hours with 1 µM Rapamycin and in the last hour 100 nM Bafilomycin A1, which inhibits the lysosomal $Na^{+}H^{+}$ ATPase, thereby preventing the activity of lysosomal acid proteases. This leads to accumulation of autophagosomes and the autophagic flux can be measured.

2.20. Deep Sequencing

Differences in the transcript levels were analyzed by deep sequencing, which was done by the in-house core facility. Next generation sequencing was performed on the Ion Torrent Proton sequencing platform (Thermo Fisher) using the Ion Total RNA-Seq Kit v2 (Thermo Fisher) with minor modifications. Total RNA for transcriptome analysis was isolated with miRNeasy micro Kit (Qiagen) from individual soleus muscles with on column DNAse treatment (RNase free DNase Set, Qiagen). Homogenization of samples before lysis was done on bead mill (Retsch, MM301) for 4 minutes at room temperature. Integrity of RNA was checked on Bioanalyzer 2100 (Agilent) and 2 µg of RNA with RIN >8.7 was used for ribosomal depletion using the Ribo Minus Kit (Thermo Fisher). Following modifications to the standard RNA-seq Library protocol were performed: Fragmented RNA was concentrated to 3 µl with SpeedVac (Eppendorf) for 10-15 minutes and all 3 µl were used for further steps. Numbers of amplification cycles were reduced to 10-12 cycles resulting in lower PCR duplication levels without any influence to quality/contribution of obtained reads. Obtained RNA libraries were diluted to 100 pM and used in a final concentration of 9 pM for template preparation on Ion OneTouch2 instrument (Thermo Fisher). For each run on the V2 Ion Torrent Chip 2 RNA libraries were pooled in equimolar ratios to obtain between 27-52M reads per sample.

2.21. Electron microscopy of muscles

Electron microscopy analysis of mouse muscles was performed in collaboration with PD Dr. Sawa Kostin, Max-Planck-Institute for Heart and Lung Research in Bad Nauheim. After pre-fixation of the whole mouse by perfusion with 3% glutaraldehyde buffer, the soleus muscles were prepared and

fixed directly after preparation in 3% glutaraldehyde buffer at room temperature. The fixative was removed by 6 times washing in 0.1 M sodium cacodylate buffer. Then the tissues were incubated for 1 hour with 1% osmium tetroxid/0.1 M cacodylate buffer, washed 3 times 10 minutes in water, dehydrated for 30 minutes in serial ethanol dilution 10%, 30%, 50% with following incubation in 1% uranyl acetate/70% ethanol for 1 hour. Uranil acetate was removed by washing in 70% ethanol overnight. Further dehydration of sections was performed in 70%, 90% and twice in 100% ethanol for 30 minutes in each solution. After dehydration the samples were infiltrated with epoxy resin, ethanol:SPURR=3:1 for 3 hours; epoxy resin, EtOH:SPURR = 1:1 for 4 hours, overnight with epoxy resin; EtOH:SPURR = 1:3 and twice 8 hours in pure SPURR, which polymerizes finally. The blocks were sectioned with an ultramicrotome. The sections were placed on copper grids. Muscle cells were visualized using a transmission electron microscope (Philips CM 10 electron microscope).

3. Results

3.1. Bioinformatics and structural analysis of Mettl21c identifies conserved SAM binding domains and a methyltransferase domain

The putative Class I MTase Mettl21c (Methyltransferase-like 21c) was originally identified in a previous study by Drexler et al., which examined the distribution of proteins in fast and slow muscles. Sequence alignment on protein level revealed for Mettl21c a similarity of 20-40% to a small group of methyltransferases namely Mettl21a-e. This protein group represents a small subfamily of the ten human Methyltransferase 16 (MTF16) enzymes and belongs to the class-I-like SAM binding methyltransferase superfamily, which utilize the ubiquitous methyl donor S-adenosylmethionine (SAM). The Mettl21 family is structurally highly conserved and consists of central seven beta-strands, five alpha helices and four distinct motifs for SAM binding. The SAM binding site is conserved in the primary sequences of four short signature motifs designated Motif 1, Motif Post 1, Motif 2 and Motif 3 [3]. Spacings in the primary sequence between the motifs are variable, but often conserved. Structurally, the motifs can be classified: Motif 1 contains the first conserved beta-strand (β1) and the following loop, Motif Post 1 consists of the second beta-strand (β2), Motif 2 corresponds the fourth beta-strand (β4), and Motif 3 includes the fifth beta-strand (β5) and the alpha-helix preceding it [191]. Of note, a hallmark of the MTF16 protein family is a distinct DXXY motif [(D/E)-X-X-(Y/F)] located after Motif 2, probably important for the positioning of the methyl group donated by SAM in the methylation reaction [149]. The first motif GxGxG at the end of the first beta-strand is a characteristic of a nucleotide-binding site and hence binds the cofactor SAM. Mettl21c contains 248 amino acids and the methyltransferase domain ranges from amino acid 52 to 232. Besides the presence of a nuclear localization sequence with a score of 5 on Mettl21c (http://nls-mapper.iab.keio.ac.jp/cgi-bin/NLS_Mapper_form.cgi; Score: 5 indicates that it may be possibly located in both the nucleus and the cytoplasm), the mass spectrometric measurements revealed newly identified mono- and dimethylation sites that were not previously indicated on phosphosite.org (Figure 8).

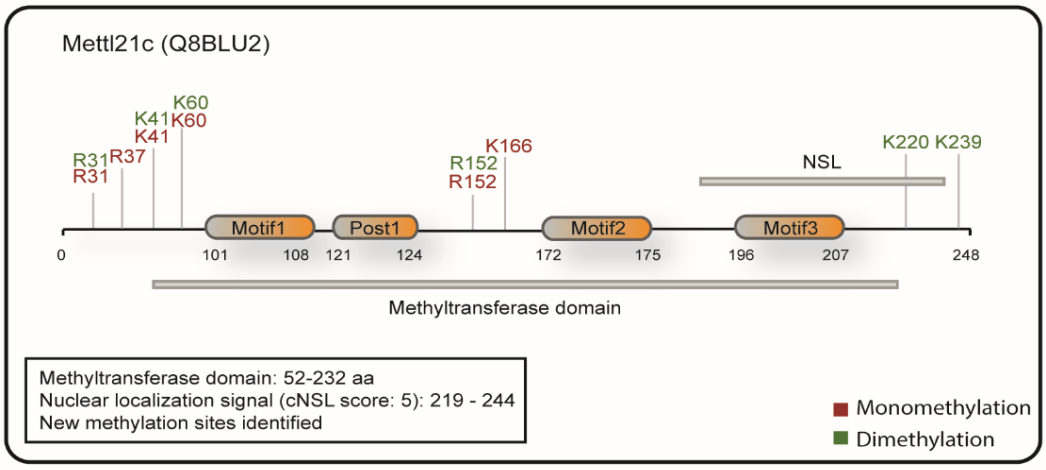

Figure 8. Sequence landscape of Mettl21c consisting of 248 amino acids, displaying four distinct motifs (Motif 1, Motif Post 1, Motif 2 and Motif 3) and indicating the methyltransferase domain, the nuclear localization signal (cNSL score: 5) and the newly identified mono- and dimethylation sites (not previously indicated on phosphosite.org).

In order to identify orthologues of Mettl21c a BLAST search was performed resulting in the identification of several Mettl21c orthologues in different species such as insects, plants and fungi. The four highly conserved motifs are highlighted in the sequence alignment (

Figure 9) and also the characteristic DXXY motif can be found in all species.

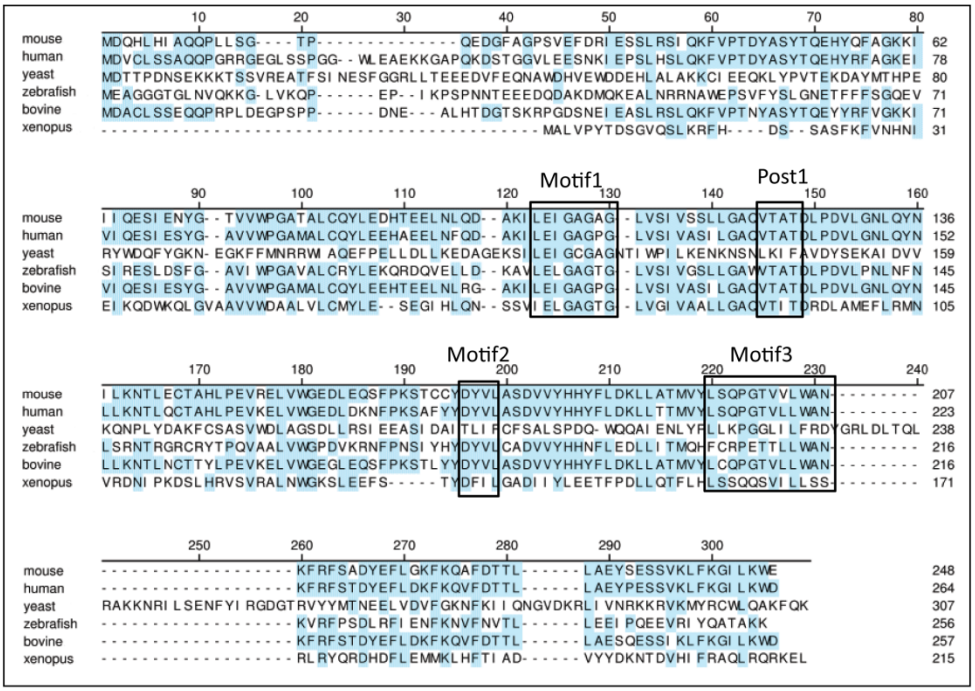

Figure 9. Sequence alignment of Mettl21c (Q8BLU2) shown for the closest homologues in human (Q5VZV1), yeast (Q9P7L6), zebrafish (B7ZVT8), bovine (A6QP81), xenopus (A4IGU3) and showed the four highly conserved methyltransferase motifs (Motif 1, Motif Post 1, Motif 2 and Motif 3).

This initial bioinformatic analysis reveals that Mettl21c belongs to the seven beta-strand MTase family and is present in a wide range of multicellular eukaryotes.

3.2. Characterization of the Mettl21c$^{-/-}$ mouse

To characterize the function of the mammalian Mettl21c more in detail, we inactivated Mettl21c by homologous recombination in mice. The mouse Mettl21c gene is located on Chromosome 1 and spans five exons over a genomic region of 10.6 kb. The resulting mRNA transcript has 1086 bp and the ATG start codon is localized at the beginning of exon 2. For inactivation of Mettl21c, the ZEN-UB1 velocigene cassette was used. It contains the beta-galactosidase coding sequence from E.coli (LacZ Gene) and a polyadenylation signal. In addition, the promoter of human ubiquitin C genes together with the neomycin phosphotransferase and a polyadenylation signal flanked by loxP sites were used for positive selection (Figure 10). The vector was purchased from velocigene (http://www.velocigene.com/komp/detail/15237). The construct was inserted by electroporation into ES cells and successful homologous recombination into the Mettl21c locus was tested by Taqman PCR to detect the mutation. Next, positive ES cell clones were used for injection into blastocysts to generate chimeric animals. The generation of ES cells and the transgenic mice were performed by the laboratory of Professor Braun and the central animal facility of the Max-Planck-Institute in Bad Nauheim. Chimeric mice were mated with cre-deleter mice, which express the cre-Recombinase in the germ line to eliminate the neomycin-resistance cassette.

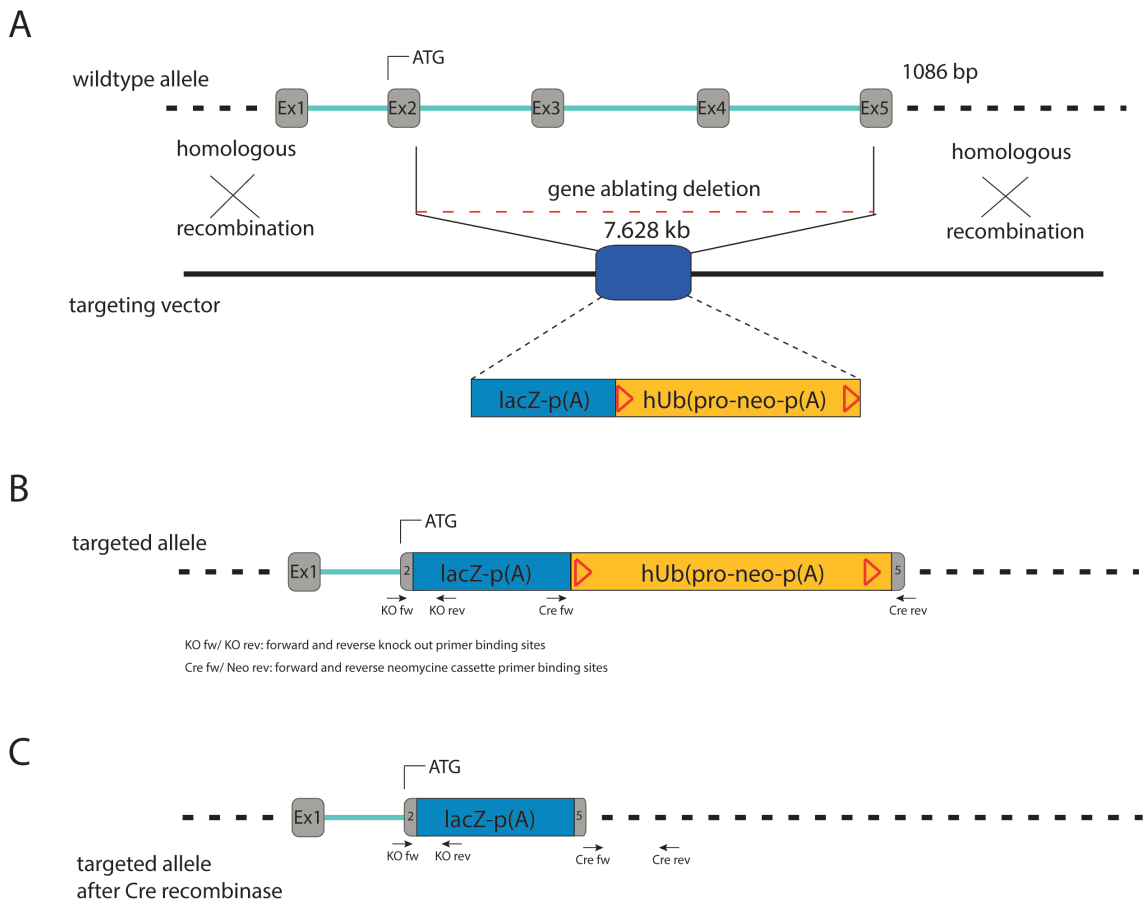

Figure 10. Schematic representation of the Mettl21c gene and the gene ablating deletion by homologous recombination. (A) The wild type and the targeting allele are displayed in 5' to 3' orientation. The five exons of Mettl21c are represented as grey rectangles and are stretching over 1086 base pairs. The coding sequence from exon 2 to exon 5 is mainly deleted by homologous recombination and the insertion of a LacZ cassette. The size of the gene ablating deletion is 7.628 kb. (B) Displaying the targeted allele with the inserted LacZ cassette and the neomycin-resistance cassette as well as the binding sites of the sequencing primers. The binding site for the reverse primer for the wild type is located in intron 2. (C) The deletion of the neomycin-resistance cassette resulted by cre-mediated recombination at the loxP sites (red triangles).

For genotyping offspring were tested by PCR to distinguish between wild type, heterozygous, and knockout animals and the excision of the neomycin cassette. The PCR strategy was based on three primers to simultaneously detect wild type, and deletion alleles. One primer (forward primer for wild type and knockout detection) is located in intron 1, the reverse wild type primer is located in intron 2 and the deletion primer is placed in the LacZ cassette. The wild type allele was identified by PCR fragment of 245 base pairs. Whereas the knockout allele created a 456 base pair fragment (Figure 11A).

Since there is no working mouse antibody available, the in vivo SILAC spike-in approach was used to confirm the absence of any translated Mettl21c protein in Mettl21c$^{-/-}$ animals. The soleus muscle from wild type and knockout animals were mixed with the soleus muscle from the fully labeled $^{13}C_6$

Lysine (Lys6) SILAC-mouse in a 1:1 ratio, respectively. The protein mixture was in-solution digested with LysC and measured by LC-MS/MS. Peptides were now measured as SILAC pairs with a distance of 6 Da and the relative peak intensity was used for relative protein quantification. The analysis of wild type animals revealed several Mettl21c SILAC peptide pairs with a 1:1 ratio. In contrast, the absence of any light peptide for Mettl21c in the knockout mouse confirmed the absence of the Mettl21c protein in homozygous animals (Figure 11B).

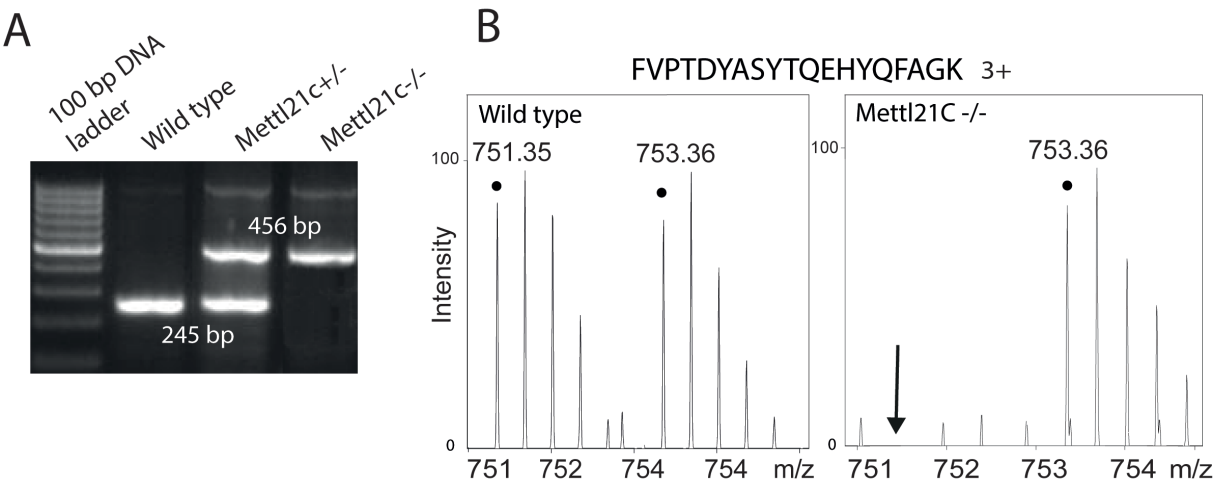

Figure 11. PCR and mass spectrometry confirmation of Mettl21c knockout. (A) The PCR fragment for a wild type is 245 bp and for a knockout mouse 456 bp. A 100 bp ladder was used as the marker. (B) Mass spectrometry measurement confirmed the knockout, due to the absence of the light peptide (in our example for ^{42}FVPTDYASYTQEHYQFAGK^{60}, Q8BLU2) of Mettl21c at a m/z ratio of 751.35 (charge 3+). White circle represents the non-labeled Mettl21c peptide, whereas the black circle labeled the Lys6 containing peptide. The arrow in B (right MS spectrum) highlights the absence of the corresponding non-labeled peak at 751.35 m/z.

3.2.1. Mettl21c is expressed in Z-disk structures of slow muscle fibers

The function of skeletal muscle cells is the coordinated contraction and elongation of millions of sarcomeres that are mainly composed of actin and myosin filaments. Several sarcomeres are arranged consecutively and are separated via Z-disks to form a myofibril. The organization of a sarcomere is a key feature of the sliding filament model. Muscle activity is related to the enzymatic and physical properties of actin, myosin, and the accessory proteins that constitute the thin and thick filaments.

The availability of a human Mettl21c antibody made it feasible to visualize the endogenous localization of Mettl21c within human skeletal muscle fibers. Longitudinal human skeletal muscle sections were immunostained with antibodies against human Mettl21c, the M-line protein Myomesin and the Z-disk marker alpha-Actinin 2. Confocal laser scanning microscopy enabled analyzing the structure of sarcomeres showing that the majority of Mettl21c co-localizes with alpha-Actinin 2, which serves as an actin filament cross-linker within the sarcomere. Double staining with Mettl21c and Myomesin showed clearly a distinct expression pattern (Figure 12).

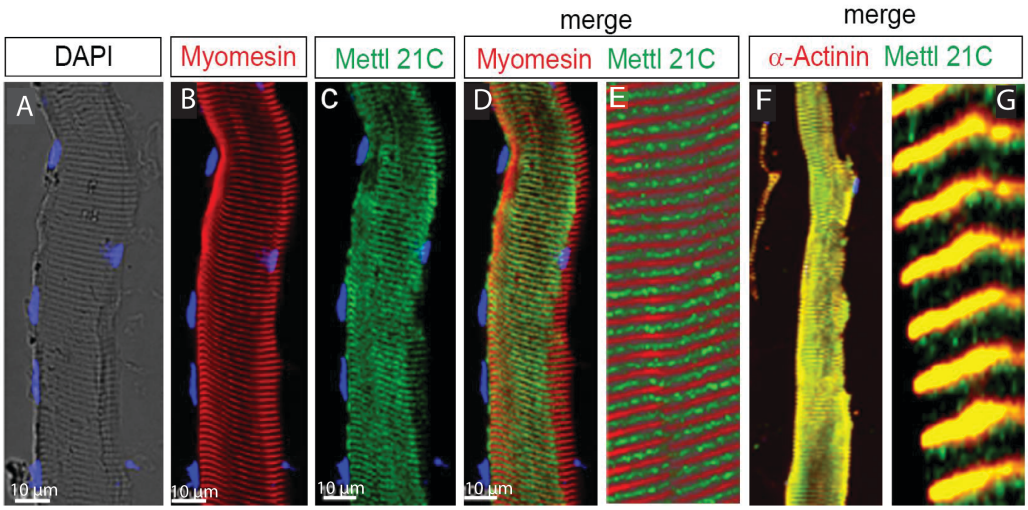

Figure 12. Mettl21c localizes to the Z-disk of striated muscle. Immunohistochemical analysis on longitudinal human skeletal muscle sections with (C, E, G) anti-Mettl21c (green), (B, D) anti-Myomesin (red, marker for M-line) and (F) anti-alpha-Actinin 2 (red, marker for Z-disk) antibodies. The counterstaining of the nucleus was done with DAPI. (A) Counterstaining with DAPI. Scale bars = 10 µm.

Next, the LacZ enzyme activity was used to analyze the expression pattern of Mettl21c in different muscle types, in order to evaluate unique anatomical structures expressing Mettl21c. The Mettl21c knockout mutant line carries an allele with the promotor of the Mettl21c gene driving a LacZ (bacterial beta-galactosidase) reporter. Comparing Mettl21c homozygous and heterozygous deletion mutants will depict, that homozygous animals have twice as much of bacterial beta-galactosidase resulting in different staining intensities.

The expression and localization of beta-galactosidase in Mettl21c hetero- and homozygous mice were followed by whole mount stainings and cryosections (20 µm slice thickness). The LacZ expression profiling revealed the highest X-Gal staining in the soleus muscle, with approximately 50% of all soleus fibers being Mettl21c/LacZ positive (Figure 13A, E). Similarly, the gluteus maximus (Figure 13B, F), which is a mixed fiber muscle [192] also showed a mosaic pattern, but with lower intensity compared to the soleus muscle. Analysis of the extensor digitorum longus (Figure 13C, G)

and the diaphragma (Figure 13D, H) muscles with predominately fast-twitch fibers [18], displayed only a weak staining for a minor fraction of ~1% of fibers with significant smaller diameter.

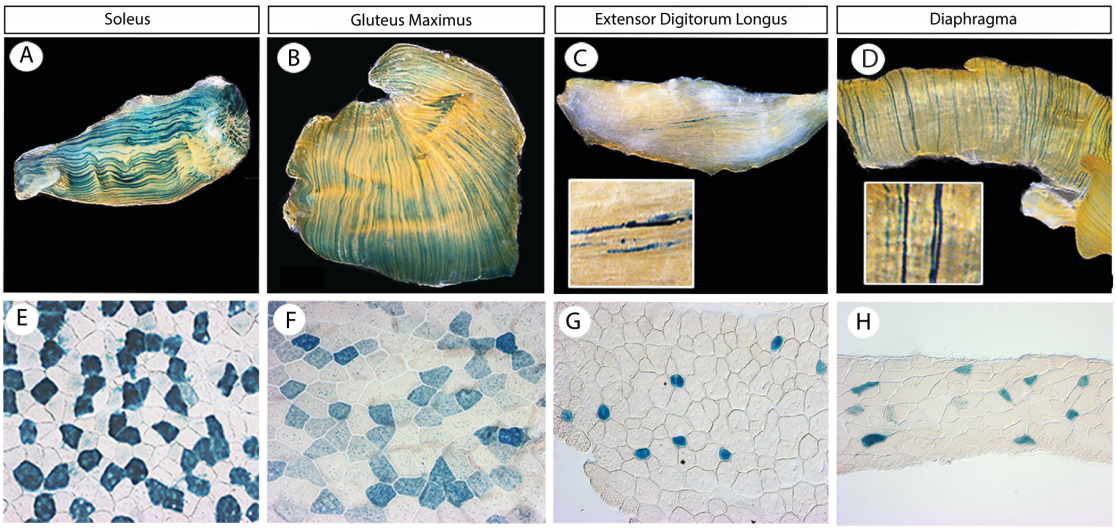

Figure 13. LacZ/Mettl21c positive cells show a mosaic pattern in different muscle types. Whole mount and corresponding transversal cryosections (20 µm slice thickness) of (A, E) soleus muscle; gluteus maximus (B, F), extensor digitorum longus (C, G) and diaphragma (D, H) muscles stained with X-Gal revealed the expression pattern of Mettl21c. The inlet in (C) and (D) shows a higher magnification of LacZ positive fibers.

Taken together, the systematic analysis of LacZ positive cells showed that Mettl21c was expressed in a specific subset of muscle fibers in different muscles. The number of LacZ positive cells reflected the proportion of slow and fast fibers within those muscles. Moreover, the soleus muscle as the slowest muscle showed the highest LacZ staining intensity suggesting that Mettl21c is predominantly expressed in slow fibers, which confirms a previous report [19].

To validate that Mettl21c is expressed in a specific subset of fiber-types immunohistochemical stainings with antibodies directed against slow myosin heavy chain I (MyHC I, slow, gene name Myh7) and against the fast MyHC IIa (MyHC IIa, fast, gene Name Myh2) in combination with LacZ stainings were performed. The expression pattern of Mettl21c/LacZ was assessed on serial cryosections (20 µm slice thickness) from soleus muscle of wild type controls, Mettl21c$^{+/-}$, and Mettl21c$^{-/-}$ littermates.

The overlap of those sections clearly revealed that Mettl21c/LacZ signals were exclusively expressed in slow-twitch muscle fibers (Figure 14A, B) since only MyHC I positive fibers were also Mettl21c/LacZ positive and MyHC II positive fibers were negative for Mettl21c/LacZ.

To clarify whether the inactivation of Mettl21c influence fiber-type specification, I counted MyHC II and MyHC I positive cells in adjacent sections after immunostainings with slow and fast MyHC

antibodies. In total, ~100 fibers for each genotype were counted and I observed ~50% MyHC IIa and 45% MyHC I positive fibers in wild-type animals. This ratio reflects exactly the fiber-type distribution in the soleus muscle as reported in previous studies [18, 193]. The analysis of Mettl21c$^{+/-}$ and Mettl21c$^{-/-}$ revealed a similar proportion compared to the wild type soleus, indicating that the inactivation of Mettl21c has no effect on the fiber-type composition in the slow soleus muscle. Each genotype was analyzed in biological triplicates.

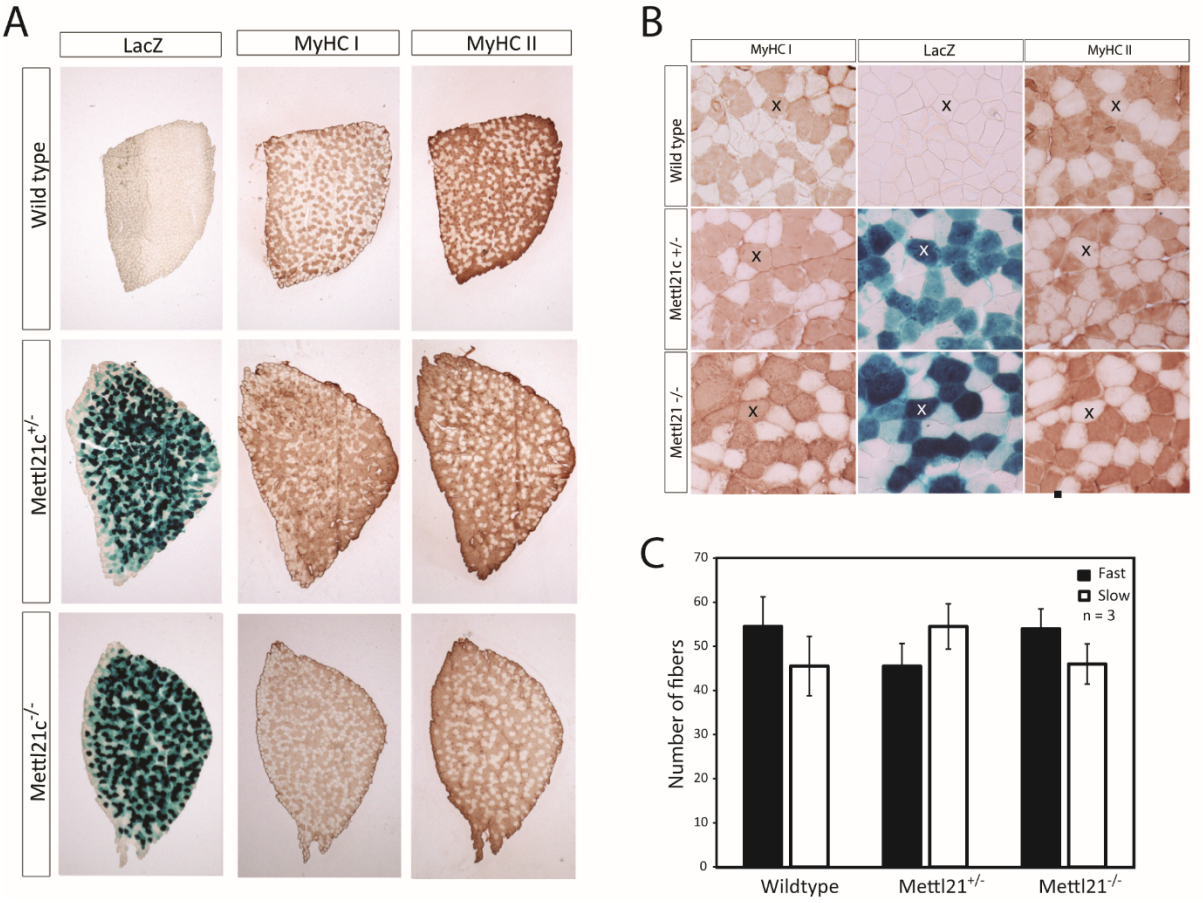

Figure 14. Mettl21c is exclusively expressed in slow-twitch muscle fibers. (A) Immunohistochemical stainings for myosin heavy chain monoclonal I antibody (MyHC I, slow) and II (MyHC II, fast) as well as LacZ stainings for serial sections (20 µm slice thickness) from soleus muscle of wild type, Mettl21c$^{+/-}$, and Mettl21c$^{-/-}$ littermates. (B) Higher magnification of panel (A). The cross indicates a Mettl21c/LacZ expressing cell and correlates it to the MyHC I and MyHC II staining. (C) Analysis of the fiber-type composition of the soleus muscle from wild type, Mettl21c$^{+/-}$, and Mettl21c$^{-/-}$ littermates. This was correlated to the total number of fibers (~100) in each section. All stainings and quantitative measurements were performed in biological triplicates.

Next, to decipher the general morphology and architecture of Mettl21c deficient soleus muscle a haematoxylin and eosin staining (H&E) was performed to visualize eosinophilic structures and nuclei of cells (Figure 15A). To monitor the carbohydrate composition of glycoproteins and proteoglycans a Lectin staining was utilized (Figure 15B). Moreover, staining for cytoplasmic, nuclei,

collagen and mucosa substances were achieved by the Trichrom method (Figure 15C). The comprehensive analysis of cellular and extracellular matrix structures by different staining procedures revealed no morphological changes between wild type and homozygous animals (Figure 15).

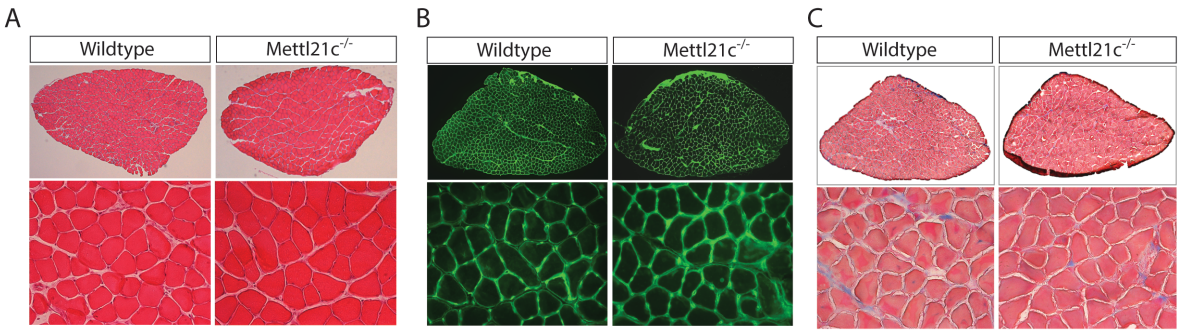

Figure 15. Mettl21c deficiency does not influence muscle morphology and fiber integrity. Representative image of (A) Haematoxylin and Eosin (H&E), (B) Lectin and (C) Trichrom staining for Mettl21c$^{-/-}$ and wild type littermate controls.

To gain a view on the intracellular localization of Mettl21c, I used U2OS and C2C12 cells transiently transfected with Flag-tagged Mettl21c for 24 hours. After fixation and permeabilization, the cells were stained with Flag antibody and counterstained with DAPI to visualize the nucleus structures. Figure 16 shows that Mettl21c is homogenously expressed in transiently transfected U2OS and C2C12 cells.

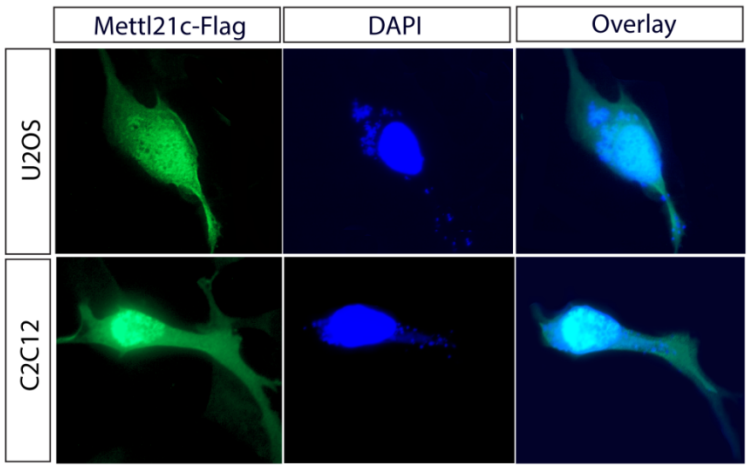

Figure 16. Mettl21c does not localize in a specific cellular compartment. Immunofluorescence microscopy of U2OS cells and C2C12 myoblasts showed that Mettl21c-Flag is expressed in cytoplasmic and nuclear structures. Localization of the Flag-tagged methyltransferase is revealed by immunofluorescence with a Cy2-labeled antibody. Counterstaining of the nucleus was done with DAPI.

Collectively, the methyltransferase Mettl21c is highly enriched in Z-disk structures and is expressed exclusively in slow-twitch muscle fibers. The deletion of the Mettl21c gene did not alter the general morphology and architecture of the soleus muscle. Localization of Mettl21c in transiently transfected cell lines revealed that Mettl21c is homogenously expressed within the nucleus and the cytoplasm.

3.2.2. Deletion of Mettl21c leads to reduced voluntary and forced running capabilities

Forced and voluntary running performance tests were chosen as a mean to characterize muscle performance in control and mutated mice. To exclude any effects based on body mass, weight and length of muscles each morphometric parameter from all experimental animals participating in the physiological tests was determined. Notably, the analysis revealed no significant differences in body weight and muscle size within the experimental groups and between different phenotypes (Figure 17A).

A voluntary running assay is based on a running wheel that is localized directly in the mouse cage and the mouse can enter the device at any time during day and night. Each rotation is counted by an online computer system and the number of rotations per day/night is a proxy of the physiological activity and muscle performance of the animal. Day and night rotations were recorded after one day of acclimation time. The running profile of wild type control group clearly confirmed higher running activity during the night since mice are nocturnal animals (Figure 17B).

The comparison to Mettl21c deficient animals showed a clear reduction in the running distance during night (Figure 17C, -53%, n=22, $p < 0.05$). Similarly, Mettl21c$^{+/-}$ animals showed also a reduced running performance (-15%; n=16), indicating a dose-dependent effect (Figure 17C) of Mettl21c on voluntary running performance.

The forced running test is an intensive test on a treadmill to monitor acute muscle endurance and to determine the time of exhaustion. These running experiments were conducted after a two day training period and the test was scheduled for 60 minutes at a speed of 12 m/min (0.6 km/h). Each exercise session was terminated at any point at which a mouse meets one out of three exhaustion criteria, including the willingness of the mouse to spend greater than 5 consecutive seconds on the shock grid without attempting to reengage the treadmill or the mouse spending greater than 50% of its time on the shock grid or if a mouse is spending three times two seconds on the shock grid. Consistently, Mettl21c$^{-/-}$ animals showed significant reduced ability to sustain a forced running activity (-64%, n=15, $p < 0.05$). Controls were able to run constantly for at least one hour, whereas

Mettl21c$^{-/-}$ animals were exhausted after 20 ± 5minutes. Of note, heterozygous animals also showed a dose-dependent effect as indicated by a slight reduction of running capability (Figure 17D).

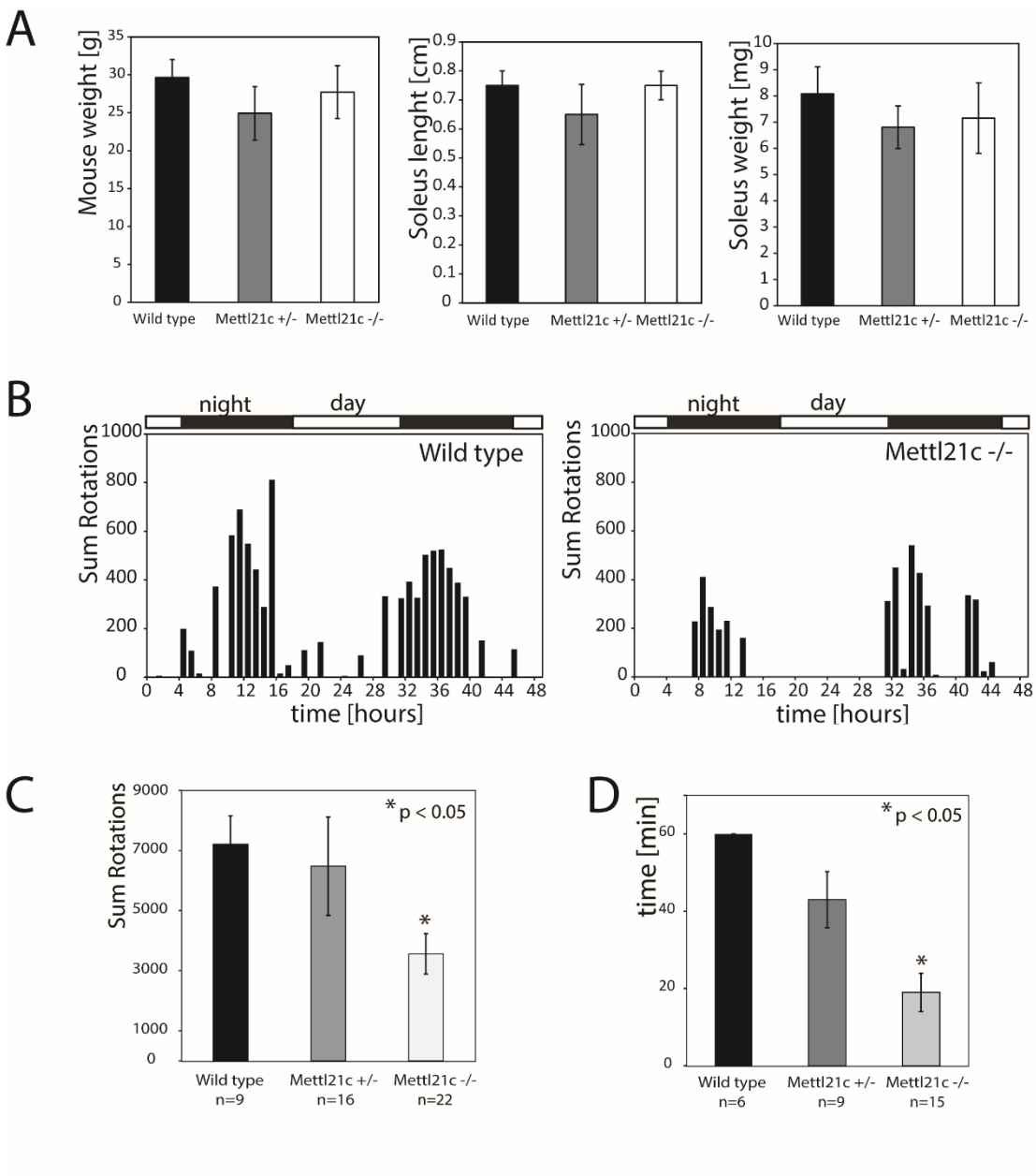

Figure 17. Deletion of Mettl21c results in significant decrease of forced and voluntary exercise performance. (A) Determination of mouse weight [g], soleus length [cm] and soleus weight [mg] for wild type littermates, Mettl21c$^{+/-}$, and Mettl21c$^{-/-}$ mice participating in the physiological tests. (B) Voluntary wheel running performance for Mettl21c$^{-/-}$ and wild type littermates monitored for two days and nights. (C) Mettl21c$^{-/-}$ demonstrated significantly reduced running durations compared to wild type littermates ($p < 0.05$). (D) Treadmill exercise performance was recorded for a 60 minutes treadmill run at 12 m/min. The exercise session was terminated at any point at which

a mouse meets one of the three exhaustion criteria. For this test Mettl21c$^{-/-}$ animals demonstrated a significantly reduced forced running performance ($p < 0.05$).

3.2.3. Proteomic and transcriptomic profiling of Mettl21c deletion mutants

In order to investigate the observed phenotype of reduced muscle performance on the molecular level, a global transcript and protein expression profiling was performed. To achieve the best correlation between transcriptomic and proteomic data, the soleus muscle from male Mettl21c$^{-/-}$ and wild type control littermates was divided into two samples. One piece of the soleus was subjected to quantitative mass spectrometry analysis and the other half was used for transcriptome analysis using a deep sequencing approach.

For the mass spectrometric analysis 20 µg of SDS-extracted protein lysate was separated by one-dimensional SDS-PAGE gel electrophoresis. Each gel lane was cut into 10 slices and then proteins were in-gel digested with the endopeptidase Trypsin. The resulting peptides were then extracted from the gel and the peptide mixture was cleaned and concentrated by stop and go extraction tips (STAGE tips). Subsequently samples were analyzed by high-resolution liquid chromatography mass spectrometry (LC-MS/MS) using 150 min LC-gradients (Figure 18A). In total, 60 samples were measured resulting in a MS measurement time of 7 days. For accurate protein quantification label-free protein quantification methods was used. To achieve statistically relevant datasets each experiment (Mettl21c$^{-/-}$ versus wild type) were performed in biological triplicates. To visualize the dataset, volcano plots were generated, which plot the log2 fold change between wild type and mutant animals and the -log10 p-values. The p-value was obtained by a t-test modified with a fudge factor of 0.1. The fudge factor ascertains that the variance of the relative difference between the experimental groups is independent of the mean of the protein expression. To control for multiple testing a permutation-based false discovery (FDR) in Perseus [194] was used. The FDR guarantees that the probability of observing a false positive but significant protein is below a certain threshold.

Alterations on the mRNA transcription level were analyzed by a deep sequencing approach using an Ion Torrent Proton (Thermo Fisher). The experiments were performed by the in-house core facility of the Max-Planck-Institute for Heart and Lung research. Isolated RNA from the soleus was first fragmented and then ligated to adapters (library). The resulting library fragments were then bound to beads and amplified by PCR. Gene transcript levels were then analyzed by massively

parallel sequencing of cDNA tags as shown in Figure 18B and then aligned to the reference transcriptome of the mouse [195].

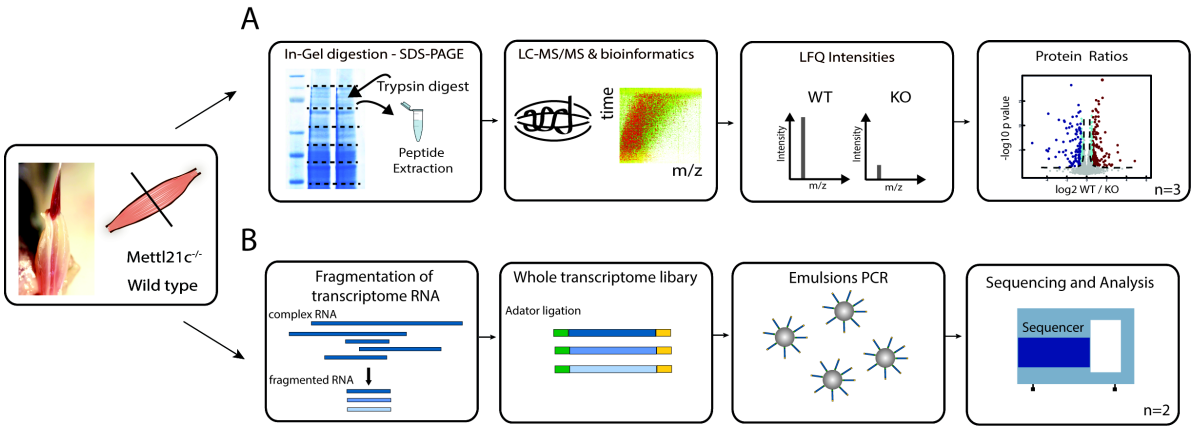

Figure 18. Generic workflow of quantitative LC-MS/MS proteomics and deep sequencing transcriptome analysis of Mettl21c$^{-/-}$ and wild type control animals. After the extraction of the soleus muscle one part was subjected to mass spectrometry and the other part to deep sequencing analysis. (A) In-depth proteome analysis was carried out by in-gel digestion. The resulting peptides were then analyzed by high-resolution LC-MS/MS. The label-free protein quantification was based on the LFQ algorithm of MaxQuant [169]. (B) The RNA was initially fragmented and then ligated to adapters (library). The library fragments were then bound to beads and amplified by PCR (emulsions PCR). The global gene transcript levels were then analyzed by massively parallel sequencing of cDNA tags with the Ion Torrent Proton.

The proteomic analysis resulted in the recording of 5576997 MS/MS fragment spectra which were used for the Andromeda search algorithm (MaxQuant, Version 1.5.2.8). To estimate the rate of false positive identified peptides and proteins the database consists of a concatenated reverse database and the false discovery rate was set to 1% on peptide and protein level. The search against the mouse Uniprot database (from 2015, a data set involving 74,265 protein sequence entries) resulted in the identification of 109772 peptides and merging this peptides to protein groups resulted in 7379 proteins. Since statistical analysis can only be performed for cases where at least two out of three conditions were detected with protein intensity, missing values were replaced by random numbers that are taken from the normal distribution. The default values are chosen to mimic low abundant protein intensities. The width parameter of this normal distribution was chosen as 0.3 of the standard deviation of all measured values and the center was shifted towards low abundance by 1.8 times of the standard deviation. This procedure increases the number of quantified proteins for 32 % (Figure 19A) and using this approach 6414 proteins were quantified. Notably, a minor fraction of 54 up and 66 down regulated proteins (absolute log2 fold change > 0.58 and -log10 p value > 1.3) could be identified. In addition, the high Pearson correlation of > 0.90 among all replicates reflected the accurate and robust protein quantification.

To verify differences between wild type and Mettl21c$^{-/-}$ animals and to gain a more systematic view on potential protein changes a principle component analysis among all phenotypes and replicates was performed. Principle component analysis helps to reduce the high-dimensionality of the data while retaining most of the variation in the data set. This analysis identifies directions that are called principle components, which can be plotted. Thereby similarities and differences between different phenotypes and replicates can be easily observed [196]. Clearly, two principle components revealed a separation between wild type and Mettl21c$^{-/-}$ animals, which made up 63.5% of the total variation. It presents a high clustering among the wild type triplicates but a heterogeneous distribution for Mettl21c$^{-/-}$ in the two-dimensional graph (Figure 19B).

The mRNA study revealed 30-50 Million raw reads of which 90% were of high quality reads. The data analysis resulted in >80% possible mapped reads using the software program “Star” [197]. In total the analysis resulted in 24448 transcripts with more than one read per gene. I detected a high Spearman correlation among the two biological replicates ranging from 0.92 to 0.95. Differentially expressed genes were assessed with DeSeq [198] and similar to the proteomics data 59 statistically significantly regulated genes were observed (absolute log2 fold change > 1 and -log10 p value > 1.3). To accomplish a proteomic-transcriptomic integrative analysis protein Uniprot identifiers were overlapped with the Ensemble Identifiers of the transcript dataset. A total number of 2534 proteins were correlated which resulted in a Pearson correlation of 0.29 (Figure 19D). Both omics approaches proved the inactivation of Mettl21c as shown in Figure 19A and C.

The comparison between the quantitative global soleus proteome and transcriptome analysis, studying differences of Mettl21c$^{-/-}$ and wild type littermates under basal conditions, revealed only a weak correlation between the respective abundances of these two classes of biological molecules.

Previous studies showed that the mouse soleus muscle contains equal number of slow and fast-twitch fibers [18, 193]. Since Mettl21c is exclusively expressed in slow-twitch muscle fibers, it is possible that a potential protein alteration is covered by non-affected fast fibers. Thus, to obtain a more detailed view on the slow fibers with inactivated Mettl21c, single fibers were isolated which were positive for the Mettl21c/LacZ staining. Thus, using fibers that are positive for the Mettl21c/LacZ expression marker enables a more focused view of the slow muscle proteome alterations.

Isolated soleus muscle was incubated with collagenase to disaggregate single fibers and heterozygous and homozygous fibers were incubated with the X-Gal staining solution. Only blue fibers were selected for subsequent MS analysis (Figure 14A+B, Figure 20A). For the experiments

~30 fibers from heterozygous and homozygous soleus muscle were isolated, respectively. The pool of slow muscle fibers was lysed and in-gel digested using SDS-PAGE gel electrophoresis.

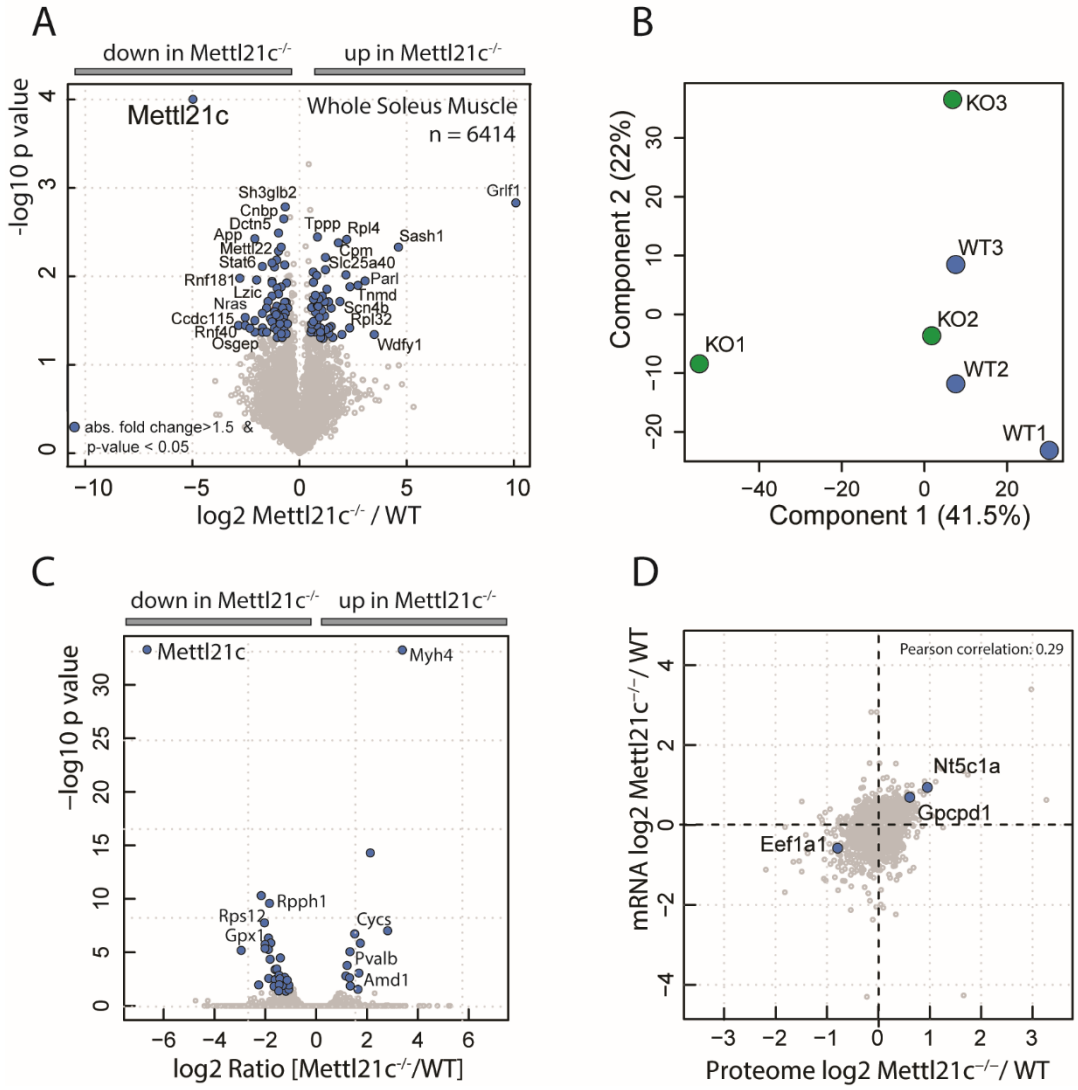

Figure 19. Proteomic and transcriptomic profiling of Mettl21c deletion mutants. (A) Volcano plot depicting significantly regulated proteins of Mettl21c$^{-/-}$ mutants in respect to wild type controls. In the proteome experiment 6414 proteins were quantified. Significant regulated proteins are colored in blue (absolute log2 fold change > 0.58 and -log10 p value > 1.3). (B) Principal component analysis showing high similarity among the wild type triplicates (blue) but a heterogeneous distribution for Mettl21c$^{-/-}$ (green). (C) Volcano plot depicting significant regulated mRNAs of Mettl21c$^{-/-}$ compared to wild type littermates. Significant regulated proteins are colored in blue (absolute log2 fold change > 1 and -log10 p value > 1.3). (D) Scatter plots visualizing the correlation of large-scale quantitative proteome and mRNA transcriptome analysis of Mettl21c deletion mutants.

The mass spectrometric analysis revealed 1564 quantified proteins and the biological samples showed a Pearson correlation between 0.97 and 0.98 (Figure 20B). The Principal component analysis revealed a high similarity among the biological replicates of Mettl21c$^{-/-}$ (green) and Mettl21c$^{+/-}$ (blue) mice (Figure 20C) and a clear separation between both groups. The label-free

protein quantification resulted in 37 statistically significantly regulated candidate genes (absolute log2 fold change > 0.58 and -log10 p value > 1.3) (Figure 21A)

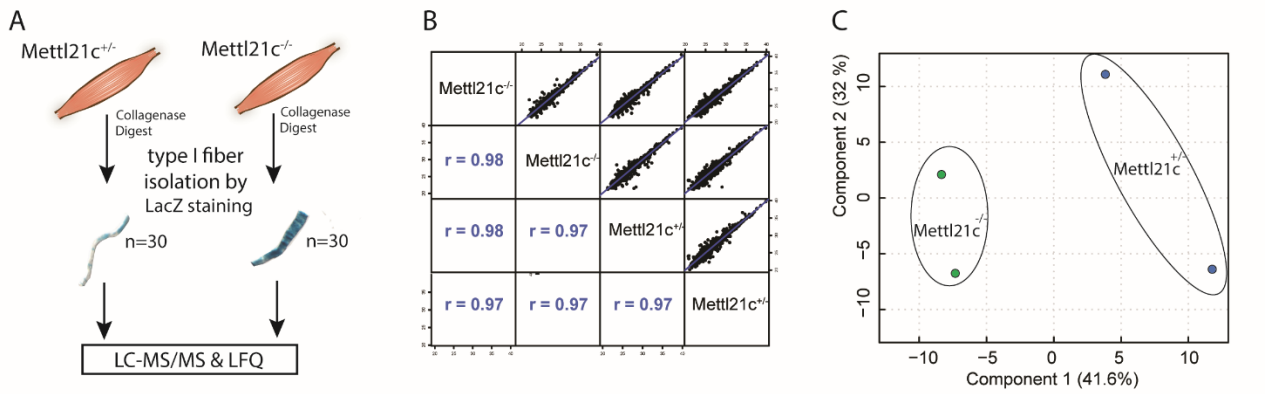

Figure 20. Characterization of the proteome of slow-twitch muscle fibers from soleus muscle of Mettl21c$^{-/-}$ and Mettl21c$^{+/-}$ mice. (A) Experimental workflow for 30 X-Gal positive/ slow-twitch fibers isolated from soleus muscle of Mettl21c$^{-/-}$ and Mettl21c$^{+/-}$ mice. Slow-twitch fiber isolation performed by collagenase digest and X-Gal staining was followed by a quantitative LC-MS/MS mass spectrometry approach (Q Exactive). (B) Pearson correlation of the soleus samples ranged from 0.97 to 0.98, representing a high correlation. (C) Principal component analysis showing high similarity among the biological replicates of Mettl21c$^{-/-}$ (green) and Mettl21c$^{+/-}$ (blue) mice.

Notably, the proteomic approach of single soleus fibers and a gene ontology term analysis provided evidence that the loss of Mettl21c alters the expression of many autophagy-related proteins and these candidates were not significantly changed in the whole soleus muscle analysis. Autophagy related proteins are summarized in Figure 21B. For example, the Ca^{2+}/Calmodulin Kinase II (Camk2g and Camk2b) is activated by Ca^{2+}/Calmodulin and can thereby regulate the autophagic process [199]. Gain-and-loss-of-function studies on Bnip3, a BH3-only protein, proved that Bnip3 modulates autophagy by FoxO-dependent regulation [28]. In muscle, several tissue-specific E3 ligases have been identified as atrophy-related genes, the F-box protein atrogin-1/MAFbx, and the MURF muscle-specific RING-finger proteins among that Trim54/Murf3 [200]. For Lamin A/C (Lmna) it was shown, that it modulates the mTorc1 signaling and leads to impaired autophagy [201]. Ulbricht et al. revealed that chaperone-assisted selective autophagy (CASA) is as a tension-induced autophagy pathway, which plays an important role for mechanotransduction in muscle. For the formation of autophagosomes during CASA the interaction of BAG3 with synaptopodin-2 (Synpo2) is of importance [202]. Here, cytoplasmic dynein 1 intermediate chain 2 was detected with increased levels in Mettl21c deficient mice and the clearance of aggregate-prone proteins is regulated by dynein, probably by modulating autophagosome-lysosome fusion [203]. In a global shRNA screening using the accumulation of the autophagy marker p62, Strohecker et al. identified, among many other candidates, Phosphorylase kinase alpha 1 (Phka1) as a potential autophagy regulator

[204]. In addition, it was also shown, that defective autophagy is the result of collagen VI deficiencies (Col6aI-III) in the ECM leading to muscular dystrophies [8].

Taken together, our analysis of the slow-twitch soleus fiber proteome revealed an alteration on many known autophagy-related proteins in Mettl21c mutants and this effect is only visible after separation of slow and fast muscle fibers.

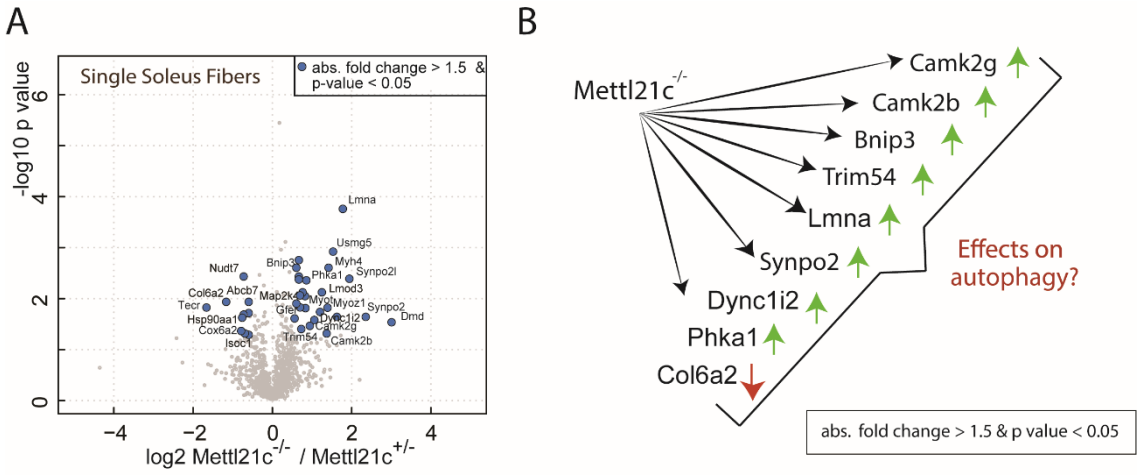

Figure 21. Loss of Mettl21c alters the expression of many know autophagy-related proteins. (A) Volcano plot depicting significantly regulated proteins of Mettl21c$^{-/-}$ mutants in respect to Mettl21c$^{+/-}$ controls. In the sub-proteome experiment of single slow-twitch soleus fibers 1564 proteins were quantified. Significant differently regulated proteins are colored in blue (absolute log2 fold change > 0.58 and -log10 p value > 1.3). (B) The expression of many autophagy-related proteins is altered in slow-twitch muscle fibers due to the Mettl21c deletion.

3.3. Mettl21c interacts with autophagic regulator proteins – Valosin-containing protein (p97) and Sequestosome-1 (p62)

In order to elucidate the molecular interplay between Mettl21c and autophagy related proteins several protein-protein interaction studies were performed. As mentioned in section 3.2., until now there is no working mouse antibody available. Hence, SILAC based affinity purification experiments using Mettl21c with different tags were performed. Mettl21c was transfected in mammalian cells such as human embryonic kidney cells (HEK 293T) and mouse myoblast cells (C2C12). After affinity purification with specific tag antibodies, enriched proteins were analyzed by the quantitative mass spectrometric workflow. Flag-tagged and GFP-tagged Mettl21c were generated by cloning the mouse Mettl21c coding sequence into the pcDNA5/TO vector containing either a C-terminal Flag- or GFP-tag. SILAC labeled cells were transfected with Flag- and/or GFP-tagged Mettl21c (under the control of the CMV promotor) as well as empty expression plasmid (TO5-Flag or TO5-GFP) for control experiments. One day post transfection, cells were harvested, lysed with modified RIPA

buffer, and immunoprecipitated using Flag and GFP antibodies in combination with Sepharose G beads. In the case of a SILAC experiment non-labeled (light) and labeled (heavy) samples, cell lysates were washed and mixed before elution. Eluted proteins were separated using SDS-PAGE, in-gel digested and subjected to LC-MS/MS analysis.

Although the overexpression of expression vectors in cell culture cells is a valuable method to screen for protein-protein interactions, this approach is often hampered by the missing expression of tissue specific proteins. To cope with these shortcomings a more physiological protein interaction screen was conducted. Here Flag-tagged Mettl21c derived from HEK 293T cells were incubated with mouse soleus lysate to enrich interaction partners from differentiated muscle tissue. For an appropriate control, beads were incubated with the tissue lysate. Control and Mettl21c samples were again analyzed by the LC-MS/MS approach.

Since each immunoprecipitation contains a large number of background binders resulting in false positive interactors each experiment was performed in duplicates and the overlap of the most common hits revealed that Mettl21c interacts predominately with co-chaperones, Heat-Shock-Proteins, autophagosomal and proteasomal proteins (Figure 22).

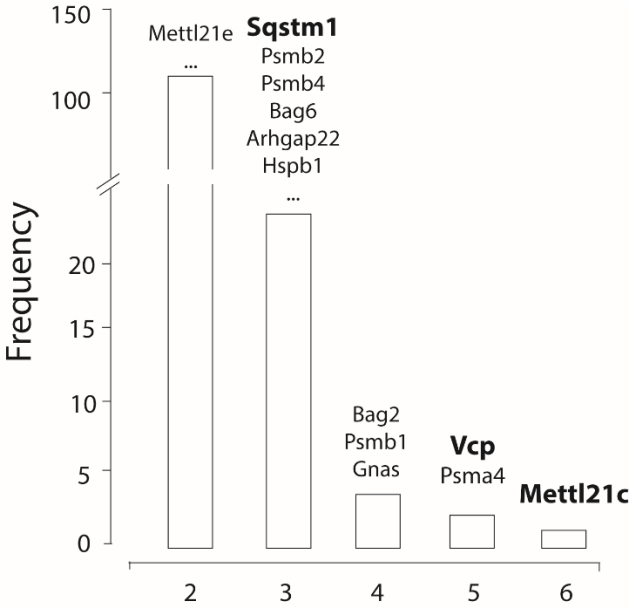

Figure 22. Mettl21c interacts predominately with co-chaperones, Heat-Shock-Proteins, autophagosomal and proteasomal proteins. Three different interaction partner screens were performed in duplicates. Flag- and GFP-tagged Mettl21c was overexpressed in SILAC-labeled C2C12 myoblasts and HEK 293T cells, immunoprecipitated, analyzed using LC-MS/MS and normalized to the controls. In addition, the Flag-tagged Mettl21c was overexpressed in HEK 293T cells, immunoprecipitated, incubated with mouse soleus lysate and analyzed using LC-MS/MS.

Notably, the Valosin-containing protein (Vcp, p97), and Sequestosome-1 (Sqstm1, p62), two autophagic adapter proteins, raised my particular attention. The two proteins are involved in transport of degradation cargo and are important regulators of these degradation pathways. As shown in Figure 23A the MS spectra revealed that the bait, GFP-tagged Mettl21c, was enriched with the highest intensity. The SILAC MS spectra for Vcp and Sqstm1 also proved that GFP-tagged Mettl21c serves as an interactor for these autophagic adapter proteins. The SILAC proteomics data were validated by western blotting (Figure 23B). To verify the Mettl21c-Vcp, and Mettl21c-Sqstm1/p62 interaction reverse immunoprecipitations with Vcp and Sqstm1/p62 from HEK 293T were performed corroborating the interaction of Mettl21c with Vcp and Sqstm1/p62 (Figure 23B).

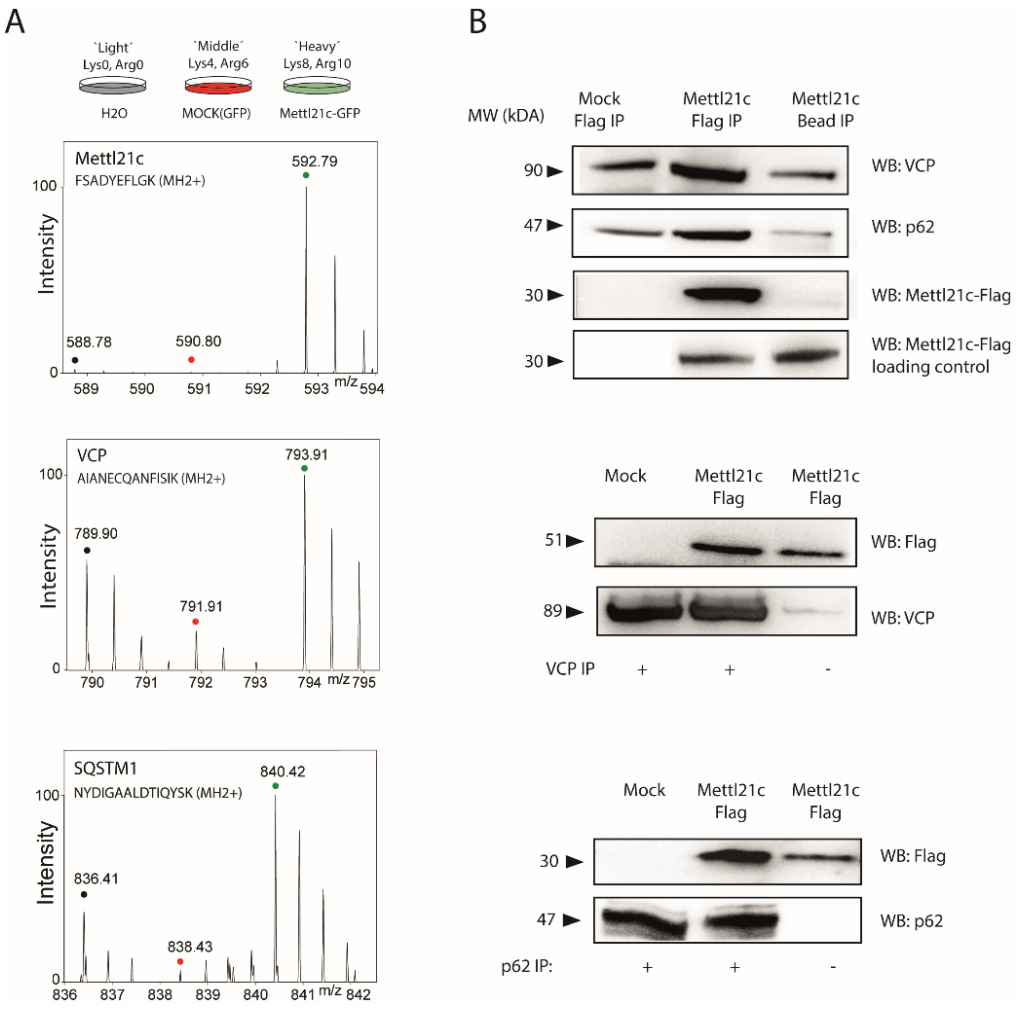

Figure 23. Mettl21c interacts with two autophagic regulator proteins, Valosin-containing protein (Vcp/p97) and Sequestosome-1 (Sqstm1/p62). (A) MS spectra from a triple SILAC experiment and (B) western blot analysis proofing the interaction of Mettl21c with Vcp and Sqstm1. Reverse immunoprecipitations with endogenous VCP and SQSTM1 from HEK 293T cells corroborating the interaction with Mettl21c.

In addition, the results also revealed an interaction between Mettl21c and its family member Mettl21e, even though it was not observed in every type of experiment, probably depending on

the expression level in the cells (Figure 22, Figure 24). Therefore, the Mettl21c-Mettl21e interaction was confirmed by overexpressing Flag-tagged Mett21c and HA-tagged Mettl21e as well as HA-tagged Mett21c and Flag-tagged Mettl21e, respectively. Immunoprecipitation and western blotting confirmed this interaction (Figure 24).

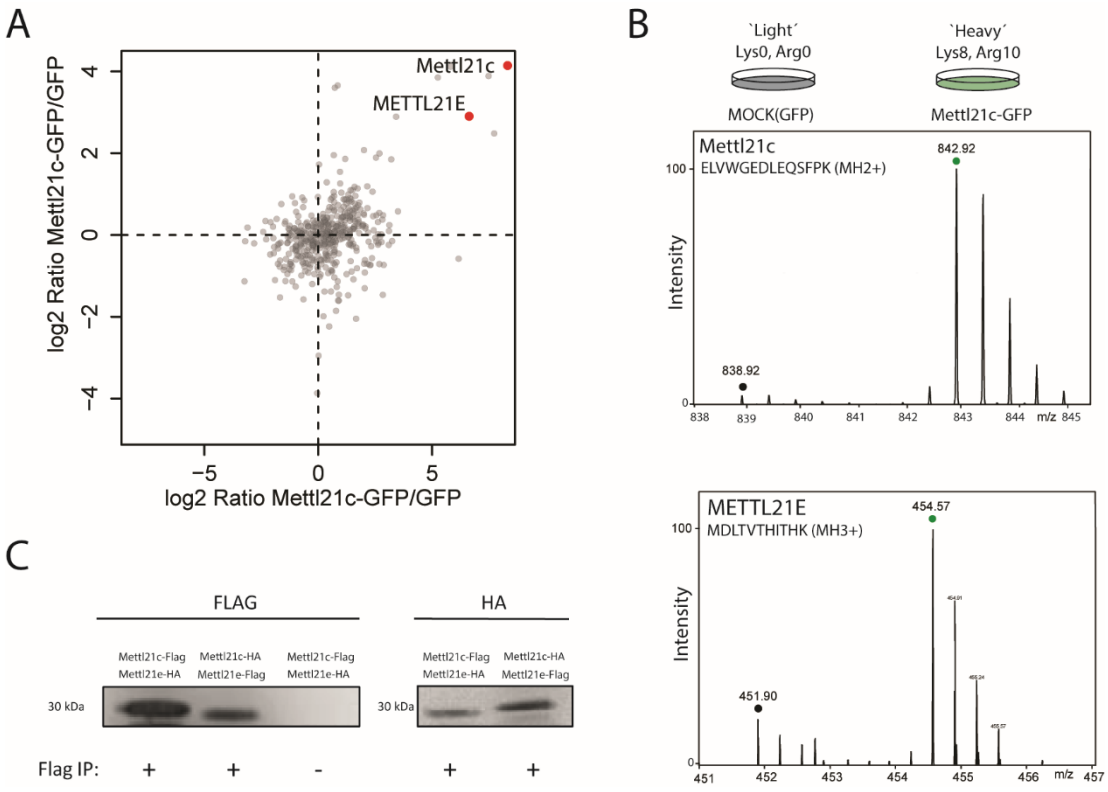

Figure 24. Mettl21c interacts with its family member Mettl21e. (A) Scatter plot and (B) MS spectra of immunoprecipitated GFP-tagged Mettl21c overexpressed in HEK 293T cells depicting the interaction of Mettl21c with endogenous METTL21E. (B) Western blot confirming the interaction between Mettl21e and Mettl21c by immunoprecipitating with Flag-antibody overexpressed Flag-tagged Mettl21c and HA-tagged Mettl21e as well as HA-tagged Mettl21c and Flag-tagged Mettl21e, respectively.

Together, these results suggest that Mettl21c plays a pivotal role in the autophagy process as it interacts with important regulators like Vcp and p62.

3.4. Mettl21c trimethylates Valosin-containing protein in vitro and in vivo

Since Mettl21c is annotated as a potential methyltransferase it would be important to identify potential substrates, which are methylated in the presence of Mettl21c. In order to identify

whether Mettl21c is able to methylate Vcp, Sqstm1 and Mettl21e, an in vitro methyltransferase assay was developed. Of note, previous studies have shown that the family member METTL21D is able to methylate VCP at position lysine-315 [3].

Both, the substrate and enzyme were overexpressed in HEK 293T cells and enriched by immunoprecipitation. This procedure ensures the presence of important cofactors for the enzymatic reaction, which might be absent in in vitro assays. The immunoprecipitated potential substrates are incubated with the methyl donor S-adenosylmethionine (SAM) and the methylation reaction is initiated with the immunoprecipitated Mettl21c (Figure 25A). To identify the methylation site(s) induced by Mettl21c activity, all reactions were analyzed by mass spectrometry. All peptide intensities were compared to the empty bead controls (without Mettl21c). As mentioned previously the consensus sequence at amino acid position 101 with the sequence "LEIGAGAG" is important for the catalytic activity of Mettl21c. Thus, a potential mutant variant of Mettl21c was generated by replacing the consensus sequence by "LEIAAAAA" resulting in impaired SAM binding [205] (Figure 25B).

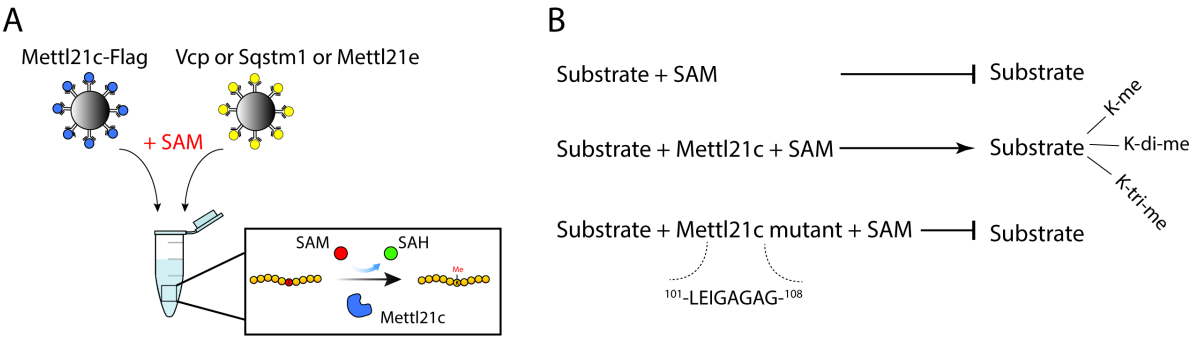

Figure 25. Experimental design for the MTase assay with Mettl21c and the potential substrates. (A) In vitro methylation assay using endogenous Flag-tagged Mettl21c and different potential substrates (Vcp, Sqstm1 and Mettl21e). The potential substrates bound to Sepharose G beads are incubated with the methyl donor S-adenosylmethionine (SAM) and the methylation reaction is initiated with beads that carry the immunoprecipitated Mettl21c-Flag. (B) The reaction of Mettl21c with the potential substrate could induce mono-, di- and trimethylation, which was analyzed by LC-MS/MS.

All components were mixed as described in the method section 2.18.4. and incubated for one hour at room temperature. Then the reactions were stopped by adding 1xLDS buffer and prepared for in-gel digestion and LC-MS/MS analysis. For the reaction of Mettl21c with Sqstm1 and Mettl21e no detectable methylation sites were observed. One reason for a missing methylation might be that these proteins are only interaction partners and no substrates. Alternatively, it is possible that the methylated peptides are not accessible for MS analysis since their length is too short or too long. In contrast, the incubation of Mettl21c and Vcp generated several methylated lysine residues. In

total I observed a sequence coverage of 88% and found 6 mono-, 3 di-, and 1 trimethylation site (Figure 26A). All mono- and dimethylation sites were equally detected in all experiments, indicating a background methylation independent of Mettl21c. However, increased trimethylation in the presence of Mettl21c was observed on the lysine at position 315 on VCP (Figure 26B, C). The MS/MS fragmentation spectrum showed an Andromeda score of 160 of the trimethylated peptide and Figure 26D depicts the presence of high mass accuracy y- and b- ions based on HCD fragmentation on a Q Exactive mass spectrometer, confirming the presence of the trimethylation at lysine-315 on VCP.

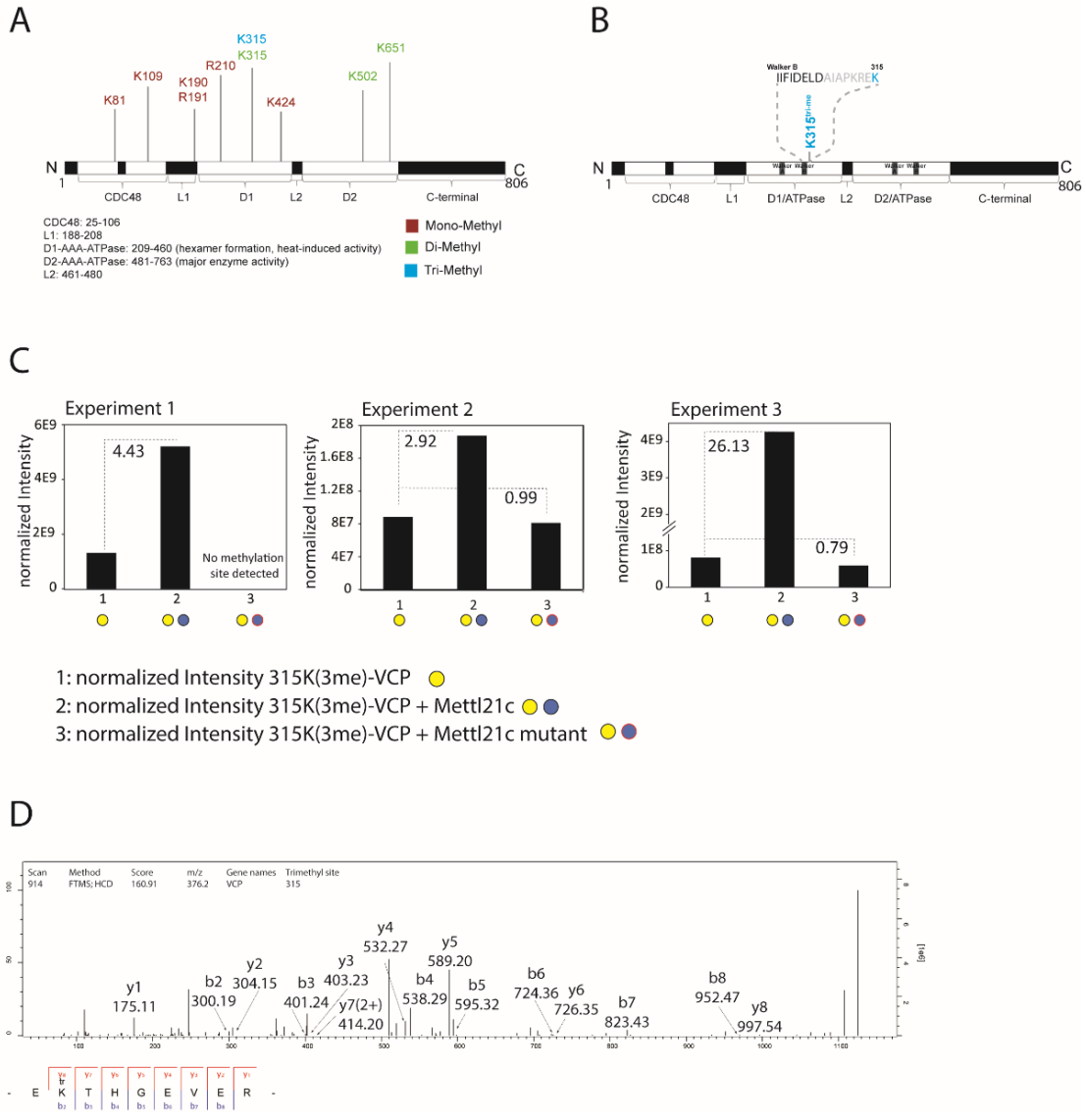

Figure 26. Mettl21c trimethylates lysine-315 of VCP. (A) MTase assay showed that Mettl21c methylates VCP at distinct lysine residues (B) but only lysine-315 is trimethylated in respect to the mutant control. (C) Bar plot displaying the upregulation of the intensity of the trimethylation of lysine-315 upon incubation with Mettl21c in respect to the control reaction and a mutant form of Mettl21c. (D) MS/MS spectrum depicts the identification of the trimethylation on lysine-315 with an Andromeda score of 160.

To investigate this trimethylation of VCP under more physiological conditions soleus muscle from wild type control and Mettl21c$^{-/-}$ was isolated and protein extracts with RIPA buffer were generated. Next, Vcp was immunoprecipitated from both genotypes and trimethylation was tested by western blotting using an anti-trimethyl antibody. The experiment revealed clearly a reduced tri-methylation in Mettl21c deficient animals compared to the wild type controls (Figure 27A). However, based on this western blot one cannot exclude the presence of other trimethylation sites, which are also less methylated in Mettl21c$^{-/-}$ animals.

To investigate the consequences of a reduced trimethylation at position 315 on Vcp, a protein interaction study using the soleus from wild type and Mettl21c$^{-/-}$ mutants was performed. After protein extraction and antibody incubation, samples were digested in-gel and LC-MS/MS analysis was conducted. As described earlier Vcp interacts with the cofactor Nsfl1c also known as p47. This interaction is important to modulate the ATPase activity of Vcp [206, 207].

The immunoprecipitation and LC-MS/MS analysis confirmed the Vcp-Nsfl1c interaction and interestingly this interaction was clearly reduced in Mettl21c deficient soleus muscle (Figure 27A, B)

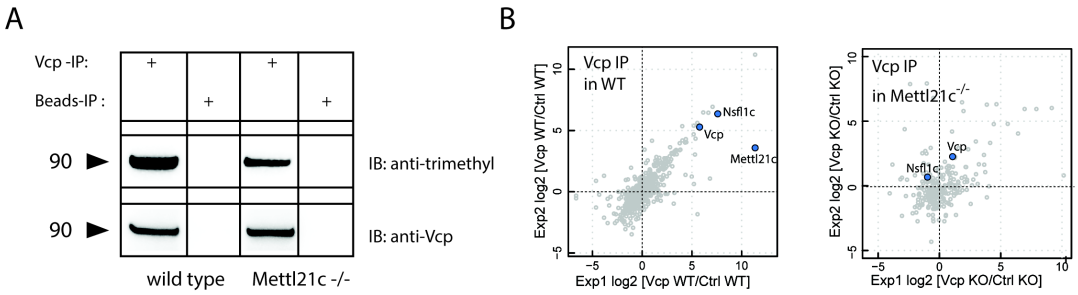

Figure 27. Reduced Vcp trimethylation on lysine-315 might compromise interaction with the Vcp cofactor Nsfl1c/p47. (A) Immunoprecipitation and western blot of control and Mettl21c$^{-/-}$ soleus muscle. (B) Scatter plots showing the log2 Ratio of Vcp-IP versus the Ctrl-IP in two quantitative mass spectrometry based protein interaction studies from soleus muscle of wild type (left plot) and Mettl21c$^{-/-}$ mutants (right plot).

Collectively, the interaction of Mettl21c and Vcp links this slow-muscle fiber specific methyltransferase to control mechanisms of autophagy. Furthermore SAM methylation assays revealed that it trimethylates mammalian VCP on lysine-315 since a 42 Da mass shift was identified in the mass spectra in comparison to an unmethylated peptide. The methylation was abolished when using a mutant form of Mettl21c with impaired SAM binding. For other interaction partners, like p62 or Mettl21e, I could not show any upregulated methylation sites compared to the controls.

3.5. Electron microscopy reveals changes in ultrastructure of Mettl21c deletion mutants

Electron microscopy is a powerful approach to monitor the ultrastructure of cellular compartments such as mitochondria or the contractile apparatus of skeletal muscle fibers.

To monitor alterations in Mettl21c deficient animals, 30- and 94-week old wild type, Mettl21c$^{+/-}$, and Mettl21c$^{-/-}$ soleus muscle were analyzed by a Philips CM 10 electron microscope.

Interestingly, I identified an accumulation of autophagosomes in Mettl21c mutants, which resemble structures found in autophagic vacuolar myopathies. Electron microscopy analysis revealed that these accumulated autophagic vacuoles are present in Mettl21c deficient and Mettl21c$^{+/-}$ myofibers but not in age-matched wild type controls. From electron microscopy analysis the sarcoplasmic reticulum appear normal (Figure 28). Since the autophagosomes are not observed in normal muscle fibers, autophagic vacuoles have been often considered as pathological hallmarks of numerous neuromuscular disorders.

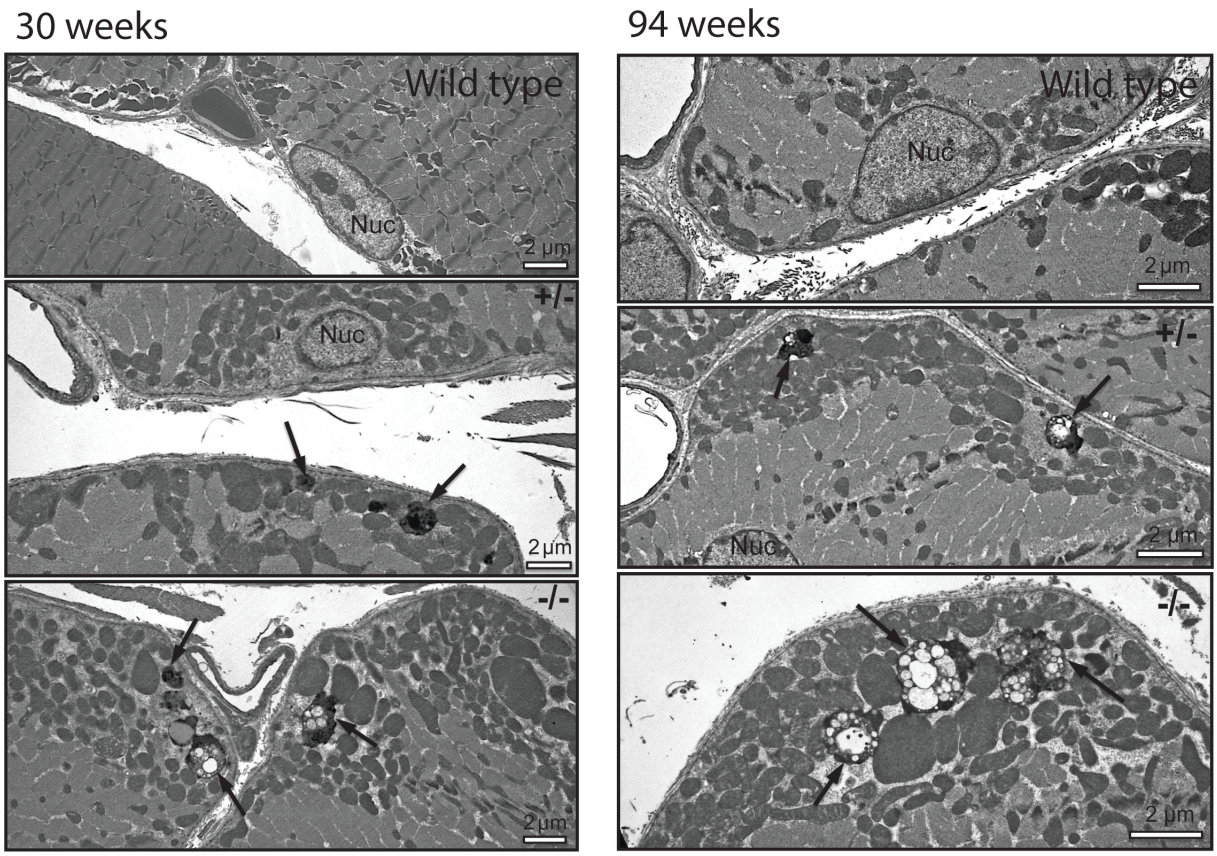

Figure 28. Electron micrographs reveal accumulation of vacuoles in Mettl21c mutants. Shown in a myofiber of a 30- and 94-week-old wild type (top), Mettl21c$^{+/-}$ (middle) and Mettl21c$^{-/-}$ (bottom) mouse. The images are representative of results obtained from three different animals per experimental group. Bars = 1 µm.

3.6. Mettl21c is associated to the autophagic flux upon denervation-induced atrophy

The inactivation of Mettl21c under steady state conditions resulted in reduced muscle performance and increased levels of proteins associated with degradation pathways. Moreover, the interaction with Vcp and its cofactor Nsfl1c suggests that Mettl21c functions as a protein that might modulate general protein degradation processes. To investigate how Mettl21c influences the process of autophagy in skeletal muscle tissue, neuronal denervation by unilaterally cutting the sciatic nerve of Mettl21c deficient and control mice for a time period of seven days was performed. The contralateral limb served as a control (Figure 29A). After seven days of denervation the soleus muscle from the control and denervated site of Mettl21c$^{-/-}$ and wild type control mice (n=3) was isolated and the muscle weights were normalized to the total body weight. Notably, wild type and Mettl21c$^{-/-}$ muscles, displayed a significant reduction of ~35% (+/- 10%) upon denervation compared to the control site, indicating muscle atrophy. However, Mettl21c deficient mice showed a similar reduction of the muscle mass compared to their wild type littermates suggesting no severe abnormalities during denervation-induced muscle atrophy (Figure 29B).

In order to characterize the role of Mettl21c$^{-/-}$ on the molecular level upon denervation, a global quantitative proteome analysis based on mass spectrometry was conducted.

The proteomic expression profiling resulted in 6482 quantifiable proteins and the analysis of biological triplicates lead to the identification of 134 up and 221 down regulated proteins in the soleus muscle of wild type compared to the control limb (Figure 29D and F). Similarly, 121 up and 203 down regulated proteins (absolute log2 fold change > 0.58 and -log10 p value > 1.3) were detected in Mettl21c$^{-/-}$ mice (Figure 29E, F). Since the main focus of this experiment was the identification of proteins related to autophagy, a systematic gene ontology term (GO) analysis was conducted. The analysis clearly showed that GO terms for mitochondrial proteins was significantly enriched but phagosomal proteins were not enriched in Mettl21c$^{-/-}$ mice compared to wild type control mice (Figure 29C, Figure 30, Figure 31) corroborating the role of Mettl21c in autophagocytosis.

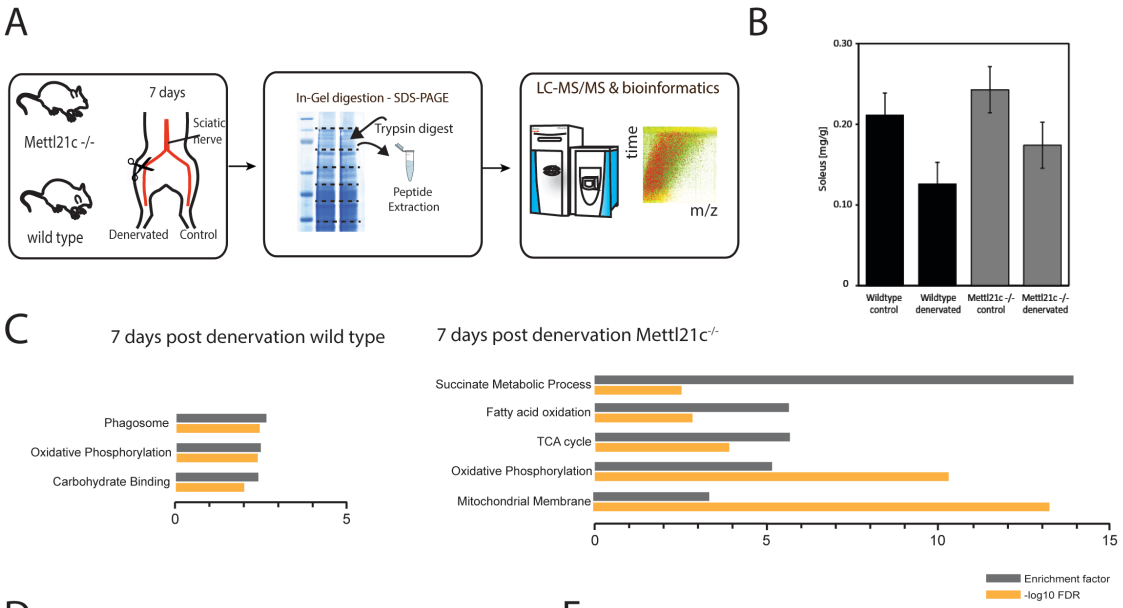

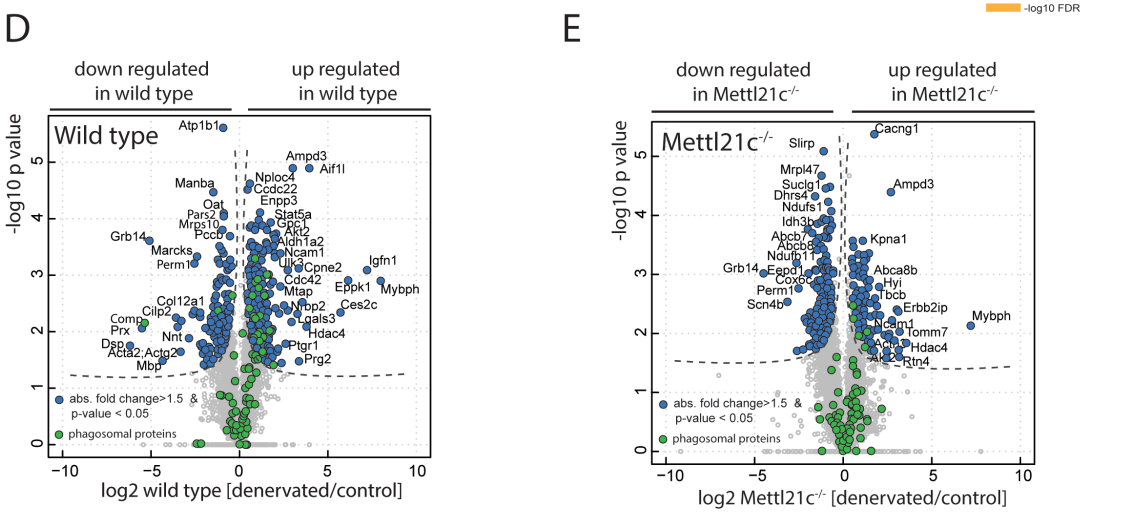

F

Sign. Regulated Proteins [Den/Ctrl]

	WT	KO
up	134	121
down	221	203

Total: 6482

Regulated Proteins

KO [Den/Ctrl] / WT [Den/Ctrl]	
up	520
down	761

Figure 29. Mettl21c regulates phagosomal and mitochondrial mechanisms during denervation-induced atrophy. (A) Experimental design for denervation-induced atrophy in Mettl21c$^{-/-}$ and wild type control mice. Unilaterally denervation by severing the sciatic nerve for a time period of seven days, with the contralateral limb serving as a control. (B) Muscle mass corrected for body weight proved a reduction in muscle mass in both wild type control (n=3, 30% reduction, $p < 0.05$) and Mettl21c$^{-/-}$ (n=3, 34% reduction, $p < 0.05$) animals. (C) Fisher exact test showing significantly regulated Go-terms for experimental animals. (D+E) Volcano plot depicting significantly regulated proteins of denervated wild type (D) and Mettl21c$^{-/-}$ mutant (E) limbs in respect to control limbs.

Significant differently regulated proteins are colored in blue (absolute log2 fold change > 0.58 and -log10 p value> 1.3). Phagosomal proteins are indicated as green circles. (F) Table showing the regulated proteins in wild type control and Mettl21c$^{-/-}$ mice.

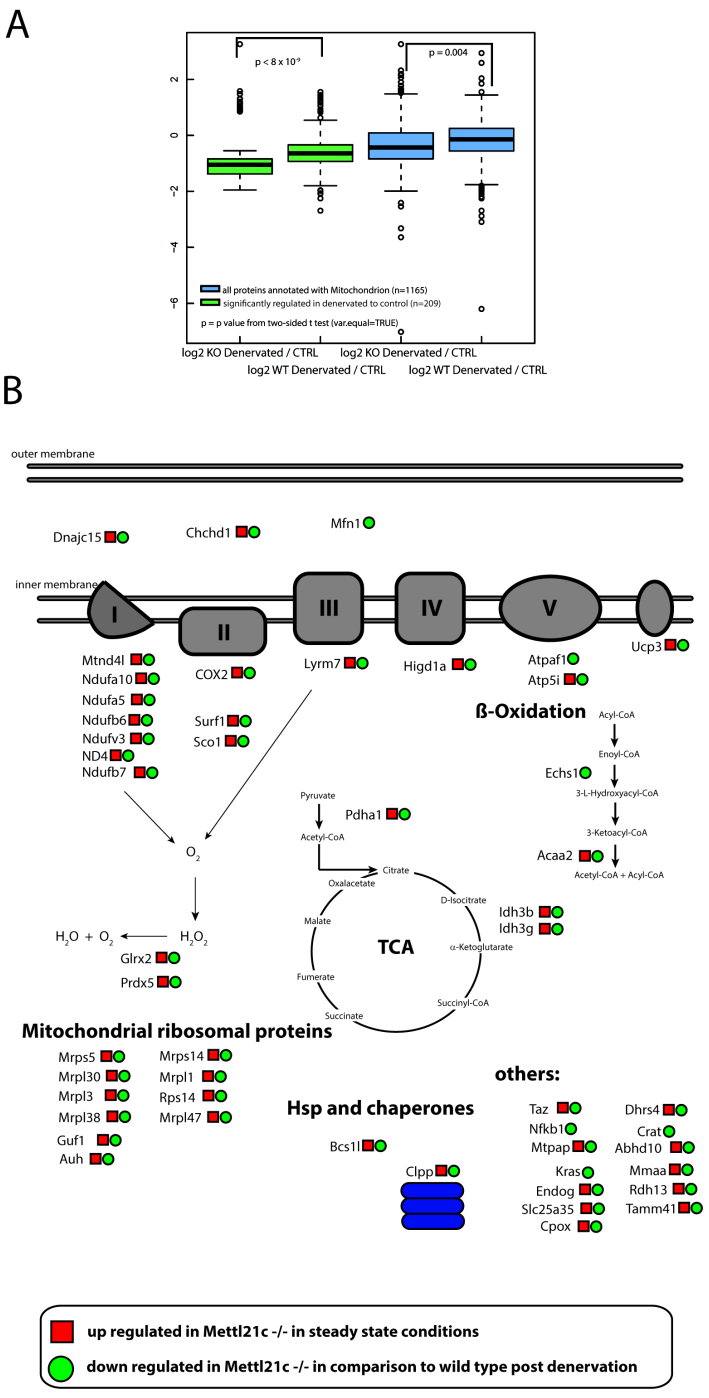

Figure 30. Increased mitophagy in Mettl21c deletion mutants. (A) Boxplot depicting regulation for all (blue) and significantly regulated (green) mitochondrial proteins from quantitative mass spectrometric analysis. (B) Mass spectrometry analysis revealing that mitochondrial proteins in Mettl21c$^{-/-}$ mice are upregulated under steady state conditions but further downregulated post denervation in comparison to wild type control mice.

Interestingly, comparison of wild type and Mettl21c mice under regular conditions revealed that mitochondrial proteins were significantly upregulated (Figure 30). Conversely, upon denervation in Mettl21c deficient animals mitochondrial proteins showed the opposite effect and were significantly downregulated in comparison to denervated wild type control mice. Since mitochondria are highly dynamic organelles mitophagy is a general process of atrophying muscle to prevent the accumulation of damaged mitochondria. Thus, the finding that Mettl21c$^{-/-}$ showed a decreased abundance of mitochondrial proteins upon denervation indicates most likely an increased level of mitochondrial clearance. In addition, the rigorous statistical analysis based on FDR calculation revealed a significant upregulation of several proteins involved in phagosomal/lysosomal transport for the denervated wild type control (Figure 31A). For example, the subunits of the V-ATPase are essential for the lysosomal hydrolase activity and the autophagic flux. Here, wild type animals showed a clear increase of this protein family (green circles in Figure 31C), whereas the denervated muscle from Mettl21c mutants (Figure 31B) did not show any upregulation of the ATP6 subunits leading to relative down regulation compared to denervated wild type animals (Figure 31A-D).

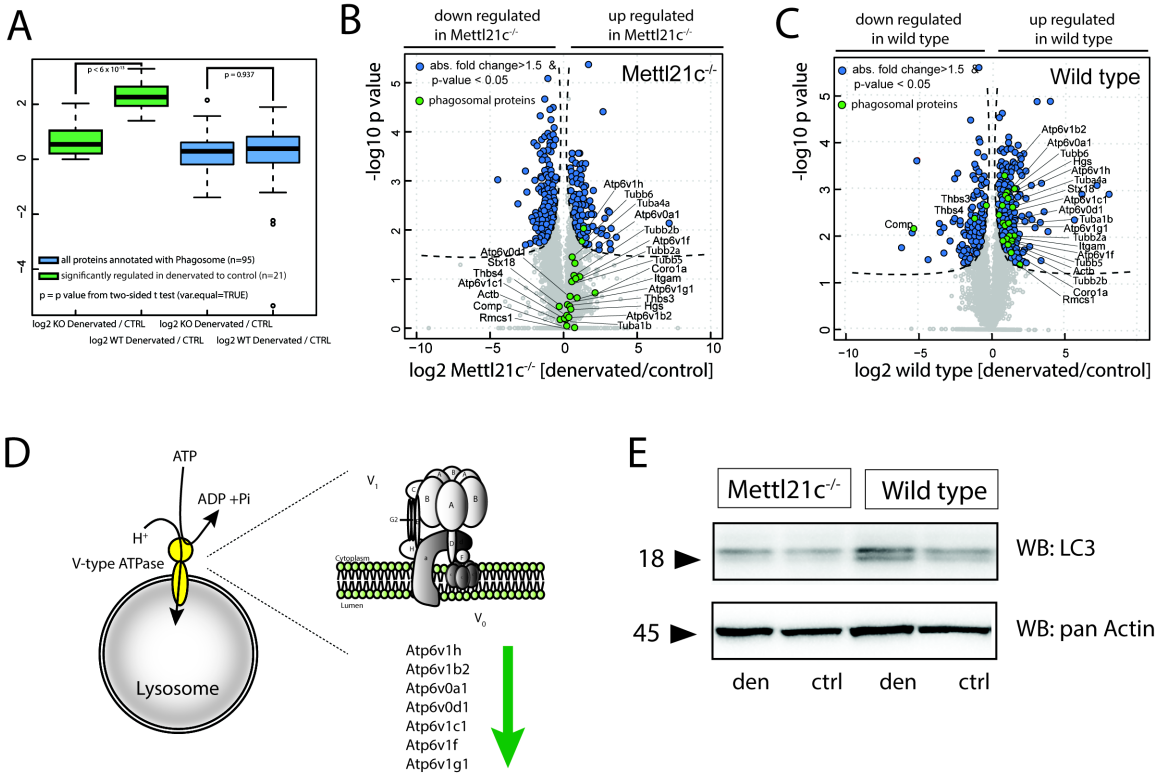

Figure 31. Mettl21c regulates the autophagic flux. (A) Boxplot showed regulation for all (blue circles) and significantly regulated (green circles) phagosomal proteins from quantitative mass spectrometric analysis. (B, C) Volcano plots shows significantly regulated proteins of denervated Mettl21c$^{-/-}$ mutants and wild type muscles compared to control muscles, respectively. Significant differently regulated proteins are colored in blue (absolute log2 fold change > 0.58 and -log10 p value > 1.3). Phagosomal proteins in the Mettl21c deficient mutants and wild type mice are

selected and labeled in green. The Volcano plot is revealing a deregulation for phagosomal proteins between wild type control and Mettl21c$^{-/-}$ animals. (D) Schematic scheme of the V-type ATPase and the deregulated subunits. (E) Western Blot of denervated and control soleus lysate of Mettl21c$^{-/-}$ and wild type littermates depicting increase of both the lipidated and unlipidated form of LC3 for wild type mice. For Mettl21c$^{-/-}$ mice the lipidation of LC3 was blocked.

The finding that lack of Mettl21c leads to dysregulation of lysosomal proteins, persuaded me to investigate the functional consequences for autophagosomal formation. Lipidated and cleaved LC3 is a general autophagic marker [48]. As shown in previous studies the induction of autophagy leads to an increase of both the lipidated and unlipidated form of LC3. Strikingly, the western blot analysis of denervated Mettl21c$^{-/-}$ clearly indicated a block of LC3 lipidation (Figure 31E), indicating a dysregulation of the autophagic flux in Mettl21c deficient mutants.

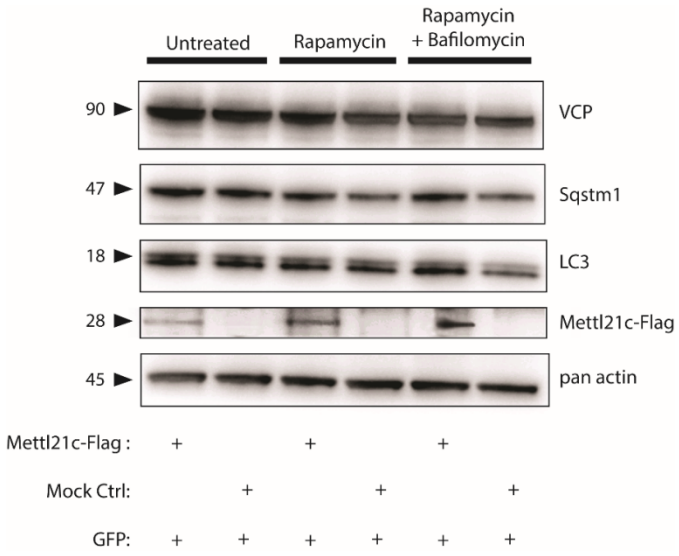

Figure 32. Mettl21c increases autophagic flux. C2C12 cells were transfected either with Flag-tagged Mettl21c or empty vector control (Mock Ctrl) as well as GFP-TO5 vector. To induce autophagy 1 µM Rapamycin was used and 100 nM BafilomycinA1 to block autophagic flux. Reliable autophagy markers, like LC3 and Sqstm1/p62, show upregulated levels, when cells were transfected with Mettl21c. The expression of VCP was not altered.

To further evaluate the function of Mettl21c cultivated C2C12 myoblasts were transient transfected with a Mettl21c-Flag fusion construct. After transfection of Mettl21c and the corresponding empty control vector, the C2C12 cells were treated with Rapamycin to induce autophagy. In addition, Bafilomycin was used to increase the pH of the lysosome, thereby blocking the autophagy flux. All cells were transfected with GFP to ensure same levels of protein content in the cell. The transfection experiments revealed that cells transfected with Mettl21c and treated with Rapamycin have increased levels of the autophagy markers LC3 and Sqstm1. In contrast, VCP was not altered upon Mettl21c transfection and autophagy induction. Similarly, simultaneous incubation of Rapamycin and Bafilomycin lead to an upregulation of LC3 and Sqstm1 in the

presence of Mettl21c (Figure 32). Taken together, the cell culture experiments suggest that expression of Mettl21c increases the levels of LC3 and Sqstm1 and thereby regulates the autophagic flux.

4. Discussion

4.1. Protein methylation in skeletal muscle

Reversible post-translational modifications (PTM) modulate several cellular processes, including cell proliferation, intracellular cell signaling, metabolic activity and even muscle contraction. Clearly, the mapping of global phosphorylation pattern by mass spectrometry helped tremendously to understand signaling events under regular and pathological conditions. Another PTM, which was initially identified to be important for epigenetic regulation of histone molecules, is the methylation of arginine and lysine residues. Previous studies proved that several non-histone proteins are strongly methylated. Such mono-, di- or trimethylation on arginine and lysine residues are known to modulate protein-protein interactions as well as enzymatic activities [92, 116-118].

The skeletal muscle is a highly dynamic organ, which can rapidly adapt to force demands, nutritional status and other environmental changes. The skeletal muscle is characterized by a heterogeneous composition of fiber-types with distinct metabolic activities. Notably, it has been shown that not only the expression of specific slow and fast MyHC molecules classify muscle fibers, but a complex expression pattern of different classes of proteins, including metabolic enzymes, signaling and structural proteins. Recently, it has been described that extensive post-translational modifications determine the ability of skeletal muscle fibers to undergo adaptive changes [19, 208]. Until now more than hundred thousand phosphorylation sites on serine, threonine, and tyrosine on skeletal muscle proteins were mapped by mass spectrometry and there is also an increasing number for the identification of ubiquitination and acetylation sites.

Although protein methylation was identified about the time as phosphorylation, the number and understanding of methylation of non-histone proteins is still in its infancy. Recently, the understanding of enzymes that catalyze the transfer of methyl groups from S-adenosylmethionine (SAM) to DNA, RNA, proteins, lipids and small molecules has greatly expanded and most of the knowledge originates from epigenetics studies [183]. Strikingly, the development of antibodies directed against protein methylation, peptide arrays, and mass spectrometry resulted in the identification of many “non-histone” methylation sites on arginine and lysine residues within the mammalian proteome. Until now ~3097 sites were annotated in common databases (www.phosphosite.org; December 2015) but this number of identified methylation sites most likely represents only the tip of the iceberg [209-213].

However, the function and dynamic regulation for most of the protein methylation events is poorly understood. One example for a known function is the methylation of specific lysine residues of the tumor suppressor p53. Besides the known functions of several phosphorylation, ubiquitination and acetylation sites, it has been shown that methylation enhances or suppresses the activity of p53 during tumorigenesis [116, 117]. The Set and MYND domain containing protein 2 (SMYD2) is mainly responsible for p53 methylation [214]. This enzyme falls into the Class VI SET domain methyltransferases. In addition, Smyd2 has an intriguing function in the cytoplasm of skeletal myocytes, where it methylates the chaperone Hsp90 which promotes the interaction between Hsp90 and the N2A domain of titin [92].

Another important protein regulating a wide range of physiological processes throughout eukaryotic organisms is Calmodulin, a key mediator of the calcium-dependent signaling, which plays an important role in skeletal muscle excitation. Several studies showed that Calmodulin is modulated by many regulatory post-translational modifications, including a trimethylation of the lysine-115 residue [102, 123, 124]. It has been shown that the trimethylation of Calmodulin results in the regulation of certain enzymes such as the NAD kinase [124, 215-217] and the trimethylation of Calmodulin controls the protein turnover rate via the ubiquitin-dependent degradation pathway [218, 219].

In comparison to other post-translational modifications, the function of methylation is not based on a charge change and the mono-, di-, and trimethylation causes only a 14, 28 or 42 Da mass increase of a protein, respectively. Nevertheless, methylation on arginine, lysine, and the N-terminus induces a wide range of protein changes. For example, protein methylation is closely associated with other PTMs and there is an obvious crosstalk to dynamic ubiquitination and phosphorylation sites [209, 220, 221]. Furthermore, protein methylation can create a binding surface to recruit other proteins, thereby regulating protein complexes and networks [222, 223]. Thus, “methyl switches” are important to modulate signals at neighboring amino acids and act as regulators for DNA binding [88, 224].

In a global SILAC-based quantitative proteome screen comparing differentially regulated proteins between slow (soleus) and fast (EDL) muscle types, the Methyltransferase-like 21c was identified as an abundant protein with high expression in the slow-twitch muscle [19]. This led to the assumption that this methyltransferase acts as a regulator for slow-twitch muscle function and identity. The aim of this study was to examine the role for Mettl21c in global muscle homeostasis in living mice. Since Mettl21c is mainly expressed in slow-twitch muscle fibers, where it interacts with autophagic adaptor proteins, this study focused on the investigation of how Mettl21c associates muscular strength with vesicular trafficking and autophagic flux. Clearly, the proper balance of

autophagy is a nodal point for optimal muscle function and there are several hints that changes in the autophagy flux are mediators for severe human muscle diseases.

Taken together, the aforementioned examples emphasize that methylation of non-histone proteins is an important tool for cells to modulate protein-protein interactions, protein stability, and activity under regular and pathophysiological conditions.

4.2. Bioinformatic analysis associates Mettl21c to cytoplasmic Class I methyltransferases

Mettl21c belongs to a small subfamily of four highly homologous (30-50% sequence homology) uncharacterized putative methyltransferases (MTases), designated Mettl21a – Mettl21e. The family members belong to Class I methyltransferases, which contain a canonical Rossmann-fold-like bundle of seven-beta-strands and display four characteristic conserved sequence motifs denoted as Motif 1, Motif Post 1, Motif 2 and 3. The crystal structure of human METTL21C (PDB: 4mtl) revealed that it consists of a seven-stranded beta-sheet adjoined by five alpha helices. The small cofactor SAM binds in the deep cleft resulting from the beta-sheet which contains a central topology switch point. All SAM-dependent methyltransferases show a structurally conserved binding domain consisting of two conserved regions. First, the conserved Motif 1, which displays the sequence GxGxG (in Mettl21c GAGAG) localized at the end of the first beta strand, proved to be important for binding of the carboxypropyl part of SAM [191]. Mutation of the glycines (G104, G106, G108) into alanines results in impaired SAM binding and hence inactivates the enzyme. However, until now the methyltransferase activity of Mettl21c was only shown by lysine-automethylation [3]. In addition, all Mettl21c orthologues contain a conserved DXXY motif located C-terminal to Motif 2. The conserved acidic residue aspartate forms one hydrogen bond to each hydroxyl of the SAM ribose part [225] and a mutation in these regions would lead to a catalytically inactive enzyme. Although the Mettl21c protein structure suggests a potential lysine and arginine methylation activity, the physiological function and protein targets for most of the Mettl21 family members are completely unknown.

Identification of specific substrates and the structural analysis of the complex with the specific methyltransferase will reveal the requirements for methyl transfer and explain substrate specificity. Many of the amino acids directly involved in substrate binding are conserved within the Mettl21 family. However, the analysis of alterations in the amino acid composition of the active site might help to determine the diverse substrate specificities, which seem to be at least chemically and functionally related.

4.3 Mettl21c is localized within Z-disk structures of skeletal muscle fibers

A recent study reported that overexpressed Flag-tagged Mettl21c is predominantly localized within the nucleus. However, none of the four main histones seems to be methylated by Mettl21c [2] and the observations made in this study revealed a pan-cellular localization of transiently overexpressed Flag-tagged Mettl21c in C2C12 myoblasts and U2OS cells. Moreover, protein-protein interaction studies detected several cytoplasmic proteins, indicating a localization of Mettl21c in the cytoplasm. In addition, immunohistochemistry using a human Mettl21c antibody and confocal microscopy revealed the endogenous localization in human skeletal muscle fibers. Co-immunostainings for Mettl21c, the M-line protein Myomesin and the Z-disk protein alpha-Actinin 2 indicated that Mettl21c is mainly localized in the Z-disk as it co-localizes with alpha-Actinin 2. Moreover, Mettl21c positive areas were also observed next to the Z-disk in the I-band. The Z-disk is responsible for force reception, transduction, transmission and acts as a sensor for mechanical stress, redirecting chemical signals. The I-band is near the edge of the sarcomere and contains mainly thin filaments. It has been shown that Z-disk proteins are involved in signaling processes and mutations of Z-disk proteins have been linked to many myofibrillar myopathies [226, 227]. Thus, protein methylation of Z-disk proteins might be a novel mechanism to modulate muscle activity and protein homeostasis as it was shown for the methyltransferase Smyd2. In a current study it was postulated that endogenous Smyd2 and titin N2A-domain colocalize in cardiomyocytes with methylated Hsp90 in the Z-disk/I-band, whereas non-methylated Hsp90 is mainly localized in the cytoplasm [228]. Whether Mettl21c shuttles between Z-disk and I-band structures should be investigated by future experiments. However, keeping in mind that the Z-disk is a high-density protein region that might result in staining artefacts, a careful evaluation of Mettl21c localization with alternative methods, including biochemical fractionation and other imaging approaches, appears mandatory.

4.4. Deficiency of slow-muscle specific Mettl21c results in reduced muscle performance

To characterize the function of Mettl21c more in detail, the gene was inactivated in the mouse by homologous recombination. The gene inactivation strategy did also introduce a reporter for the Mettl21c gene activity (LacZ cassette) into the Mettl21c locus. Comparison of wild type and Mettl21c deficient animals revealed no alterations in body weight, locomotor behavior, and fertility under baseline conditions. Morphometric analysis of several muscle tissues revealed no changes of

muscle size and muscle weight, indicating that Mettl21c is dispensable for skeletal muscle development.

Co-localization experiments with slow MyHC I (gene Myh7) and X-Gal staining showed that Mettl21c is mainly expressed in slow-twitch muscle fibers. Interestingly, although the heart muscle is also a “slow” muscle, Mettl21c is not expressed in heart muscle or any other muscle related tissue, including smooth muscle, suggesting that Mettl21c has primary a function in slow fibers. Since Mettl21c is mainly expressed in slow fibers all subsequent experiments were performed with the slowest mouse muscle, the soleus, which contains ~45% slow type I fibers. Surprisingly, inactivation of Mettl21c did not result in morphological changes, including fiber diameter, fiber-type composition, and extracellular matrix proteins of the soleus muscle.

Oxidative slow-twitch muscles are mainly involved in posture and endurance performance. Slow fibers have an increased level of mitochondria and more myoglobin for oxygen transport. Slow fibers also express higher levels of heat shock proteins to cope with increased metabolic activity and higher levels of reactive oxygen species. Similar to SETD1A and SMYD2 function, it might be possible that Mettl21c is associated to chaperone functions to deal with the higher cellular stress in slow fibers compared to fibers with lower metabolic activity [92, 131]. One of the key findings in this study was that Mettl21c deficient mice showed a reduced running capacity in comparison to their wild type littermates. Forced high-impact treadmill running and the moderate intensity voluntary wheel running experiments revealed a significant reduction of more than 50% in endurance capacity of Mettl21c deficient animals. Heterozygous mice having only one allele of Mettl21c showed a weak dose-dependent effect.

The soleus muscle acts as an important antigravity muscle in the leg and due to the anatomical distribution of these slow muscles it is assumed that they might acts as a neutral alignment of the hindlimb extremity. It is proposed that slow muscles reduce the fatigue in adjacent larger fast skeletal muscles and ensure the physical rest for situations, when powerful bursts of movement are needed [229]. It is worth questioning whether changes in a rather small population of fibers can affect the global muscle performance. Earlier experiments showed that already a slight transition from fast- to slow-twitch fibers can increase the resistance to fatigue [230, 231]. For example, mice lacking PGC-1alpha showed a decrease of endurance exercise capacity and resistance to fatigue [232].

A reduced muscle performance is tightly associated with a potential imbalance of catabolic and anabolic processes. The equilibrium between protein synthesis and protein breakdown is vital for all cells and is controlled by several cellular systems. For example, the ubiquitin-proteasome system (UPS) regulates the elimination of single proteins and smaller aggregates by hydrolysis in the

proteasome. The autophagosomal-lysosomal pathway is able to clear entire organelles and large protein aggregates [28]. An unbalanced regulation of the autophagic flux is detrimental for the global homeostasis of skeletal muscles under regular and workload conditions. Moreover, autophagy is important for the maintenance of exercise capacity. Reduced or excessive autophagy results in several muscle diseases with reduced physiological capacity [8-10]. Mettl21c appears to be pivotal for the molecular homeostasis in slow-twitch skeletal muscle fibers and consequently for the maintenance of a physiological balance between endurance and muscle fatigue. Thus, future experiments to elucidate whether Mettl21c expression is induced by exercise would help to better understand the function of this new protein.

Thus, identification of Mettl21c targets that promote skeletal muscle homeostasis would increase our understanding how metabolic and contractile properties of muscle fibers are co-regulated. A potential mechanism might be that slow fibers deficient for Mettl21c influence other fibers by the release or receipt of myokines as it was shown that autophagy is important for endosome trafficking and some forms of exo-and endocytosis [233].

4.5. EM analysis reveals massive accumulation of multivesicular autophagosomes and vacuoles

An assessment of muscle biopsy on electron microscopy enables a definite diagnosis of several muscular disorders. Since the analysis with a confocal microscope did not show any morphological changes between control and Mettl21c deficient muscle sections, a more comprehensive analysis with a transmission electron microscope of soleus muscle sections from 30- and 94-week old Mettl21c$^{-/-}$ mice were performed. Notably, the Mettl21c deficient soleus muscles displayed an accumulation of multivesicular autophagosomes and vacuoles indicating a dysregulation of protein degradation via the autophagosomal-lysosomal system. The enhanced accumulation of autophagic vacuoles might also reflect increased cellular oxidative stress, since pathological accumulation of autophagic vacuoles has been implicated in several human diseases, including ALS [5], lysosomal storage diseases [234], IBMPFD [235], and muscular dystrophies [234, 236-238]. Importantly, autophagosomes are not detectable under regular steady-state conditions in muscle fibers. There are two main groups of autophagic vacuolar myopathies including lysosomal myopathies. One group shows primary defects in lysosomal proteins including Pompe and Danon disease. In contrast, autophagic vacuoles in rimmed vacuolar myopathies are caused by extra-lysosomal defects and are usually observed at later stages of the disease. This group includes sporadic inclusion body myositis (sIBM) and myofibrillar myopathies. Thus, the analysis of the ultrastructure

of Mettl21c deficient skeletal muscle tissue revealed a potential association to autophagy processes reflected by the accumulation of multivesicular autophagosomes.

4.6. Global proteome analysis revealed association to autophagy pathways

In order to verify a potential dysregulation of autophagic pathways, a quantitative transcriptome and proteome analysis of the soleus muscle from control and Mettl21c deficient animals was conducted. The initial immunohistochemical experiments showed equal fiber-type compositions between control and Mettl21c deficient muscles. In line with these results the quantitative mass spectrometric analysis of MyHC proteins using only unique peptides for the different Myosin isoforms confirmed this trend. However, the fast myosin heavy chain MyHC IIb (gene Myh4) was upregulated on the transcript and protein level in Mettl21c deficient fibers compared to wild type fibers. The identification of quantitative differences of MyHC compositions in Mettl21c mutants might reflect the high sensitivity of transcriptomic and proteomic approaches which is not reached by immunohistochemistry.

The fastest Myosin, Myh4, is optimized for maximal strength and speed. Hence, increased expression of Myh4 in slow muscle fibers might reduce endurance. Strikingly, under basal conditions the type IIb Myh4 is barely detectable in slow soleus muscle and it has been shown that unweighting the soleus hindlimb by suspension or microgravity results in slow to fast fiber-type conversion, with de novo expression of the Myh4 isoform mRNA [239-241]. The expression of myosin isoforms in muscle is mainly regulated by transcriptional control [242] and the understanding how myofilament proteins are modulated by post-translational protein modifications just emerges [243-245]. For example, a previous study showed that fast fibers have higher phosphorylation levels in order to counteract the quick reduction of force that is followed by contractile activity [243]. Hence, methylation is described as a modification with a slower turnover than other post-translational modifications. The physiological relevance might be a long-term regulation to maintain the endurance phenotype of slow type I fibers [246]. The mechanism how Mett21c suppresses the Myh4 gene expression or protein abundance is completely unknown.

Previously, systematic proteo-genomic experiments showed only a weak correlation between global gene expression patterns and protein abundances, reflecting the existence of post-transcriptional and post-translational regulatory mechanisms. Here, the comparison of transcript and protein levels of the soleus muscle from wild type and Mettl21c deficient mice revealed a Pearson correlation of 0.29. Similar, a recent global analysis of transcript-protein relationships in

liver tissue of different inbred strains of mice with a variety of gene mutations, reported a correlation between transcript and protein levels of 0.27, which varied depending on the cellular location and the biological function of the gene [247]. This indicated that the knowledge of protein levels is essential to estimate the real protein concentrations under regular and perturbed conditions. In addition to the different regulatory stages of transcriptome and proteome, the low correlations can also occur due to different technical procedures.

The combined proteo-genomic analysis revealed an overlap of 2534 proteins from soleus tissue. Only a minor fraction of 15 proteins were equally and significantly regulated on transcript and protein level between Mettl21c$^{-/-}$ and control mice. Since the mouse soleus muscle contains equal numbers of fast and slow fibers a complete lysis will most likely dilute a potential phenotype in one of the fiber-types, respectively. Thus, to avoid a potential contamination of proteins derived from fast type II fibers, the soleus of heterozygous (Mettl21c/LacZ) and homozygous (LacZ/LacZ) animals were separated by collagenase digestion and individual fibers were stained according to their beta-galactosidase activity. Notably, the collection of ~30 LacZ positive fibers is sufficient to perform an in-depth quantitative proteome analysis. Of note, this approach depends on LacZ positive fibers and wild type fibers without LacZ activity cannot be used as controls. However, heterozygous Mettl21c mice are very similar to wild type controls and show only a very mild phenotype concerning reduced voluntary running activity, which qualifies them for a control.

The mass spectrometric analysis of isolated type I soleus fibers from hetero- and homozygous animals allowed a more focused view on the effects of Mettl21c deficient type I fibers. Interestingly, the inactivation of Mettl21c resulted in reduced levels of many autophagy-related proteins, including the BCL2/Adenovirus E1B 19kDa Interacting Protein 3 (Bnip3) [28], the striated muscle-specific tripartite motif (TRIM) protein 54 (also known as Murf3) [200] and the collagen 6aII (Col6a2) [8]. These candidates were not significantly regulated when comparing intact soleus muscles from wild type and Mettl21c deficient mice. However, a direct association of those autophagy-related proteins to the Mettl21c methyltransferase activity is difficult, since there are no techniques available to conduct an in-depth enrichment of methylated proteins. Thus, future experiments with endogenous antibodies directed against Mettl21c and immunoprecipitations after induction of autophagy will help to identify whether those candidates are direct targets of Mettl21c.

Taken together, the fiber-selective proteome provides a valuable approach for a more focused analysis of specific fiber-types. Analysis of the proteome of Mettl21c mutants suggests a close association of Mettl21c with autophagy marker proteins. Moreover, Mettl21c is a novel marker for

slow type I fibers and the Mettl21c expression can be used as a reporter for other mouse models with a type I fiber dependent muscle phenotype.

4.7. Protein-protein interaction studies unraveled a Mettl21c–VCP interaction

The reduced muscle activity, the increased number of autophagosomes, and the down regulation of several autophagy marker proteins suggests a potential association of Mettl21c to protein degradation mechanisms. Thus, a systematic identification of cofactors and substrates for Mettl21c would help to uncover the function of this novel methyltransferase within the complex autophagy network. Hence, I used SILAC based quantitative interactome screenings coupled to high-resolution mass spectrometry to identify potential substrates for Mettl21c. Immunoprecipitations with tagged Mettl21c fusion proteins identified the chaperone VCP (Valosin-containing-protein) as the most significant interactor. In addition, recombinant Flag-tagged Mettl21c protein isolated from HEK 293T cells was incubated with mouse soleus lysate to identify potential in vivo interaction partners. Interestingly, these experiments confirmed the Mettl21c-VCP interaction as well as several other proteasomal proteins, chaperones, and heat shock proteins. Proteasomal proteins are important for protein quality control, ensuring polypeptide processing, facilitating correct protein folding and changing the physiological state of proteins. In addition, earlier experiments showed that the methylation of chaperones can modulate protein interaction, activity, stability and turnover [248].

Defects in the protein quality control system induce proteotoxic cell stress, which is especially detrimental for the skeletal muscle homeostasis. Important catabolic factors for the balance of the homeostasis are the ubiquitin-proteasome and autophagy-lysosome systems together with the large family of heat shock proteins and chaperons [8, 28].

It has been shown that VCP is an important regulator during the maturation of autophagosomes. Inactivation of VCP results in a defect of lysosomal fusion processes and results in an accumulation of Sequestosome-1/p62 (Sqstm1) positive protein aggregates and non-digested autophagosomes, which are called rimmed vacuoles [70, 235, 249]. Interestingly, in many immunoprecipitation experiments from this study, the autophagic cargo protein Sequestosome-1/p62 was identified as a potential interaction partner of Mettl21c.

So far, several human diseases have been associated with mutations of VCP, like the IBM, the IBMPFD [250, 251], and ALS [252, 253]. The main characteristics of these diseases are muscle weakness and cognitive delay. VCP is an essential protein conserved throughout evolution from archaea to mammals and it is a cytosolic AAA-ATPase. VCP has multiple cellular roles, such as DNA

replication, mitosis, protein degradation, unfolded protein response, endocytosis, membrane fusion, and organelle biogenesis [72, 254].

Notably, VCP activity is tightly regulated through cofactor and substrate binding [255-257]. For example, under regular conditions NSFL1C binds to the N-terminal domain of VCP, reduces the diameter of the p97 hexameric ring and results in the inhibition of the ATPase activity [206, 207]. N-ethylmaleimide-sensitive factor (NSF) is also an ATPase known to be involved in transport vesicle/target membrane fusion and fusions between membrane compartments. NSFL1C binds as a trimer to the hexamer structure of cytosolic VCP and is required for VCP-mediated remodeling of Golgi cisternae from mitotic Golgi fragments.

In order to understand the Mettl21c dependent Vcp activity in more detail, Vcp immunoprecipitation experiments from mouse soleus lysate of Mettl21c$^{-/-}$ and wild type littermates were performed. Consistently, this reverse immunoprecipitation confirmed the interaction of Vcp and Mettl21c and showed in addition the interaction with Nsfl1c/p47. Interestingly, the Vcp-Nsfl1c interaction was drastically downregulated in Mettl21c deficient mice. Mutations in VCP are closely associated with the onset of pathological disorders by altering N-domain and D1 conformations and cause defects in interdomain communications between the neighboring subunits [258]. This changes cofactor binding, leading to substrate accumulation, which might indicate that the Mettl21c dependent methylation coordinates the interaction of the Nsfl1c trimer and Vcp hexamer.

Besides VCP mutations resulting in enhanced cofactor binding, there are also VCP mutant variants, which results in a loss of the NSFL1C interaction. For example, the P137L mutant of VCP, causing the onset of the pathology of IBMPFD patients, completely abolishes the VCP interactions with NSFL1C and also other known interactors like Ufd1 and Npl4 [259]. In the latter case it is assumed that the substrate accumulation resulted in an impairment of transferring degradable proteins to the proteasome system for further processing [259].

Thus, it seems that VCP interactions with its substrates and cofactors are dependent on post-translational modifications and the Mettl21c-promoted trimethylation suggest a new mechanism to modulate VCP activity under regular and disease-related conditions.

Another important finding from the SILAC based quantitative interactome screenings was the interaction between Mettl21c and endogenously expressed Mettl21e, another member of the methyltransferase 21 family. Due to the low Mettl21c and Mettl21e expression in mammalian cells, a co-expression of Flag- and HA-tagged fusion proteins was performed in HEK 293T cells. The observation that Mettl21e was enriched by Mettl21c immunoprecipitation and vice versa suggests a hetero-dimerization of these methyltransferases. Uniprot Blast search analysis revealed a 40%

sequence homology for these two methyltransferases. As indicated from biogps data (biogps.org) both methyltransferases are exclusively expressed in skeletal muscle tissue, suggesting a similar function within the skeletal muscle. A synergistic function has already been described for the mRNA methylation by Mettl3 and Mettl14 [260], the DNA methylation by Dnmt3a and Dnmt3b [223], and the protein methylation by Prmt1 and Prmt4 [261]. Furthermore, the transcriptome analysis revealed enhanced mRNA levels of Mettl21e in Mettl21c deficient animals. This result will be further validated using real-time PCR assays in future experiments.

It remains elusive, whether there is a functional cooperation between Mettl21c and Mettl21e, which will provide an insight into the dynamic methylome of different muscle fiber-types [262-264]. Although Mettl21c$^{-/-}$ animals showed only a mild phenotype under regular conditions, the induction of stress conditions like physical exercise and atrophy revealed that Mettl21e can only partially compensate for the loss of Mettl21c. However, a simultaneous inactivation of both methyltransferases by homologous recombination would be challenging since both genes are localized on chromosome 1 in 200 kb proximity. Alternatively, future experiments with the Crisper-Cas technology inactivating Mettl21e in a Mettl21c$^{-/-}$ background will help to investigate a potential functional compensation between both proteins. Taken together, the quantitative interactome studies showed a potential hetero-dimerization between two methyltransferases and depict a functional role of Mettl21c during protein degradation in slow muscle fibers by the interaction with the known autophagy markers Vcp, Sqstm1 and several heat shock proteins.

4.8. Trimethylation of lysine-315 of VCP facilitates cofactor binding

Coupling in vitro methylation assays to mass spectrometry allows the identification of methylated peptides by the characteristic multiple 14 Da mass shifts. As a novel finding the MTase assay showed that Mettl21c does not only interact but also trimethylates the mammalian VCP on lysine-315 residue. Notably, VCP methylation was reduced when using a SAM binding mutant of Mettl21c. The in vitro SAM assay for the potential interaction partners Sqstm1 and Mettl21e showed no methylation sites in respect to the controls, indicating that Mettl21c specifically trimethylates VCP. In addition, the incubation of Mettl21e and VCP did not show any methylated peptides. Although it is possible that potential Mettl21e dependent methylation sites are not accessible for the mass spectrometric measurements, it is likely that VCP is not a substrate of Mettl21e. Alternatively, it might be possible that a co-factor for Mettl21e was missing. However, the combined incubation of Mettl21c and Mettl21e did not enhance the methylation of VCP.

It has been shown that the family member METTL21D can trimethylate VCP and results in the reduction of the ATPase activity [2, 3]. It might be possible that VCP is methylated by tissue-specific

methyltransferases in order to differentially regulate its cellular function. Since VCP is expressed ubiquitously, a tissue specific methylation might be a potential regulator for the VCP activity [28, 72]. In addition, it has been reported that the deletion or the loss of function of VCP leads to disturbed aggresome formation and defects in the degradation pathways [265-267]. Therefore, the specific regulation by selective methylation might be the explanation for the varying effects in different muscles and muscle fiber-types in response to the same stimulus [1, 268].

Until now the effect of the trimethylation on lysine-315 for the ATPase activity is controversially discussed. VCP consists of two ATPase domains (denoted as D1 and D2) and an N-terminal adaptor domain [269]. The identified trimethylation site, lysine-315, lies in proximity to the Walker B motif of the first ATPase/D1 domain [2]. A recent study suggested that the trimethylation mediated by METTL21D negatively impacts the activity of the ATPase/D1 domain, but it had no effect on the activity of the ATPase/D2 domain [2]. Conversely, two studies showed no changes of the ATPase activity in METTL21D deficient cells compared to wild type control cells [3, 270].

In the presented study the Vcp immunoprecipitation from Mettl21c deficient soleus muscles showed a clear reduction of Vcp trimethylation using a pan-trimethyl antibody. The remaining signal can be explained by the presence of other trimethylation sites on this protein or from trimethylated Vcp originating from fast fibers of the soleus muscle. It was shown that methylation leads to a modulation of cofactor and substrate binding [271, 272]. Hence, the reduced trimethylation of lysine-315 of Vcp results in impaired function due to loss of the inhibitory Nsfl1c/p47 cofactor binding which might enhance the ATPase activity of Vcp in disease models like IBMPFD. The ATPase activity of Vcp is the primary defect causing the pathological phenotype of accumulation of non-degradable proteins [11]. Future aims are the measurement of the ATPase activity of Vcp and the correct formation of the hexameric structure of Vcp in Mettl21c deficient mice in order to detect the in vivo effects of the reduced trimethylation on lysine-315.

Another example for trimethylation is given by several human HSP70 (HSPA) proteins which are trimethylated by METTL21A, another Mettl21 family member, which regulates the affinity of the chaperone for the monomeric and fibrillar forms of the Parkinson disease associated protein alpha-synuclein. This chaperone-targeting by specific methyltransferases suggests the existence of a post-translational modification code for chaperons that was termed “chaperone code” similar to the well-known “histone-code”. Thus, the functional characterization of methylation patterns on proteins involved in protein stability will decipher the pathophysiological mechanisms in several disease models. The reduced trimethylation on lysine-315 of Vcp in Mettl21c deficient mice resulted in the loss of cofactor binding and this suggests that the trimethylation might modulate the ATPase activity of Vcp.

4.9. Accumulation of mitochondria in Mettl21c deficient mice

Autophagy is an important mechanism to clear large protein aggregates and entire organelles, accompanied with an efficient recycling of amino acids [28]. In contrast to the ubiquitin–proteasome system, the formation of autophagosomes enables the cell to degrade whole mitochondria and the depletion of those structures.

The quantitative proteome analysis comparing Mettl21c$^{-/-}$ and wild type littermates under basal conditions revealed a significant upregulation of several mitochondrial proteins, including mitochondrial core proteins of the oxidative phosphorylation complex as well as metabolic components. Mitochondria are crucial for aerobic energy production, regulation of cell signaling, apoptosis and mitophagy. Thus, a correct balance between mitochondrial fusion, mixing of mitochondrial material and the division of mitochondria into smaller components (fission) is essential for the homeostasis and performance of the whole skeletal muscle tissue [273]. A possible explanation for the accumulation of mitochondrial proteins in Mettl21c deficient mice might be a dysregulation in mitochondrial clearance processes. For example, the deletion of important autophagy key players shows dysfunctional elimination of aged and defective mitochondria [274, 275]. Alternatively, the reduced muscle performance in Mettl21c$^{-/-}$ animals might be compensated by an increased level of mitochondrial proteins. Thus, a reduced methylation of so far unknown target proteins may be responsible to regulate the dynamic of mitochondrial biogenesis and degradation. In order to assess mitochondrial ATP synthesis investigation of oxidative phosphorylation of intact cells or isolated mitochondria might help to explain the physiological relevance of Mettl21c for mitochondrial functions. However, Mettl21c expression is restricted to slow fibers and the isolation of mitochondria from intact soleus muscle will result in many mitochondria from fast fibers, which do not express Mettl21c. Alternatively, one could also isolate single fibers and measure first the mitochondrial respiration followed by the analysis of the fiber-type composition by single fiber proteomics.

In contrast to the steady state situation, muscle atrophy induced by denervation, results in an enhanced clearance of mitochondrial proteins in Mettl21c deficient mice compared to denervated control animals. This conflicting result might be caused by a different mechanism that allows mitochondria to commit suicide (termed as mitoptosis). It was shown that mitoptosis is induced by reactive oxygen species (ROS). This causes an opening of the permeability transition pores in the inner mitochondrial membrane. Massive mitoptosis can result in apoptosis, programmed cell death due to release of proapoptotic proteins from the mitochondrial intermembrane space [276].

In addition, cellular stress is accompanied with an enhanced unfolded protein response (UPR) and ubiquitin proteasome system (UPS) activity. Since Vcp is closely associated with the UPR and UPS

function, a reduced level of trimethylation in Mettl21c deficient animals might enhance the degradation of mitochondria under denervated conditions. Reduced Vcp levels induce ER stress and increase the abundance of polyubiquitinated proteins [277]. Although Vcp levels were not changed between control and Mettl21c$^{-/-}$ animals under regular and denervated conditions, reduced trimethylation might be responsible for the faster down regulation of mitochondrial proteins upon neuronal denervation. Thus, further analysis is required to elucidate the link between Mettl21c dependent methylation and programmed organelle degradation under cellular stress conditions.

Another class of proteins, which was strikingly regulated upon denervation, were phagosomal proteins, such as V-type ATPases and proteins from the tubulin network.
The acidic conditions in the autolysosome are provided by activation of hydrolases and are important to degrade the cargo consisting of proteins and organelles. To produce a low pH within the lysosome the activity of several ATP-dependent proton pump V-ATPases is essential and this macro-protein complex consists of eight V1, six V0 and two accessory subunits [278].

The presented study revealed a clear upregulation of 7 ATPase subunits upon sciatic nerve denervation in wild type mice, whereas Mettl21c$^{-/-}$ mutants do not respond to this stimulus and the identified ATPase subunits were not upregulated. This suggests that the formation or correct function of autolysosomes is disturbed in the absence of Mettl21c. Although it is long known that Vcp governs critical steps in the ubiquitin-dependent protein quality control like the delivery of protein substrates to the proteasome, recent finding now have uncovered that Vcp also fulfills important functions in the autophagosomal-lysosomal pathway. One key step in autophagy is the lipidation of the ubiquitin-like modifier LC3/Atg8 which decorates autophagosomal membranes. This is performed with the help of autophagic adaptor molecules like Sqstm1 and Nbr1, which link LC3 to ubiquitin-labeled structures, thereby initiating the recruitment of autophagosomal membranes and engulfment. It was shown that in patients carrying a missense mutation in VCP suffers from impaired autophagy, causing an accumulation of SQSTM1 and lipidated LC3, and inducing LC3-positive vacuoles that failed to mature [279].

Furthermore, in a recent study Johnson et al. gave insights into the molecular mechanism underlying the action of Vcp in the autophagy pathway. They used the fly muscle as a model organism and could show that lysosomes consist of a highly dynamic network of tubules that changes constantly upon a given stimuli. Reduced levels of Vcp resulted in impaired lysosomal vesicle formation and this implicates that the AAA-ATPase Vcp is a key player for the dynamics and integrity of the tubular lysosomal network. Vcp deficient flies show aggregates of damaged

proteins and their ability to move was reduced [71]. Although the quantitative proteome analysis revealed no changes of Vcp in Mettl21c$^{-/-}$, the reduced trimethylation in the absence of Mettl21c might be crucial for the activity of Vcp and hampers the formation and/or activity of autolysosomes.

In order to investigate the impairment of autophagy induction upon denervation of Mettl21c$^{-/-}$ mice in more detail, the lipid association of the autophagy marker protein Microtubule-associated protein light chain 3 (LC3) was used for western blot analysis. During denervation-induced autophagy, cytosolic LC3 (LC3-I) covalently conjugates to phosphatidylethanolamine to generate a lipidated form of LC3 (LC3-II), which displays a higher electrophoretic mobility and is indicative of autophagy [280]. For Mettl21c deficient mice, immunoblot analysis revealed a significant reduction in LC3-II levels compared to lipidated LC3-II levels in the denervated wild type situation. This indicates a reduced induction of the autophagic process. However, a direct association of Mettl21c and LC3 is not known. Importantly, inactivation of key players of the autophagosomal biogenesis like the autophagy related protein Atg7 also abolishes LC3 processing. Atg7 is a key player in the biogenesis of autophagy and functions as an E1-like ligase, which conjugates Atg5 to Atg12, a necessary step for the formation of a functional autophagosome. Furthermore, it converts LC3 (Atg8) from an immature, cytosolic form to a mature autophagosomal membrane protein by adding a phosphatidylethanolamine group [281].

While loss of function of Mettl21c in the mouse resulted in autophagic impairment, gain-of-function-studies by overexpressing Mettl21c in HEK 293T cells have also shown to modulate autophagy. In this complementary cell culture assay, control cells were compared to Flag-tagged Mettl21c overexpressed cells. In order to monitor autophagic flux, the lipidation of LC3 as well as the expression of the autophagosomal cargo proteins SQSTM1 and VCP was analyzed. In order to induce autophagy rapamycin was used, a lipophilic macrolide antibiotic that is a well-established and potent inducer of autophagy. Autophagy is negatively regulated by mTOR, a kinase that senses the availability of nutrients and energy and integrates inputs from growth factors and stress signaling. Rapamycin functions as an allosteric inhibitor of the kinase activity of mTOR [48]. In addition, the combinatory treatment of Rapamycin, an autophagy inducer, and Bafilomycin A1, that neutralizes lysosomal acidification and stalls autophagy, results in accumulation of autophagosomes by blocking autophagosome-lysosome fusion. This technique is named “autophagometer” as it provides one with static levels of endogenous LC3-II, and helps to render misinterpretations due to possible alteration in LC3-II levels upon autophagic induction [282].

As a clear indication for the upregulation of autophagy in control and Mettl21c overexpression cells, lipidated LC3-II and SQSTM1 was found to be accumulated after the treatment with

Rapamycin and even more after the combinatory treatment with Rapamycin and Bafilomycin A1; while expression of VCP was not affected. Interestingly, the accumulation of LC3 and SQSTM1 was more pronounced in Mettl21c overexpressing cells.

Strikingly, the accumulation of SQSTM1, an indicator for ubiquitinated proteins [77], is usually described as inhibition of autophagy [48]. In our cell culture based assay it seems that the expression level of SQSTM1 is restored. Similar results were obtained in other studies indicating that upon starvation the level of SQSTM1 does not always inversely correlate with autophagic activity. This suggests that three factors, autophagic degradation, transcriptional upregulation, and availability of lysosomal-derived amino acids lead to restoration of SQSTM1 during autophagy [283]. Furthermore, it was shown that cells can use the key autophagic cargo adaptor protein SQSTM1 itself to regulate autophagic activity. Overexpression of SQSTM1 significantly increases the basal level of autophagy in mammalian cells by disrupting the association between Bcl-2 and Beclin 1 [284].

Enhanced autophagy activity was also found after overexpression of the two autophagic key players Atg7 and Atg5, which are essential for the autophagosome formation [281, 285]. Enhanced autophagy proved to be beneficial for the mammalian lifespan by presumably reducing misfolded proteins and aggregates, improving insulin sensitivity and reducing oxidative stress. For future experiments, it would be of great interest to elucidate whether a moderate Mettl21c overexpression functions beneficial for a balanced homeostasis of the skeletal muscle and thereby improves the physical activity in mammalians. Taken together, this gain-of-function assay proved that Mettl21c is able to regulate the autophagic flux in cell culture.

4.10. Conclusions

Muscle can rapidly respond to physiological changes by fine-tuning the balance between catabolic and anabolic processes, a process known as muscle plasticity. Autophagy is a pathway by which cytoplasmic components including macromolecules and organelles are degraded by the autophagosome-lysosome system. The proper regulation of autophagy flux is important for whole body homeostasis under basal and stress conditions. Skeletal muscle acts as an indispensable metabolic center that responds to global energy demands. Defective and excessive autophagy is both referred to be harmful and is associated to several human muscle diseases and the understanding of the molecular mechanisms that control autophagy in skeletal muscle has only recently begun to emerge.

The proposed study demonstrates the phenotypic consequences of slow-muscle specific Mettl21c deletion in mice. The inactivation results in the physiological impairment of muscular endurance and the accumulation of autophagic vacuoles. In addition, Mettl21c deficient mice suffer from a lysosomal defect indicated by the occurrence of impaired lysosomal vesicles after denervation-induced atrophy. Dysfunctional autophagy is associated with many pathologies, where impaired muscle performance and health is the first diagnose.

In this study Vcp was identified as a novel substrate for Mettl21c, which trimethylates Vcp at lysine-315. The molecular mechanism, underlying the observed effects on the impairment of autophagic flux in slow-twitch muscle fibers in mice deficient for Mettl21c, is probably based on reduced trimethylation of Vcp on lysine-315. This site lies in close proximity to the Walker B motif of the ATPase/D1 domain. The reduced trimethylation of Vcp in slow-twitch muscle fibers might results in the loss of cofactor binding, like it was shown here for the interaction of Vcp and the inhibitory cofactor Nsfl1c/p47. In addition, alterations in cofactor binding might modulate the ATPase activity of VCP. Several disease models like IBMPFD and ALS show that the ATPase activity of VCP is the primary defect causing the pathological phenotype of accumulation of non-degradable proteins [11].

Hence, the understanding about fiber-type specific regulation of autophagy will help to understand muscle homeostasis as well as the onset of degenerative diseases in humans that are associated with disrupted VCP function, resulting in muscle weakness as a first symptom. Thus, the tissue specific expression of methyltransferases defines a novel mechanism regulating proteostasis in skeletal muscle tissue and the extension of this study will help to elucidate the complex network of protein methylation and muscle loss under diseased conditions. In addition, the dissection of the autophagy pathway and its role in metabolic disorders and myopathies is of great clinical relevance and has great therapeutic potential.

5. References

1. Schiaffino, S., et al., *Mechanisms regulating skeletal muscle growth and atrophy.* FEBS J, 2013. **280**(17): p. 4294-314.
2. Cloutier, P., et al., *A newly uncovered group of distantly related lysine methyltransferases preferentially interact with molecular chaperones to regulate their activity.* PLoS Genet, 2013. **9**(1): p. e1003210.
3. Kernstock, S., et al., *Lysine methylation of VCP by a member of a novel human protein methyltransferase family.* Nat Commun, 2012. **3**: p. 1038.
4. Schuberth, C. and A. Buchberger, *UBX domain proteins: major regulators of the AAA ATPase Cdc48/p97.* Cell Mol Life Sci, 2008. **65**(15): p. 2360-71.
5. Yoshihara, T., et al., *Ultrastructural and histochemical study of the motor end plates of the intrinsic laryngeal muscles in amyotrophic lateral sclerosis.* Ultrastruct Pathol, 1998. **22**(2): p. 121-6.
6. Disatnik, M.H., G. Buraggi, and D. Mochly-Rosen, *Localization of protein kinase C isozymes in cardiac myocytes.* Exp Cell Res, 1994. **210**(2): p. 287-97.
7. Sim, A.T. and J.D. Scott, *Targeting of PKA, PKC and protein phosphatases to cellular microdomains.* Cell Calcium, 1999. **26**(5): p. 209-17.
8. Grumati, P., et al., *Autophagy is defective in collagen VI muscular dystrophies, and its reactivation rescues myofiber degeneration.* Nat Med, 2010. **16**(11): p. 1313-20.
9. Grumati, P., et al., *Physical exercise stimulates autophagy in normal skeletal muscles but is detrimental for collagen VI-deficient muscles.* Autophagy, 2011. **7**(12): p. 1415-23.
10. He, C., et al., *Exercise-induced BCL2-regulated autophagy is required for muscle glucose homeostasis.* Nature, 2012. **481**(7382): p. 511-5.
11. Manno, A., et al., *Enhanced ATPase activities as a primary defect of mutant valosin-containing proteins that cause inclusion body myopathy associated with Paget disease of bone and frontotemporal dementia.* Genes Cells, 2010. **15**(8): p. 911-22.
12. Janssens, A., et al., *Estimation of post-operative forced expiratory volume by functional respiratory imaging.* Eur Respir J, 2015. **45**(2): p. 544-6.
13. Burkholder, T.J., et al., *Relationship between muscle fiber-types and sizes and muscle architectural properties in the mouse hindlimb.* J Morphol, 1994. **221**(2): p. 177-90.
14. Morgan, J.E. and T.A. Partridge, *Muscle satellite cells.* Int J Biochem Cell Biol, 2003. **35**(8): p. 1151-6.
15. Frontera, W.R. and J. Ochala, *Skeletal muscle: a brief review of structure and function.* Calcif Tissue Int, 2015. **96**(3): p. 183-95.
16. Staron, R.S., *Human skeletal muscle fiber-types: delineation, development, and distribution.* Can J Appl Physiol, 1997. **22**(4): p. 307-27.
17. Pette, D., H. Peuker, and R.S. Staron, *The impact of biochemical methods for single muscle fibre analysis.* Acta Physiol Scand, 1999. **166**(4): p. 261-77.
18. Schiaffino, S. and C. Reggiani, *Fiber-types in mammalian skeletal muscles.* Physiol Rev, 2011. **91**(4): p. 1447-531.
19. Drexler, H.C., et al., *On marathons and Sprints: an integrated quantitative proteomics and transcriptomics analysis of differences between slow and fast muscle fibers.* Mol Cell Proteomics, 2012. **11**(6): p. M111 010801.
20. Caiozzo, V.J., et al., *Single-fiber myosin heavy chain polymorphism: how many patterns and what proportions?* Am J Physiol Regul Integr Comp Physiol, 2003. **285**(3): p. R570-80.
21. Termin, A., R.S. Staron, and D. Pette, *Myosin heavy chain isoforms in histochemically defined fiber-types of rat muscle.* Histochemistry, 1989. **92**(6): p. 453-7.
22. Izumo, S., B. Nadal-Ginard, and V. Mahdavi, *All members of the MHC multigene family respond to thyroid hormone in a highly tissue-specific manner.* Science, 1986. **231**(4738): p. 597-600.

23. Aravamudan, B., et al., *Denervation effects on myonuclear domain size of rat diaphragm fibers.* J Appl Physiol (1985), 2006. **100**(5): p. 1617-22.
24. Li, J.B. and A.L. Goldberg, *Effects of food deprivation on protein synthesis and degradation in rat skeletal muscles.* Am J Physiol, 1976. **231**(2): p. 441-8.
25. Paul, A.C. and N. Rosenthal, *Different modes of hypertrophy in skeletal muscle fibers.* J Cell Biol, 2002. **156**(4): p. 751-60.
26. Biolo, G., T. Cederholm, and M. Muscaritoli, *Muscle contractile and metabolic dysfunction is a common feature of sarcopenia of aging and chronic diseases: from sarcopenic obesity to cachexia.* Clin Nutr, 2014. **33**(5): p. 737-48.
27. Muscaritoli, M., et al., *Consensus definition of sarcopenia, cachexia and pre-cachexia: joint document elaborated by Special Interest Groups (SIG) "cachexia-anorexia in chronic wasting diseases" and "nutrition in geriatrics".* Clin Nutr, 2010. **29**(2): p. 154-9.
28. Sandri, M., *Autophagy in skeletal muscle.* FEBS Lett, 2010. **584**(7): p. 1411-6.
29. Sandri, M., *Autophagy in health and disease. 3. Involvement of autophagy in muscle atrophy.* Am J Physiol Cell Physiol, 2010. **298**(6): p. C1291-7.
30. Sacheck, J.M., et al., *Rapid disuse and denervation atrophy involve transcriptional changes similar to those of muscle wasting during systemic diseases.* FASEB J, 2007. **21**(1): p. 140-55.
31. Li, W., et al., *A ubiquitin ligase transfers preformed polyubiquitin chains from a conjugating enzyme to a substrate.* Nature, 2007. **446**(7133): p. 333-7.
32. Hoeller, D., et al., *E3-independent monoubiquitination of ubiquitin-binding proteins.* Mol Cell, 2007. **26**(6): p. 891-8.
33. Passmore, L.A. and D. Barford, *Getting into position: the catalytic mechanisms of protein ubiquitylation.* Biochem J, 2004. **379**(Pt 3): p. 513-25.
34. Murton, A.J., D. Constantin, and P.L. Greenhaff, *The involvement of the ubiquitin proteasome system in human skeletal muscle remodelling and atrophy.* Biochim Biophys Acta, 2008. **1782**(12): p. 730-43.
35. Solomon, V. and A.L. Goldberg, *Importance of the ATP-ubiquitin-proteasome pathway in the degradation of soluble and myofibrillar proteins in rabbit muscle extracts.* J Biol Chem, 1996. **271**(43): p. 26690-7.
36. Du, J., et al., *Activation of caspase-3 is an initial step triggering accelerated muscle proteolysis in catabolic conditions.* J Clin Invest, 2004. **113**(1): p. 115-23.
37. Williams, A.B., et al., *Sepsis stimulates release of myofilaments in skeletal muscle by a calcium-dependent mechanism.* FASEB J, 1999. **13**(11): p. 1435-43.
38. Wing, S.S., A.L. Haas, and A.L. Goldberg, *Increase in ubiquitin-protein conjugates concomitant with the increase in proteolysis in rat skeletal muscle during starvation and atrophy denervation.* Biochem J, 1995. **307 (Pt 3)**: p. 639-45.
39. Medina, R., S.S. Wing, and A.L. Goldberg, *Increase in levels of polyubiquitin and proteasome mRNA in skeletal muscle during starvation and denervation atrophy.* Biochem J, 1995. **307 (Pt 3)**: p. 631-7.
40. Tiao, G.M., et al., *Identification of Altered Gene Expression in Skeletal Muscle during Sepsis Using Differential Display.* J Surg Res, 1996. **64**(1): p. 63-7.
41. Tawa, N.E., Jr., R. Odessey, and A.L. Goldberg, *Inhibitors of the proteasome reduce the accelerated proteolysis in atrophying rat skeletal muscles.* J Clin Invest, 1997. **100**(1): p. 197-203.
42. Combaret, L., et al., *Manipulation of the ubiquitin-proteasome pathway in cachexia: pentoxifylline suppresses the activation of 20S and 26S proteasomes in muscles from tumor-bearing rats.* Mol Biol Rep, 1999. **26**(1-2): p. 95-101.
43. Combaret, L., et al., *Torbafylline (HWA 448) inhibits enhanced skeletal muscle ubiquitin-proteasome-dependent proteolysis in cancer and septic rats.* Biochem J, 2002. **361**(Pt 2): p. 185-92.
44. Reggiori, F., et al., *Autophagy: more than a nonselective pathway.* Int J Cell Biol, 2012. **2012**: p. 219625.

45. Lippai, M. and P. Low, *The role of the selective adaptor p62 and ubiquitin-like proteins in autophagy.* Biomed Res Int, 2014. **2014**: p. 832704.
46. Mizushima, N., T. Yoshimori, and Y. Ohsumi, *The role of Atg proteins in autophagosome formation.* Annu Rev Cell Dev Biol, 2011. **27**: p. 107-32.
47. Ding, W.X., S. Manley, and H.M. Ni, *The emerging role of autophagy in alcoholic liver disease.* Exp Biol Med (Maywood), 2011. **236**(5): p. 546-56.
48. Klionsky, D.J., et al., *Guidelines for the use and interpretation of assays for monitoring autophagy in higher eukaryotes.* Autophagy, 2008. **4**(2): p. 151-75.
49. Boya, P., F. Reggiori, and P. Codogno, *Emerging regulation and functions of autophagy.* Nat Cell Biol, 2013. **15**(7): p. 713-20.
50. Funderburk, S.F., Q.J. Wang, and Z. Yue, *The Beclin 1-VPS34 complex--at the crossroads of autophagy and beyond.* Trends Cell Biol, 2010. **20**(6): p. 355-62.
51. Furuya, N., et al., *The evolutionarily conserved domain of Beclin 1 is required for Vps34 binding, autophagy and tumor suppressor function.* Autophagy, 2005. **1**(1): p. 46-52.
52. Fimia, G.M., et al., *Ambra1 regulates autophagy and development of the nervous system.* Nature, 2007. **447**(7148): p. 1121-5.
53. Liang, C., et al., *Autophagic and tumour suppressor activity of a novel Beclin1-binding protein UVRAG.* Nat Cell Biol, 2006. **8**(7): p. 688-99.
54. Zhong, Y., Q.J. Wang, and Z. Yue, *Atg14L and Rubicon: yin and yang of Beclin 1-mediated autophagy control.* Autophagy, 2009. **5**(6): p. 890-1.
55. Sun, Q., et al., *The RUN domain of rubicon is important for hVps34 binding, lipid kinase inhibition, and autophagy suppression.* J Biol Chem, 2011. **286**(1): p. 185-91.
56. Seglen, P.O. and P.B. Gordon, *3-Methyladenine: specific inhibitor of autophagic/lysosomal protein degradation in isolated rat hepatocytes.* Proc Natl Acad Sci U S A, 1982. **79**(6): p. 1889-92.
57. Takats, S., et al., *Autophagosomal Syntaxin17-dependent lysosomal degradation maintains neuronal function in Drosophila.* J Cell Biol, 2013. **201**(4): p. 531-9.
58. Itakura, E., C. Kishi-Itakura, and N. Mizushima, *The hairpin-type tail-anchored SNARE syntaxin 17 targets to autophagosomes for fusion with endosomes/lysosomes.* Cell, 2012. **151**(6): p. 1256-69.
59. Hegedus, K., et al., *Evolutionarily conserved role and physiological relevance of a STX17/Syx17 (syntaxin 17)-containing SNARE complex in autophagosome fusion with endosomes and lysosomes.* Autophagy, 2013. **9**(10): p. 1642-6.
60. Wani, W.Y., et al., *Regulation of autophagy by protein post-translational modification.* Lab Invest, 2015. **95**(1): p. 14-25.
61. Masiero, E., et al., *Autophagy is required to maintain muscle mass.* Cell Metab, 2009. **10**(6): p. 507-15.
62. Masiero, E. and M. Sandri, *Autophagy inhibition induces atrophy and myopathy in adult skeletal muscles.* Autophagy, 2010. **6**(2): p. 307-9.
63. Raben, N., et al., *Suppression of autophagy in skeletal muscle uncovers the accumulation of ubiquitinated proteins and their potential role in muscle damage in Pompe disease.* Hum Mol Genet, 2008. **17**(24): p. 3897-908.
64. Pankiv, S., et al., *p62/SQSTM1 binds directly to Atg8/LC3 to facilitate degradation of ubiquitinated protein aggregates by autophagy.* J Biol Chem, 2007. **282**(33): p. 24131-45.
65. Ciani, B., et al., *Structure of the ubiquitin-associated domain of p62 (SQSTM1) and implications for mutations that cause Paget's disease of bone.* J Biol Chem, 2003. **278**(39): p. 37409-12.
66. Rogov, V., et al., *Interactions between autophagy receptors and ubiquitin-like proteins form the molecular basis for selective autophagy.* Mol Cell, 2014. **53**(2): p. 167-78.
67. Fujita, N., et al., *Recruitment of the autophagic machinery to endosomes during infection is mediated by ubiquitin.* J Cell Biol, 2013. **203**(1): p. 115-28.

68. Nagy, P., et al., *Different effects of Atg2 and Atg18 mutations on Atg8a and Atg9 trafficking during starvation in Drosophila.* FEBS Lett, 2014. **588**(3): p. 408-13.
69. Arndt, V., et al., *Chaperone-assisted selective autophagy is essential for muscle maintenance.* Curr Biol, 2010. **20**(2): p. 143-8.
70. Ju, J.S., et al., *Valosin-containing protein (VCP) is required for autophagy and is disrupted in VCP disease.* J Cell Biol, 2009. **187**(6): p. 875-88.
71. Johnson, A.E., et al., *VCP-dependent muscle degeneration is linked to defects in a dynamic tubular lysosomal network in vivo.* Elife, 2015. **4**.
72. Halawani, D. and M. Latterich, *p97: The cell's molecular purgatory?* Mol Cell, 2006. **22**(6): p. 713-7.
73. Abramzon, Y., et al., *Valosin-containing protein (VCP) mutations in sporadic amyotrophic lateral sclerosis.* Neurobiol Aging, 2012. **33**(9): p. 2231 e1-2231 e6.
74. Clemen, C.S., et al., *Strumpellin is a novel valosin-containing protein binding partner linking hereditary spastic paraplegia to protein aggregation diseases.* Brain, 2010. **133**(10): p. 2920-41.
75. Liewluck, T., et al., *A novel VCP mutation underlies scapuloperoneal muscular dystrophy and dropped head syndrome featuring lobulated fibers.* Muscle Nerve, 2014. **50**(2): p. 295-9.
76. Gonzalez, M.A., et al., *A novel mutation in VCP causes Charcot-Marie-Tooth Type 2 disease.* Brain, 2014. **137**(Pt 11): p. 2897-902.
77. Pankiv, S., et al., *p62/SQSTM1 binds directly to Atg8/LC3 to facilitate degradation of ubiquitinated protein aggregates by autophagy.* Journal of Biological Chemistry, 2007. **282**(33): p. 24131-24145.
78. Kim, P.K., et al., *Ubiquitin signals autophagic degradation of cytosolic proteins and peroxisomes.* Proc Natl Acad Sci U S A, 2008. **105**(52): p. 20567-74.
79. Kraft, C., et al., *Mature ribosomes are selectively degraded upon starvation by an autophagy pathway requiring the Ubp3p/Bre5p ubiquitin protease.* Nat Cell Biol, 2008. **10**(5): p. 602-10.
80. Dargemont, C. and B. Ossareh-Nazari, *Cdc48/p97, a key actor in the interplay between autophagy and ubiquitin/proteasome catabolic pathways.* Biochim Biophys Acta, 2012. **1823**(1): p. 138-44.
81. Cantoni, G.L., *Methylation of nicotinamide with soluble enzyme system from rat liver.* J Biol Chem, 1951. **189**(1): p. 203-16.
82. Ambler, R.P. and M.W. Rees, *Epsilon-N-Methyl-lysine in bacterial flagellar protein.* Nature, 1959. **184**: p. 56-7.
83. Murray, K., *The Occurrence of Epsilon-N-Methyl Lysine in Histones.* Biochemistry, 1964. **3**: p. 10-5.
84. Gold, M., J. Hurwitz, and M. Anders, *The enzymatic methylation of RNA and DNA.* Biochem Biophys Res Commun, 1963. **11**: p. 107-14.
85. Petrossian, T.C. and S.G. Clarke, *Uncovering the human methyltransferasome.* Mol Cell Proteomics, 2011. **10**(1): p. M110 000976.
86. Lei, H., et al., *De novo DNA cytosine methyltransferase activities in mouse embryonic stem cells.* Development, 1996. **122**(10): p. 3195-205.
87. Komatsu, S., et al., *Overexpression of SMYD2 relates to tumor cell proliferation and malignant outcome of esophageal squamous cell carcinoma.* Carcinogenesis, 2009. **30**(7): p. 1139-46.
88. Cho, H.S., et al., *RB1 methylation by SMYD2 enhances cell cycle progression through an increase of RB1 phosphorylation.* Neoplasia, 2012. **14**(6): p. 476-86.
89. Luo, J., et al., *Aberrant methylation profile of 14-3-3 sigma and its reduced transcription/expression levels in Chinese sporadic female breast carcinogenesis.* Med Oncol, 2010. **27**(3): p. 791-7.

90. Kondo, Y., et al., *Alterations of DNA methylation and histone modifications contribute to gene silencing in hepatocellular carcinomas.* Hepatol Res, 2007. **37**(11): p. 974-83.
91. Schulze, A., et al., *Creatine deficiency syndrome caused by guanidinoacetate methyltransferase deficiency: diagnostic tools for a new inborn error of metabolism.* J Pediatr, 1997. **131**(4): p. 626-31.
92. Donlin, L.T., et al., *Smyd2 controls cytoplasmic lysine methylation of Hsp90 and myofilament organization.* Genes Dev, 2012. **26**(2): p. 114-9.
93. Schubert, H.L., J.D. Phillips, and C.P. Hill, *Structures along the catalytic pathway of PrmC/HemK, an N5-glutamine AdoMet-dependent methyltransferase.* Biochemistry, 2003. **42**(19): p. 5592-9.
94. Rathert, P., et al., *Specificity of protein lysine methyltransferases and methods for detection of lysine methylation of non-histone proteins.* Mol Biosyst, 2008. **4**(12): p. 1186-90.
95. Sampath, S.C., et al., *Methylation of a histone mimic within the histone methyltransferase G9a regulates protein complex assembly.* Mol Cell, 2007. **27**(4): p. 596-608.
96. Hegazi, M.F., R.T. Borchard, and R.L. Schowen, *Letter: SN2-like transition state for methyl transfer catalyzed by catechol-O-methyl-transferase.* J Am Chem Soc, 1976. **98**(10): p. 3048-9.
97. Mato, J.M., et al., *S-adenosylmethionine synthesis: molecular mechanisms and clinical implications.* Pharmacol Ther, 1997. **73**(3): p. 265-80.
98. Williams, K.T. and K.L. Schalinske, *Homocysteine metabolism and its relation to health and disease.* Biofactors, 2010. **36**(1): p. 19-24.
99. Perna, A.F., et al., *Homocysteine, a new cardiovascular risk factor, is also a powerful uremic toxin.* J Nephrol, 1999. **12**(4): p. 230-40.
100. Grove, T.L., et al., *A radically different mechanism for S-adenosylmethionine-dependent methyltransferases.* Science, 2011. **332**(6029): p. 604-7.
101. Rowe, P.M., L.S. Wright, and F.L. Siegel, *Calmodulin N-methyltransferase. Partial purification and characterization.* J Biol Chem, 1986. **261**(15): p. 7060-9.
102. Magnani, R., et al., *Calmodulin methyltransferase is an evolutionarily conserved enzyme that trimethylates Lys-115 in calmodulin.* Nat Commun, 2010. **1**: p. 43.
103. Zhang, X., H. Wen, and X. Shi, *Lysine methylation: beyond histones.* Acta Biochim Biophys Sin (Shanghai), 2012. **44**(1): p. 14-27.
104. Greer, E.L. and Y. Shi, *Histone methylation: a dynamic mark in health, disease and inheritance.* Nat Rev Genet, 2012. **13**(5): p. 343-57.
105. Klein, R.R. and R.L. Houtz, *Cloning and developmental expression of pea ribulose-1,5-bisphosphate carboxylase/oxygenase large subunit N-methyltransferase.* Plant Mol Biol, 1995. **27**(2): p. 249-61.
106. Clarke, S.G., *Protein methylation at the surface and buried deep: thinking outside the histone box.* Trends Biochem Sci, 2013. **38**(5): p. 243-52.
107. Jenuwein, T., *The epigenetic magic of histone lysine methylation.* FEBS J, 2006. **273**(14): p. 3121-35.
108. Sims, R.J., 3rd, K. Nishioka, and D. Reinberg, *Histone lysine methylation: a signature for chromatin function.* Trends Genet, 2003. **19**(11): p. 629-39.
109. Shi, Y., et al., *Histone demethylation mediated by the nuclear amine oxidase homolog LSD1.* Cell, 2004. **119**(7): p. 941-53.
110. Allis, C.D., et al., *New nomenclature for chromatin-modifying enzymes.* Cell, 2007. **131**(4): p. 633-6.
111. Cloos, P.A., et al., *Erasing the methyl mark: histone demethylases at the center of cellular differentiation and disease.* Genes Dev, 2008. **22**(9): p. 1115-40.
112. Santos-Rosa, H., et al., *Active genes are tri-methylated at K4 of histone H3.* Nature, 2002. **419**(6905): p. 407-11.
113. Lachner, M. and T. Jenuwein, *The many faces of histone lysine methylation.* Curr Opin Cell Biol, 2002. **14**(3): p. 286-98.

114. Lachner, M., et al., *Trilogies of histone lysine methylation as epigenetic landmarks of the eukaryotic genome.* Cold Spring Harb Symp Quant Biol, 2004. **69**: p. 209-18.
115. Reinberg, D., et al., *Steps toward understanding the inheritance of repressive methyl-lysine marks in histones.* Cold Spring Harb Symp Quant Biol, 2004. **69**: p. 171-82.
116. Kruse, J.P. and W. Gu, *Modes of p53 regulation.* Cell, 2009. **137**(4): p. 609-22.
117. Chuikov, S., et al., *Regulation of p53 activity through lysine methylation.* Nature, 2004. **432**(7015): p. 353-60.
118. Shi, X., et al., *Modulation of p53 function by SET8-mediated methylation at lysine 382.* Mol Cell, 2007. **27**(4): p. 636-46.
119. Kouskouti, A., et al., *Gene-specific modulation of TAF10 function by SET9-mediated methylation.* Mol Cell, 2004. **14**(2): p. 175-82.
120. Kunizaki, M., et al., *The lysine 831 of vascular endothelial growth factor receptor 1 is a novel target of methylation by SMYD3.* Cancer Res, 2007. **67**(22): p. 10759-65.
121. Just, S., et al., *The myosin-interacting protein SMYD1 is essential for sarcomere organization.* J Cell Sci, 2011. **124**(Pt 18): p. 3127-36.
122. Diehl, F., et al., *Cardiac deletion of Smyd2 is dispensable for mouse heart development.* PLoS One, 2010. **5**(3): p. e9748.
123. Oh, S.H. and D.M. Roberts, *Analysis of the state of post-translational calmodulin methylation in developing pea plants.* Plant Physiol, 1990. **93**(3): p. 880-7.
124. Roberts, D.M., et al., *Trimethyllysine and protein function. Effect of methylation and mutagenesis of lysine 115 of calmodulin on NAD kinase activation.* J Biol Chem, 1986. **261**(4): p. 1491-4.
125. Lee, J.Y., et al., *Novel Function of Lysine Methyltransferase G9a in the Regulation of Sox2 Protein Stability.* PLoS One, 2015. **10**(10): p. e0141118.
126. Park, J.H., et al., *Protein arginine methyltransferase 5 is a key regulator of the MYCN oncoprotein in neuroblastoma cells.* Mol Oncol, 2015. **9**(3): p. 617-27.
127. Lee, J.C., et al., *Protein L-isoaspartyl methyltransferase regulates p53 activity.* Nat Commun, 2012. **3**: p. 927.
128. Naeem, H., et al., *The activity and stability of the transcriptional coactivator p/CIP/SRC-3 are regulated by CARM1-dependent methylation.* Mol Cell Biol, 2007. **27**(1): p. 120-34.
129. Shen, E.C., et al., *Arginine methylation facilitates the nuclear export of hnRNP proteins.* Genes Dev, 1998. **12**(5): p. 679-91.
130. Smith, W.A., et al., *Arginine methylation of RNA helicase a determines its subcellular localization.* J Biol Chem, 2004. **279**(22): p. 22795-8.
131. Cho, H.S., et al., *Enhanced HSP70 lysine methylation promotes proliferation of cancer cells through activation of Aurora kinase B.* Nat Commun, 2012. **3**: p. 1072.
132. Lee, Y.H., et al., *Regulation of coactivator complex assembly and function by protein arginine methylation and demethylimination.* Proc Natl Acad Sci U S A, 2005. **102**(10): p. 3611-6.
133. Cheng, D., et al., *The arginine methyltransferase CARM1 regulates the coupling of transcription and mRNA processing.* Mol Cell, 2007. **25**(1): p. 71-83.
134. Mazur, P.K., et al., *SMYD3 links lysine methylation of MAP3K2 to Ras-driven cancer.* Nature, 2014. **510**(7504): p. 283-7.
135. Cazanove, O., et al., *Methylation of Xilf3 by Xprmt1b alters its DNA, but not RNA, binding activity.* Biochemistry, 2008. **47**(32): p. 8350-7.
136. Petrossian, T. and S. Clarke, *Bioinformatic Identification of Novel Methyltransferases.* Epigenomics, 2009. **1**(1): p. 163-175.
137. Tkaczuk, K.L., et al., *Structural and evolutionary bioinformatics of the SPOUT superfamily of methyltransferases.* BMC Bioinformatics, 2007. **8**: p. 73.
138. Wlodarski, T., et al., *Comprehensive structural and substrate specificity classification of the Saccharomyces cerevisiae methyltransferome.* PLoS One, 2011. **6**(8): p. e23168.

139. Katz, J.E., M. Dlakic, and S. Clarke, *Automated identification of putative methyltransferases from genomic open reading frames.* Mol Cell Proteomics, 2003. **2**(8): p. 525-40.
140. Kagan, R.M. and S. Clarke, *Widespread occurrence of three sequence motifs in diverse S-adenosylmethionine-dependent methyltransferases suggests a common structure for these enzymes.* Arch Biochem Biophys, 1994. **310**(2): p. 417-27.
141. Aktas, M., et al., *S-adenosylmethionine-binding properties of a bacterial phospholipid N-methyltransferase.* J Bacteriol, 2011. **193**(14): p. 3473-81.
142. Hanzelmann, P. and H. Schindelin, *The structural and functional basis of the p97/valosin-containing protein (VCP)-interacting motif (VIM): mutually exclusive binding of cofactors to the N-terminal domain of p97.* J Biol Chem, 2011. **286**(44): p. 38679-90.
143. Imbert, G., et al., *Cloning of the gene for spinocerebellar ataxia 2 reveals a locus with high sensitivity to expanded CAG/glutamine repeats.* Nat Genet, 1996. **14**(3): p. 285-91.
144. Thompson, T.G., et al., *A novel cDNA detects homozygous microdeletions in greater than 50% of type I spinal muscular atrophy patients.* Nat Genet, 1995. **9**(1): p. 56-62.
145. Dewey, C.M., et al., *TDP-43 aggregation in neurodegeneration: are stress granules the key?* Brain Res, 2012. **1462**: p. 16-25.
146. Abe, K., et al., *Induction of nitrotyrosine-like immunoreactivity in the lower motor neuron of amyotrophic lateral sclerosis.* Neurosci Lett, 1995. **199**(2): p. 152-4.
147. Shaw, P.J., et al., *Oxidative damage to protein in sporadic motor neuron disease spinal cord.* Ann Neurol, 1995. **38**(4): p. 691-5.
148. Huang, J., et al., *METTL21C is a potential pleiotropic gene for osteoporosis and sarcopenia acting through the modulation of the NF-kappaB signaling pathway.* J Bone Miner Res, 2014. **29**(7): p. 1531-40.
149. Jakobsson, M.E., et al., *Saccharomyces cerevisiae Eukaryotic Elongation Factor 1A (eEF1A) Is Methylated at Lys-390 by a METTL21-Like Methyltransferase.* PLoS One, 2015. **10**(6): p. e0131426.
150. Couttas, T.A., et al., *Methylation of translation-associated proteins in Saccharomyces cerevisiae: Identification of methylated lysines and their methyltransferases.* Proteomics, 2012. **12**(7): p. 960-72.
151. Lipson, R.S., K.J. Webb, and S.G. Clarke, *Two novel methyltransferases acting upon eukaryotic elongation factor 1A in Saccharomyces cerevisiae.* Arch Biochem Biophys, 2010. **500**(2): p. 137-43.
152. Dzialo, M.C., et al., *A new type of protein lysine methyltransferase trimethylates Lys-79 of elongation factor 1A.* Biochem Biophys Res Commun, 2014. **455**(3-4): p. 382-9.
153. Aebersold, R. and M. Mann, *Mass spectrometry-based proteomics.* Nature, 2003. **422**(6928): p. 198-207.
154. Altelaar, A.F., J. Munoz, and A.J. Heck, *Next-generation proteomics: towards an integrative view of proteome dynamics.* Nat Rev Genet, 2013. **14**(1): p. 35-48.
155. Cutillas, P.R. and J.F. Timms, *Approaches and applications of quantitative LC-MS for proteomics and activitomics.* Methods Mol Biol, 2010. **658**: p. 3-17.
156. Karas, M., D. Bachmann, and F. Hillenkamp, *Influence of the wavelength in high-irradiance ultraviolet laser desorption mass spectrometry of organic molecules , . 57(14): p. 2935-2939.* Analytical Chemistry, 1985. **57**(14): p. 2935-2939.
157. Dole, M.M., L. L.; Hines, R. L.; Mobley, R. C.; Ferguson, L. D.; Alice, M. B., *Molecular beams of macroions.* The Journal of Chemical Physics. **49**(5): p. 2240-2249.
158. Fenn, J.B., et al., *Electrospray ionization for mass spectrometry of large biomolecules.* Science, 1989. **246**(4926): p. 64-71.
159. Wilkins, M.R., et al., *From proteins to proteomes: large scale protein identification by two-dimensional electrophoresis and amino acid analysis.* Biotechnology (N Y), 1996. **14**(1): p. 61-5.
160. Wisniewski, J.R., et al., *Universal sample preparation method for proteome analysis.* Nat Methods, 2009. **6**(5): p. 359-62.

161. Anderson, N.L. and N.G. Anderson, *The human plasma proteome: history, character, and diagnostic prospects.* Mol Cell Proteomics, 2002. **1**(11): p. 845-67.
162. Rappsilber, J. and M. Mann, *Analysis of the topology of protein complexes using cross-linking and mass spectrometry.* CSH Protoc, 2007. **2007**: p. pdb prot4594.
163. Cox, J. and M. Mann, *Quantitative, high-resolution proteomics for data-driven systems biology.* Annu Rev Biochem, 2011. **80**: p. 273-99.
164. Cox, J. and M. Mann, *MaxQuant enables high peptide identification rates, individualized p.p.b.-range mass accuracies and proteome-wide protein quantification.* Nat Biotechnol, 2008. **26**(12): p. 1367-72.
165. Bantscheff, M., et al., *Quantitative mass spectrometry in proteomics: critical review update from 2007 to the present.* Anal Bioanal Chem, 2012. **404**(4): p. 939-65.
166. Ong, S.E., et al., *Stable isotope labeling by amino acids in cell culture, SILAC, as a simple and accurate approach to expression proteomics.* Mol Cell Proteomics, 2002. **1**(5): p. 376-86.
167. Kruger, M., et al., *SILAC mouse for quantitative proteomics uncovers kindlin-3 as an essential factor for red blood cell function.* Cell, 2008. **134**(2): p. 353-64.
168. Trudgian, D.C., et al., *Comparative evaluation of label-free SINQ normalized spectral index quantitation in the central proteomics facilities pipeline.* Proteomics, 2011. **11**(14): p. 2790-7.
169. Cox, J., et al., *Accurate proteome-wide label-free quantification by delayed normalization and maximal peptide ratio extraction, termed MaxLFQ.* Mol Cell Proteomics, 2014. **13**(9): p. 2513-26.
170. Bantscheff, M., et al., *Quantitative mass spectrometry in proteomics: a critical review.* Anal Bioanal Chem, 2007. **389**(4): p. 1017-31.
171. Meissner, F. and M. Mann, *Quantitative shotgun proteomics: considerations for a high-quality workflow in immunology.* Nat Immunol, 2014. **15**(2): p. 112-7.
172. Iribarne, J.V., Thomson, B.A., *On the evaporation of small ions from charged droplets.* Journal of Chemical Physics, 1976. **6**(64): p. 2287-2294.
173. Nguyen, S. and J.B. Fenn, *Gas-phase ions of solute species from charged droplets of solutions.* Proc Natl Acad Sci U S A, 2007. **104**(4): p. 1111-7.
174. Wilm, M., *Principles of electrospray ionization.* Mol Cell Proteomics, 2011. **10**(7): p. M111 009407.
175. Domon, B. and R. Aebersold, *Mass spectrometry and protein analysis.* Science, 2006. **312**(5771): p. 212-7.
176. Mann, M. and N.L. Kelleher, *Precision proteomics: the case for high resolution and high mass accuracy.* Proc Natl Acad Sci U S A, 2008. **105**(47): p. 18132-8.
177. Makarov, A., *Electrostatic axially harmonic orbital trapping: a high-performance technique of mass analysis.* Anal Chem, 2000. **72**(6): p. 1156-62.
178. Hu, Q., et al., *The Orbitrap: a new mass spectrometer.* J Mass Spectrom, 2005. **40**(4): p. 430-43.
179. Kingdon, K.H., *A Method for the Neutralization of Electron Space Charge by Positive Ionization at Very Low Gas Pressures.* Phys. Rev. , 1923. **21**(4): p. 408.
180. Syka, J.E., et al., *Novel linear quadrupole ion trap/FT mass spectrometer: performance characterization and use in the comparative analysis of histone H3 post-translational modifications.* J Proteome Res, 2004. **3**(3): p. 621-6.
181. Makarov, A., et al., *Dynamic range of mass accuracy in LTQ Orbitrap hybrid mass spectrometer.* J Am Soc Mass Spectrom, 2006. **17**(7): p. 977-82.
182. Olsen, J.V., et al., *A dual pressure linear ion trap Orbitrap instrument with very high sequencing speed.* Mol Cell Proteomics, 2009. **8**(12): p. 2759-69.
183. Liu, C., et al., *Histone methylation in higher plants.* Annu Rev Plant Biol, 2010. **61**: p. 395-420.
184. Wolfe, R.R., *The underappreciated role of muscle in health and disease.* Am J Clin Nutr, 2006. **84**(3): p. 475-82.

185. Niwa, H., K. Yamamura, and J. Miyazaki, *Efficient selection for high-expression transfectants with a novel eukaryotic vector.* Gene, 1991. **108**(2): p. 193-9.
186. Lowry, O.H., et al., *Protein measurement with the Folin phenol reagent.* J Biol Chem, 1951. **193**(1): p. 265-75.
187. Shevchenko, A., et al., *In-gel digestion for mass spectrometric characterization of proteins and proteomes.* Nat Protoc, 2006. **1**(6): p. 2856-60.
188. Michalski, A., et al., *Mass spectrometry-based proteomics using Q Exactive, a high-performance benchtop quadrupole Orbitrap mass spectrometer.* Mol Cell Proteomics, 2011. **10**(9): p. M111 011015.
189. Lange O., M.A., Denisov E., Balschun *Accelerating spectral acquisition rate of Orbitrap mass spectrometry.* W.Proc. 58th Conf. Amer. Soc. Mass Spectrom, 2010.
190. Scheltema, R.A., et al., *The Q Exactive HF, a Benchtop mass spectrometer with a pre-filter, high-performance quadrupole and an ultra-high-field Orbitrap analyzer.* Mol Cell Proteomics, 2014. **13**(12): p. 3698-708.
191. Petrossian, T.C. and S.G. Clarke, *Multiple Motif Scanning to identify methyltransferases from the yeast proteome.* Mol Cell Proteomics, 2009. **8**(7): p. 1516-26.
192. Manttari, S. and M. Jarvilehto, *Comparative analysis of mouse skeletal muscle fibre type composition and contractile responses to calcium channel blocker.* BMC Physiol, 2005. **5**(1): p. 4.
193. Wigston, D.J. and A.W. English, *Fiber-Type Proportions in Mammalian Soleus Muscle during Postnatal-Development.* Journal of Neurobiology, 1992. **23**(1): p. 61-70.
194. Tusher, V.G., R. Tibshirani, and G. Chu, *Significance analysis of microarrays applied to the ionizing radiation response (vol 98, pg 5116, 2001).* Proceedings of the National Academy of Sciences of the United States of America, 2001. **98**(18): p. 10515-10515.
195. Christodoulou, D.C., et al., *Quantification of gene transcripts with deep sequencing analysis of gene expression (DSAGE) using 1 to 2 microg total RNA.* Curr Protoc Mol Biol, 2011. **Chapter 25**: p. Unit25B 9.
196. Ringner, M., *What is principal component analysis?* Nat Biotechnol, 2008. **26**(3): p. 303-4.
197. Dobin, A., et al., *STAR: ultrafast universal RNA-seq aligner.* Bioinformatics, 2013. **29**(1): p. 15-21.
198. Anders, S. and W. Huber, *Differential expression analysis for sequence count data.* Genome Biology, 2010. **11**(10).
199. Pfisterer, S.G., et al., *Ca2+/calmodulin-dependent kinase (CaMK) signaling via CaMKI and AMP-activated protein kinase contributes to the regulation of WIPI-1 at the onset of autophagy.* Mol Pharmacol, 2011. **80**(6): p. 1066-75.
200. Perera, S., et al., *Developmental regulation of MURF ubiquitin ligases and autophagy proteins nbr1, p62/SQSTM1 and LC3 during cardiac myofibril assembly and turnover.* Dev Biol, 2011. **351**(1): p. 46-61.
201. Ramos, F.J., M. Kaeberlein, and B.K. Kennedy, *Elevated MTORC1 signaling and impaired autophagy.* Autophagy, 2013. **9**(1): p. 108-109.
202. Ulbricht, A., et al., *Cellular mechanotransduction relies on tension-induced and chaperone-assisted autophagy.* Curr Biol, 2013. **23**(5): p. 430-5.
203. Ravikumar, B., et al., *Dynein mutations impair autophagic clearance of aggregate-prone proteins.* Nat Genet, 2005. **37**(7): p. 771-6.
204. Strohecker, A.M., et al., *Identification of 6-phosphofructo-2-kinase/fructose-2,6-bisphosphatase as a novel autophagy regulator by high content shRNA screening.* Oncogene, 2015.
205. Kozbial, P.Z. and A.R. Mushegian, *Natural history of S-adenosylmethionine-binding proteins.* BMC Struct Biol, 2005. **5**: p. 19.
206. Kondo, H., et al., *p47 is a cofactor for p97-mediated membrane fusion.* Nature, 1997. **388**(6637): p. 75-8.

207. Meyer, H.H., H. Kondo, and G. Warren, *The p47 co-factor regulates the ATPase activity of the membrane fusion protein, p97.* FEBS Lett, 1998. **437**(3): p. 255-7.
208. Lundby, A., et al., *Proteomic analysis of lysine acetylation sites in rat tissues reveals organ specificity and subcellular patterns.* Cell Rep, 2012. **2**(2): p. 419-31.
209. Pang, C.N., E. Gasteiger, and M.R. Wilkins, *Identification of arginine- and lysine-methylation in the proteome of Saccharomyces cerevisiae and its functional implications.* BMC Genomics, 2010. **11**: p. 92.
210. Uhlmann, T., et al., *A method for large-scale identification of protein arginine methylation.* Mol Cell Proteomics, 2012. **11**(11): p. 1489-99.
211. Bremang, M., et al., *Mass spectrometry-based identification and characterisation of lysine and arginine methylation in the human proteome.* Mol Biosyst, 2013. **9**(9): p. 2231-47.
212. Fisk, J.C., et al., *Proteomic analysis reveals diverse classes of arginine methylproteins in mitochondria of trypanosomes.* Mol Cell Proteomics, 2013. **12**(2): p. 302-11.
213. Lott, K., et al., *Global proteomic analysis in trypanosomes reveals unique proteins and conserved cellular processes impacted by arginine methylation.* J Proteomics, 2013. **91**: p. 210-25.
214. Huang, J., et al., *Repression of p53 activity by Smyd2-mediated methylation.* Nature, 2006. **444**(7119): p. 629-32.
215. Roberts, D.M., et al., *Expression of a calmodulin methylation mutant affects the growth and development of transgenic tobacco plants.* Proc Natl Acad Sci U S A, 1992. **89**(17): p. 8394-8.
216. Harding, S.A., S.H. Oh, and D.M. Roberts, *Transgenic tobacco expressing a foreign calmodulin gene shows an enhanced production of active oxygen species.* EMBO J, 1997. **16**(6): p. 1137-44.
217. Gregori, L., et al., *Specific Recognition of Calmodulin from Dictyostelium-Discoideum by the Atp, Ubiquitin-Dependent Degradative Pathway.* Journal of Biological Chemistry, 1985. **260**(9): p. 5232-5235.
218. Hershko, A., *Ubiquitin-mediated protein degradation.* J Biol Chem, 1988. **263**(30): p. 15237-40.
219. Hershko, A., *The ubiquitin pathway for protein degradation.* Trends Biochem Sci, 1991. **16**(7): p. 265-8.
220. Esteve, P.O., et al., *Regulation of DNMT1 stability through SET7-mediated lysine methylation in mammalian cells.* Proc Natl Acad Sci U S A, 2009. **106**(13): p. 5076-81.
221. Kontaki, H. and I. Talianidis, *Lysine methylation regulates E2F1-induced cell death.* Mol Cell, 2010. **39**(1): p. 152-60.
222. Bannister, A.J., et al., *Selective recognition of methylated lysine 9 on histone H3 by the HP1 chromo domain.* Nature, 2001. **410**(6824): p. 120-4.
223. Li, J.Y., et al., *Synergistic function of DNA methyltransferases Dnmt3a and Dnmt3b in the methylation of Oct4 and Nanog.* Mol Cell Biol, 2007. **27**(24): p. 8748-59.
224. Kurash, J.K., et al., *Methylation of p53 by Set7/9 mediates p53 acetylation and activity in vivo.* Mol Cell, 2008. **29**(3): p. 392-400.
225. Cheng, X., *Structure and function of DNA methyltransferases.* Annu Rev Biophys Biomol Struct, 1995. **24**: p. 293-318.
226. Selcen, D. and O. Carpen, *The Z-disk diseases.* Adv Exp Med Biol, 2008. **642**: p. 116-30.
227. Maloyan, A. and J. Robbins, *Autophagy in desmin-related cardiomyopathy: thoughts at the halfway point.* Autophagy, 2010. **6**(5): p. 665-6.
228. Voelkel, T., et al., *Lysine methyltransferase Smyd2 regulates Hsp90-mediated protection of the sarcomeric titin springs and cardiac function.* Biochim Biophys Acta, 2013. **1833**(4): p. 812-22.
229. Hitomi, Y., et al., *Seven skeletal muscles rich in slow muscle fibers may function to sustain neutral position in the rodent hindlimb.* Comp Biochem Physiol B Biochem Mol Biol, 2005. **140**(1): p. 45-50.

230. Kim, S.H., et al., *PGC-1alpha mediates a rapid, exercise-induced downregulation of glycogenolysis in rat skeletal muscle.* J Physiol, 2015. **593**(3): p. 635-43.
231. Quiat, D., et al., *Concerted regulation of myofiber-specific gene expression and muscle performance by the transcriptional repressor Sox6.* Proc Natl Acad Sci U S A, 2011. **108**(25): p. 10196-201.
232. Leone, T.C., et al., *PGC-1alpha deficiency causes multi-system energy metabolic derangements: muscle dysfunction, abnormal weight control and hepatic steatosis.* PLoS Biol, 2005. **3**(4): p. e101.
233. Ojima, K., et al., *The importance of subfragment 2 and C-terminus of myosin heavy chain for thick filament assembly in skeletal muscle cells.* Anim Sci J, 2015. **86**(4): p. 459-67.
234. Kollmann, K., et al., *Cell biology and function of neuronal ceroid lipofuscinosis-related proteins.* Biochim Biophys Acta, 2013. **1832**(11): p. 1866-81.
235. Weihl, C.C., et al., *Transgenic expression of inclusion body myopathy associated mutant p97/VCP causes weakness and ubiquitinated protein inclusions in mice.* Hum Mol Genet, 2007. **16**(8): p. 919-28.
236. Terrill, J.R., et al., *Oxidative stress and pathology in muscular dystrophies: focus on protein thiol oxidation and dysferlinopathies.* FEBS J, 2013. **280**(17): p. 4149-64.
237. Tohma, H., et al., *Quantification of ceroid and lipofuscin in skeletal muscle.* J Histochem Cytochem, 2011. **59**(8): p. 769-79.
238. Nakae, Y., et al., *Early onset of lipofuscin accumulation in dystrophin-deficient skeletal muscles of DMD patients and mdx mice.* J Mol Histol, 2004. **35**(5): p. 489-99.
239. Diffee, G.M., et al., *Control of myosin heavy chain expression: interaction of hypothyroidism and hindlimb suspension.* Am J Physiol, 1991. **261**(6 Pt 1): p. C1099-106.
240. Loughna, P.T., et al., *Disuse and passive stretch cause rapid alterations in expression of developmental and adult contractile protein genes in skeletal muscle.* Development, 1990. **109**(1): p. 217-23.
241. Swoap, S.J., et al., *Control of beta-myosin heavy chain expression in systemic hypertension and caloric restriction in the rat heart.* Am J Physiol, 1995. **269**(4 Pt 1): p. C1025-33.
242. Schiaffino, S. and C. Reggiani, *Molecular diversity of myofibrillar proteins: gene regulation and functional significance.* Physiol Rev, 1996. **76**(2): p. 371-423.
243. Bozzo, C., et al., *Nerve influence on myosin light chain phosphorylation in slow and fast skeletal muscles.* Febs Journal, 2005. **272**(22): p. 5771-5785.
244. Larsson, L. and B. Ramamurthy, *Aging-related changes in skeletal muscle. Mechanisms and interventions.* Drugs Aging, 2000. **17**(4): p. 303-16.
245. Larsson, L., et al., *Effects of aging on regulation of muscle contraction at the motor unit, muscle cell, and molecular levels.* Int J Sport Nutr Exerc Metab, 2001. **11 Suppl**: p. S28-43.
246. Zee, B.M., et al., *In vivo residue-specific histone methylation dynamics.* J Biol Chem, 2010. **285**(5): p. 3341-50.
247. Ghazalpour, A., et al., *Comparative analysis of proteome and transcriptome variation in mouse.* PLoS Genet, 2011. **7**(6): p. e1001393.
248. Yang, X.J., *Multisite protein modification and intramolecular signaling.* Oncogene, 2005. **24**(10): p. 1653-62.
249. Ching, J.K., et al., *mTOR dysfunction contributes to vacuolar pathology and weakness in valosin-containing protein associated inclusion body myopathy.* Hum Mol Genet, 2013. **22**(6): p. 1167-79.
250. Watts, G.D., et al., *Inclusion body myopathy associated with Paget disease of bone and frontotemporal dementia is caused by mutant valosin-containing protein.* Nat Genet, 2004. **36**(4): p. 377-81.
251. Weihl, C.C., *Valosin containing protein associated fronto-temporal lobar degeneration: clinical presentation, pathologic features and pathogenesis.* Curr Alzheimer Res, 2011. **8**(3): p. 252-60.

252. Majounie, E., et al., *Mutational analysis of the VCP gene in Parkinson's disease.* Neurobiol Aging, 2012. **33**(1): p. 209 e1-2.
253. Johnson, J.O., et al., *Exome sequencing reveals VCP mutations as a cause of familial ALS.* Neuron, 2010. **68**(5): p. 857-64.
254. Marza, E., et al., *Genome-wide screen identifies a novel p97/CDC-48-dependent pathway regulating ER-stress-induced gene transcription.* EMBO Rep, 2015. **16**(3): p. 332-40.
255. Ramadan, K., et al., *Cdc48/p97 promotes reformation of the nucleus by extracting the kinase Aurora B from chromatin.* Nature, 2007. **450**(7173): p. 1258-62.
256. Rabinovich, E., et al., *AAA-ATPase p97/Cdc48p, a cytosolic chaperone required for endoplasmic reticulum-associated protein degradation.* Mol Cell Biol, 2002. **22**(2): p. 626-34.
257. Zhang, X., et al., *Altered cofactor regulation with disease-associated p97/VCP mutations.* Proc Natl Acad Sci U S A, 2015. **112**(14): p. E1705-14.
258. Tang, W.K. and D. Xia, *Altered intersubunit communication is the molecular basis for functional defects of pathogenic p97 mutants.* J Biol Chem, 2013. **288**(51): p. 36624-35.
259. Erzurumlu, Y., et al., *A unique IBMPFD-related P97/VCP mutation with differential binding pattern and subcellular localization.* Int J Biochem Cell Biol, 2013. **45**(4): p. 773-82.
260. Wang, Y., et al., *N6-methyladenosine modification destabilizes developmental regulators in embryonic stem cells.* Nat Cell Biol, 2014. **16**(2): p. 191-8.
261. Kleinschmidt, M.A., et al., *The protein arginine methyltransferases CARM1 and PRMT1 cooperate in gene regulation.* Nucleic Acids Res, 2008. **36**(10): p. 3202-13.
262. Smith, V., et al., *Functional analysis of the genes of yeast chromosome V by genetic footprinting.* Science, 1996. **274**(5295): p. 2069-2074.
263. Winzeler, E.A., et al., *Functional characterization of the S. cerevisiae genome by gene deletion and parallel analysis.* Science, 1999. **285**(5429): p. 901-6.
264. Giaever, G., et al., *Functional profiling of the Saccharomyces cerevisiae genome.* Nature, 2002. **418**(6896): p. 387-91.
265. Kobayashi, T., A. Manno, and A. Kakizuka, *Involvement of valosin-containing protein (VCP)/p97 in the formation and clearance of abnormal protein aggregates.* Genes to Cells, 2007. **12**(7): p. 889-901.
266. Wojcik, C., M. Yano, and G.N. DeMartino, *RNA interference of valosin-containing protein (VCP/p97) reveals multiple cellular roles linked to ubiquitin/proteasome-dependent proteolysis.* J Cell Sci, 2004. **117**(Pt 2): p. 281-92.
267. Dalal, S., et al., *Distinct roles for the AAA ATPases NSF and p97 in the secretory pathway.* Mol Biol Cell, 2004. **15**(2): p. 637-48.
268. Yamada, E., et al., *Mouse skeletal muscle fiber-type-specific macroautophagy and muscle wasting are regulated by a Fyn/STAT3/Vps34 signaling pathway.* Cell Rep, 2012. **1**(5): p. 557-69.
269. Yamanaka, K., Y. Sasagawa, and T. Ogura, *Recent advances in p97/VCP/Cdc48 cellular functions.* Biochim Biophys Acta, 2012. **1823**(1): p. 130-7.
270. Fusser, M., et al., *Lysine Methylation of the Valosin-Containing Protein (VCP) Is Dispensable for Development and Survival of Mice.* PLoS One, 2015. **10**(11): p. e0141472.
271. Mowen, K.A., et al., *Arginine methylation of STAT1 modulates IFNalpha/beta-induced transcription.* Cell, 2001. **104**(5): p. 731-41.
272. Biggar, K.K. and S.S. Li, *Non-histone protein methylation as a regulator of cellular signalling and function.* Nat Rev Mol Cell Biol, 2015. **16**(1): p. 5-17.
273. Wai T., L.T., *Mitochondrial Dynamics and Metabolic Regulation.* Trends in Endocrinology & Metabolism, 2016.
274. Wang, K. and D.J. Klionsky, *Mitochondria removal by autophagy.* Autophagy, 2011. **7**(3): p. 297-300.
275. Masiero, E., et al., *Autophagy Is Required to Maintain Muscle Mass.* Cell Metabolism, 2009. **10**(6): p. 507-515.

276. Skulachev, V.P., *Mitochondria in the programmed death phenomena; a principle of biology: "it is better to die than to be wrong".* IUBMB Life, 2000. **49**(5): p. 365-73.
277. Wojcik, C., et al., *Valosin-containing protein (p97) is a regulator of endoplasmic reticulum stress and of the degradation of N-end rule and ubiquitin-fusion degradation pathway substrates in mammalian cells.* Mol Biol Cell, 2006. **17**(11): p. 4606-18.
278. Mauvezin, C., et al., *Autophagosome-lysosome fusion is independent of V-ATPase-mediated acidification.* Nat Commun, 2015. **6**: p. 7007.
279. Ju, J.S. and C.C. Weihl, *p97/VCP at the intersection of the autophagy and the ubiquitin proteasome system.* Autophagy, 2010. **6**(2): p. 283-5.
280. Tanida, I., T. Ueno, and E. Kominami, *LC3 and Autophagy.* Methods Mol Biol, 2008. **445**: p. 77-88.
281. Pattison, J.S., H. Osinska, and J. Robbins, *Atg7 induces basal autophagy and rescues autophagic deficiency in CryABR120G cardiomyocytes.* Circ Res, 2011. **109**(2): p. 151-60.
282. Ju, J.S., et al., *Quantitation of "autophagic flux" in mature skeletal muscle.* Autophagy, 2010. **6**(7): p. 929-35.
283. Sahani, M.H., E. Itakura, and N. Mizushima, *Expression of the autophagy substrate SQSTM1/p62 is restored during prolonged starvation depending on transcriptional upregulation and autophagy-derived amino acids.* Autophagy, 2014. **10**(3): p. 431-41.
284. Zhou, L., et al., *Bcl-2-dependent upregulation of autophagy by sequestosome 1/p62 in vitro.* Acta Pharmacol Sin, 2013. **34**(5): p. 651-6.
285. Pyo, J.O., et al., *Overexpression of Atg5 in mice activates autophagy and extends lifespan.* Nat Commun, 2013. **4**: p. 2300.

6. List of figures

7. Abbreviations

°C	Degree Celsius
µl	Microliter
3MA	3-Methyladenine
AAA-ATPase	ATPase associated with diverse cellular activities
ABC	Ammonium bicarbonate
ACN	Acetonitrile
ALS	Amyotrophic lateral sclerosis
Arg0	L-arginine
Arg10	13C6 15N4-labeled L-arginine
Arg6	13C6-labeled L-arginine
Atg	Autophagy-related genes
BSA	Bovine Serum Albumin
CASA	Chaperone-assisted selective autophagy
CID	Collision induced dissociation
CMA	Chaperone-mediated autophagy
CMV	Cytomegalovirus promotor
cNSL	Nuclear localization signal
CRM	Charge residue model
DAPI	4’,6-diamidino-2-phenylindole
dFBS	Dialyzed fetal bovine serum
DLAD	DNase II-like acid Dnase
DMD	Duchenne muscular dystrophy
DMEM	Dulbecco’s Modified Eagle’s Medium
DMSO	Dimethyl Sulphoxide
DTT	Dithiothreitol
E1	Ubiquitin-activating enzyme
E2	Ubiquitin-conjugating enzyme
E3	Ubiquitin-ligase enzyme
EDTA	Ethylenediamenetetraacetic acid
eFT	Enhanced Fourier Transformation
ESI	Electrospray ionization
FASP	Filter-aided sample preparation
FD	Frontotemporal dementia
FDR	False Discovery Rate
FT	Fourier Transformed
FT-ICR	Fourier transform ion cyclotron resonance analyzer
fw	Forward
GAA	Guanidinoacetic acid
GO	Gene ontology
H&E	Haematoxylin/Eosin
HBS	HEPES Buffered Saline
HCD	Higher energy collisional dissociation

HF	High field
HOPS	Homotypic fusion and vacuole protein sorting
IAA	Iodoacetamide
IBM	Inclusion body myopathy
IBMPFD	Paget disease of bone-frontotemporal dementia
iTRAQ	Isobaric tags for relative and absolute quantitation
LacZ	Beta-galactosidase coding sequence from E.coli
LB	Luria-Bertani
LC-MS/MS	Liquid Chromatography-Tandem Mass Spectrometry
LIR	LC3-interacting region
Lys0	L-lysine
Lys4	4,4,5,5-D_4-L-Lysine
Lys6	$^{13}C_6$ Lysine
Lys8	$^{13}C_6$ $^{15}N_2$-labeled L-lysine
LysC	Lysyl endopeptidase
M	Molar
m/z	Mass/charge
MALDI	Matrix-assisted laser desorption
MALDI	Matrix-assisted laser desorption/ionization
mg	Milligram
MS/MS	Tandem Mass Spectrometry
MTase	Methyltransferase
MTF16	Methyltransferase 16
MyHC	Myosin heavy chain
MyHC I	Myosin heavy chain monoclonal I
MyHC II	Myosin heavy chain monoclonal II
OCT	Optimal cutting temperature
PAS	Phagophore assembly site
PBS	Phosphate-buffered saline
PCA	Principal Component Analysis
PCR	Polymerase chain reaction
PD	Parkinson disease
PDB	Paget's disease of the bone
PE	Phosphatidylethanolamine
PI3-P	Phosphatidylinositol-triphosphate
PMSF	Phenylmethanesulphonyl fluoride
PSG	Penicillin-Streptavidin-L-Glutamine
PSM	Peptide spectrum match
PTM	Post-translational modification
rev	Reverse
ROS	Reactive oxygen species
RPLC	Reversed-phase liquid chromatography
SAH	S-adenosyl-homocysteine
SAM	S-adenosylmethionine
SAX	Strong anion exchange chromatography

SCX	Strong cation exchange chromatography
SDS-PAGE	Sodium dodecyl sulphate Polyacrylamide Gel Electrophoresis
SEC	Size exclusion chromatography
sIBM	Sporadic inclusion body myositis
SILAC	Stable isotope labeling with amino acids in cell culture
SR	Sarcoplasmic reticulum
StageTips	Stop and go extraction tips
TE	Tris-EDTA
TFA	Trifluoroacetic acid
TOF	Time-of-flight
TRIM	Tripartite motif
UBA	Ubiquitin-binding domain containing
UHPLC	Ultra-high pressure reversed phase chromatography
UPS	Ubiquitin-proteasomal system
UVRAG	Ultraviolet irradiation resistance associated gene
X-Gal	5-bromo-4-chloroindoxyl-beta-galactosidase
XIC	Extracted-ion chromatogram

8. Acknowledgements

This dissertation would not have been possible without the inspiration and support of my supervisors, colleagues, friends, and my family.

First and foremost, I am truly grateful to my supervisors Professor Dr. Dr. Thomas Braun and Professor Dr. Marcus Krüger for giving me the opportunity to pursue my PhD thesis at the Biomolecular Mass Spectrometry division of the Max-Planck-Institute for Heart and Lung Research. I really appreciated the incredible work environment that allowed me to grow as a scientist. Thank you for your never-ending enthusiasm, keeping your office door always open and believing in me.
I express my appreciation to Professor Dr. Katja Sträßer for her willingness to be my second corrector and supporting my doctoral graduation.

I am also grateful to the members of my institute for creating a perfect research environment to work in. Special thanks to Hendrik for all your patience in answering the many questions and for being such a good friend. Special thanks to Jens for many valuable discussions and listening to my statistical problems. Special thanks to Sriram for your motivation and sharing all the PhD issues with me. Special thanks to Tanja for being an irreplaceable support in the lab and friend through my PhD. Special thanks to Sylvia for all the scientific and technical discussions and help, your laughs and friendship. Thanks for a really great time.
I also extend my gratitude to Stefan, Brigitte, Natalie, Sabrina, Ellen, Birgit and Kerstin for their input towards my project and their continuous support.

Finally, my special gratitude and love goes to my family. Especially, my husband Peter and my lovely daughters Alina and Sophia, my parents and parents-in-law gave me continuous support, love and encouragement which always kept me motivated and without I could not have done my PhD. I dedicate this dissertation to them.

Soraya Hölper

9. Curriculum Vitae

Der Lebenslauf wurde aus der elektronischen Version der Arbeit entfernt.